NTNU

Norwegian University of
Science and Technology

Numerical Modelling of Focussed Wave Hydrodynamics and Focused Wave-structure Interaction with REEF3D

Thevaher Amarachaharam

Coastal and Marine Engineering and Management
Submission date: July 2016
Supervisor: Hans Sebastian Bihs, BAT
Co-supervisor: Mayilvahanan Alagan Chella, BAT
Ankit Aggarwal, BAT

Norwegian University of Science and Technology
Department of Civil and Transport Engineering

ERASMUS +: ERASMUS MUNDUS MOBILITY PROGRAMME

Master of Science in

COASTAL AND MARINE ENGINEERING AND MANAGEMENT

CoMEM

NUMERICAL MODELING OF FOCUSED WAVE HYDRODYNAMICS AND FOCUSED WAVE-STRUCTURE INTERACTION WITH REEF3D

Norwegian University of Science and Technology
7 July 2016

Amarachaharam Thevaher

The Erasmus+: Erasmus Mundus MSc in Coastal and Marine Engineering and Management is an integrated programme including mobility organized by five European partner institutions, coordinated by Norwegian University of Science and Technology (NTNU).

The joint study programme of 120 ECTS credits (two years full-time) has been obtained at two or three of the five CoMEM partner institutions:

- Norges Teknisk- Naturvitenskapelige Universitet (NTNU) Trondheim, Norway
- Technische Universiteit (TU) Delft, The Netherlands
- Universitat Politècnica de Catalunya (UPC). BarcelonaTech. Barcelona, Spain
- University of Southampton, Southampton, Great Britain
- City University London, London, Great Britain

During the first three semesters of the programme, students study at two or three different universities depending on their track of study. In the fourth and final semester an MSc project and thesis has to be completed. The two-year CoMEM programme leads to a multiple set of officially recognized MSc diploma certificates. These will be issued by the universities that have been attended by the student. The transcripts issued with the MSc Diploma Certificate of each university include grades/marks and credits for each subject.

Information regarding the CoMEM programme can be obtained from the programme coordinator:

Øivind A. Arntsen, Dr.ing.
Associate professor in Marine Civil Engineering
Department of Civil and Transport Engineering
NTNU Norway
Telephone: +4773594625 Cell: +4792650455 Fax: + 4773597021
Email: oivind.arntsen@ntnu.no

CoMEM URL: https://www.ntnu.edu/studies/mscomem

CoMEM Thesis

This thesis was completed by:
Amarachaharam Thevaher

Under supervision of:
Hans Bihs , Asscociate professor NTNU
Mayilvahanan Alagan Chella, Postdoc, NTNU

As a requirement to attend the degree of
Erasmus+: Erasmus Mundus Master in Coastal and Marine Engineering and Management (CoMEM)

Taught at the following educational institutions:

Norges Teknisk- Naturvitenskapelige Universitet (NTNU)
Trondheim, Norway

Technische Universiteit (TU) Delft
Delft, The Netherlands

At which the student has studied from August 2014 to July 2016.

NORWEGIAN UNIVERSITY OF SCIENCE AND TECHNOLOGY
DEPARTMENT OF CIVIL AND TRANSPORT ENGINEERING

Report Title:	Date:07/07/2016			
Numerical Modeling of Focused Wave Hydrodynamics and Focused Wave-structure Interaction with REEF3D	Number of pages (incl. appendices):87			
	Master Thesis	X	Project Work	
Name:				
Amrachaharam Thevaher				
Professor in charge/supervisor:				
Prof. Hans Bihs				
Other external professional contacts/supervisors:				
Dr. Mayilvahanan Alagan Chella, Ankit Agarwal				

Abstract:
General irregular sea state can generate very steep waves which can induce unpleasant dynamic wave loading to the structures. Sometimes these wave loads exceed upper design limits of the structure thus resulting in the failures of the structures. Sub-structure of wind turbines, offshore oil platforms and ships are some of the structures which needs more attention in designing because of larger individual and economic risks associated with these structures.

Focused waves are a group of waves used to investigate high steep wave kinematics in a numerical or in an experimental model. Each wave component's phase angle is tuned to get focused at a particular time and location. REEF3D is an open source numerical model governed by mass and momentum balance of Navier Stokes equation. This study uses REEF3D numerical model to simulate and investigate the focused wave kinematics and nature of the focused wave-structure interaction. REEF3D simulation cases are validated with available experimental data on focused waves. Two-dimensional studies are carried-out to investigate focused wave steepness kinematic correlations. Later vertical cylinder in a three dimensional domain to study wave structure interaction kinematics and wave forces. There are some signicant ndings in this thesis which improved the understanding of focused wave modeling in REEF3D.

This thesis will enhance the future studies on focused wave modeling in REEF3D.

Keywords:

1. CoMEM
2. REEF3D
3. Focused wave
4. Vertical cylinder

_____

MASTER THESIS

(TBA4920 Marine Civil Engineering, master thesis)

Spring 2016
for
Amarachaharam Thevaher

Numerical modelling of focussed wave hydrodynamics and focussed wave-structure interaction with REEF3D

BACKGROUND

Extreme waves are huge waves at sea and their interaction with a structure exerts a huge hydrodynamic load on it. The knowledge concerning the characteristics and kinematics of extreme waves is inevitable to understand the physical processes and the associated higher-order effects on structures, e.g. ringing. For the global design of marine structures e.g. offshore wind turbine structures, extreme wave conditions need to be considered. Numerical modelling of extreme waves with a random wave groups is more demanding as it requires much longer simulation times.

TASK DESCRIPTION

In the present master thesis, the extreme waves and their interaction with a slender cylinder will be investigated using the open-source CFD model REEF3D which is based on the three dimensional Navier-Stokes equations.

- The characteristics and kinematics of extreme waves will be investigated with first and second-order focussed waves.
- The results of first and second order focussed waves will be compared with experimental data in order to validate the numerical model for modelling focused waves.
- The numerical model for simulating wave forces from focussed waves will be evaluated with experimental data. The study further investigates the interaction of focussed waves with a cylinder for different wave and environmental conditions. This includes the analysis of wave forces from the first and second order focussed waves.

In addition, the free surface flow features and the associated hydrodynamics around a cylinder will be studied in detail.

General about content, work and presentation
The text for the master thesis is meant as a framework for the work of the candidate. Adjustments might be done as the work progresses. Tentative changes must be done in cooperation and agreement with the professor in charge at the Department.

In the evaluation thoroughness in the work will be emphasized, as will be documentation of independence in assessments and conclusions. Furthermore the presentation (report) should be well organized and edited; providing clear, precise and orderly descriptions without being unnecessary voluminous.

The report shall include:

- Standard report front page (from DAIM, http://daim.idi.ntnu.no/)
- Title page with abstract and keywords.(template on: http://www.ntnu.no/bat/skjemabank) CoMEM students must include CoMEM as one of the keywords.
- CoMEM page (Only CoMEM students)
- Preface
- Summary and acknowledgement. The summary shall include the objectives of the work, explain how the work has been conducted, present the main results achieved and give the main conclusions of the work.
- Table of content including list of figures, tables, enclosures and appendices.
- A list explaining important terms and abbreviations should be included.
- List of symbols should be included
- The main text.
- Clear and complete references to material used, both in text and figures/tables. This also applies for personal and/or oral communication and information.
- Thesis task description (these pages) signed by professor in charge as Attachment 1.
- The report musts have a complete page numbering.

The thesis can as an alternative be made as a scientific article for international publication, when this is agreed upon by the Professor in charge. Such a report will include the main points as given above, but where the main text includes both the scientific article and a process report.

Submission procedure
Procedures relating to the submission of the thesis are described in IVT faculty webpage
http://www.ntnu.edu/ivt/master-s-thesis-regulations

On submission of the thesis the candidate shall submit to the professor in charge a CD/DVD('s) or a link to a net-cloud including the report in digital form as pdf and Word (or other editable form) versions and the underlying material (such as data collection, time series etc.).

Documentation collected during the work, with support from the Department, shall be handed in to the Department together with the report.

According to the current laws and regulations at NTNU, the report is the property of NTNU. The report and associated results can only be used following approval from NTNU (and external cooperation partner if applicable). The Department has the right to make use of the results from the work as if conducted by a Department employee, as long as other arrangements are not agreed upon beforehand.

Start and submission deadlines
The work on the Master Thesis starts on: - 02nd February 2016

The thesis report as described above shall be submitted digitally in DAIM at the latest on:-
07th July 2016 at 11:59PM.

Professor in charge: Hans Bihs

Other supervisors: Mayilvahanan Alagan Chella, Ankit Aggarwal

Trondheim, Date:- _____

_____
Professor in charge (sign)

Numerical Modeling of Focused Wave Hydrodynamics and Focused Wave-structure Interaction with REEF3D

A Masters' Thesis
submitted to the Faculty of Civil & Transport Engineering
at the Norwagian University of Science and Technology

by

Amarachaharam Thevaher

Acknowledgments

This master thesis work is done in order to meet the requirements of the two year Erasmus Mundus Coastal Engineering and Management (CoMEM) course. This thesis is carried out at the Department of Civil and Transport Engineering in NTNU. I hereby thanking all the academic and administrative staffs for their supports in accomplishing this task.

I specially thank Associate professor Øivind Arnsten for coordinating and arranging all the academic matters to begin my thesis at NTNU. I am grateful to Associate Professor Hans Bihs for his supervision and letting me work on REEF3D at the department. I have to thank my co-supervisor Postdoctoral Researcher Mayilvahanan Alagan Chella for spending his valuable time with me on clarifying matters on the whole process of writing my thesis. I also thanks PhD Candidate Ankit Aggarwal to help me on technical matters.

Finally, I would like to thank Mrs Sonja Marie Ekrann Hammer and Mariette van Tillburg for their administrative support through out the whole CoMEM master program.

Abstract

General irregular sea state can generate very steep waves which can induce unpleasant dynamic wave loading to the structures. Sometimes these wave loads exceed upper design limits of the structure thus resulting in the failures of the structures. Sub-structure of wind turbines, offshore oil platforms and ships are some of the structures which needs more attention in designing because of larger individual and economic risks associated with these structures.

Focused waves are a group of waves used to investigate high steep wave kinematics in a numerical or in an experimental model. Each wave component's phase angle is tuned to get focused at a particular time and location. REEF3D is an open source numerical model governed by mass and momentum balance of Navier Stokes equation. This study uses REEF3D numerical model to simulate and investigate the focused wave kinematics and nature of the focused wave-structure interaction. REEF3D simulation cases are validated with available experimental data on focused waves. Two-dimensional studies are carried-out to investigate focused wave steepness kinematic correlations. Later vertical cylinder in a three dimensional domain to study wave structure interaction kinematics and wave forces. There are some significant findings in this thesis which improved the understanding of focused wave modeling in REEF3D.

This thesis will enhance the future studies on focused wave modeling in REEF3D.

Contents

List of Figures

List of Tables

Chapter 1

Introduction

1.1 Ocean waves

Waves are generated in the ocean due to wind fetch or due to seismic activities such as earthquakes or due to tides or due to man-made activities. Waves are basically energy propagation and spreading in the ocean domain from where the energy concentrated. In all these mentioned causes there is an energy input. Wind and tidal waves are the dominant wave phenomenon in the sea. In nature these wave characteristics are not usually regular in both spatial and temporal domains. So they are called irregular waves. These irregular waves can be interpreted as a combination of regular waves. There are many theories explaining both regular and irregular waves and their hydrodynamics. Study of regular and irregular wave hydrodynamics and its characteristic changes in the surf zone is highly correlated to many other Engineering disciplines such as morphology of the sea bed, wave interaction against both submerged and emerged structures, coastal zone protection and sustainable offshore developments.

Linear wave theory, Stokes higher order theories, Cnoidal and Solitary wave theories are the common regular wave theories used. Linear wave theory is the simplest wave theory for applications but it is derived upon the assumption of the wave height is so small that the kinematic and dynamic boundary condition at the free surface is equal to the still water level rather than the distributed free surface. Therefore it has many limitations when it comes to practice. Even though there are some applications in which linear wave theory becomes significant(Young, 1999). As an example deep sea low steep wave kinematics can be studied with linear wave theory. Limiting steepness (wave height to wave length ratio in deep water) of linear wave assumption lies around 0.05 to 0.08 (Svendson and Hansen, 1976). Beyond this steepness linear wave theory fails to capture non-linear effects. Stokes second order wave theory compromises some drawbacks in the linear wave theory for higher steepness cases. Stoke's higher order theories are getting more and more complicated for further increment in the steepness. Ocean waves exert dynamic forces on the offshore structures. To design such an offshore structure one has to understand the complete nature of this dynamic forcing. Down scaled prototype laboratory models to study these irregular wave kinematics always come with the higher price tag, instrumental and scaling errors. A handy and comparatively less expensive way to overcome this hurdle is modeling this irregular sea state in a computer with all the physics behind it.

Constant or linear relations do not represent a sea state because of its irregularities. Therefore representing irregular sea-state is only possible through the means of spectral parameters. Distribution of wave energy over its frequency of occurrence is called the wave energy spectrum. JONSWAP and Pierson Moskowitz are the commonly used spectrum for the wind waves. Wave energy spectrum almost represents all wave characters with some approximations in a young sea state (Arntsen Ø.A, 2000).

1.2 Focused waves

Dynamic forcing on offshore structural foundations and ships increases with increasing wave height. This extreme loading can pose certain threat to the structural stability or they can topple the ships unless they are designed for these conditions. There are statistical evidences for such kinds of extreme wave events from the past. The famous one in the North Sea is called New year wave which happened in 1995 at Draupner offshore platform which exceeded 18.5m while the sea state had a significant wave height of 12m at that time (Walker et al., 2004). Other than this there are many incidents happened including overturning ships(Slunyaev et al., 2011) and damaging structures(Kharif et al., 2009). These extreme waves are the result of an super positioning of many irregular wave phases at a particular time and at a particular point in space (Bihs et al., 2016). This wave-wave non-linear interaction creates very complex hydrodynamic and kinematic phenomenon at the focus point. This extreme event has very low probability of occurrence as it needs super positioning of many waves from the ambient sea state. The resulting extreme wave is highly non-linear due to its supreme steepness.

Modeling these extreme cases in the laboratory is a bit challenging. Because laboratory generated storm waves are mainly regular or from random wave tests. Regular waves are not the representation of extreme waves. And it is almost unpredictable and impossible to capture non-linear extreme wave with laboratory generated random waves. Because, random wave series necessarily doesn't need to generate an extreme wave in a particular time interval given (Ning et al., 2009). To overcome these modeling barriers a predefined focused wave group can be used in which several wave components in a spectrum focuses simultaneously at a position in space and time. This outcome almost represents the shape of random extreme wave profile. The whole thesis is all about this predefined focused wave group, its kinematics and its interaction with a structure. Focused wave group study has been so far extensively used by many researchers to investigate extreme wave kinematics. Johannessen and Swan had used a double Fourier function to study focused waves (Johannessen and Swan, 1997), and they examined odd and even higher order components in spread sea wave groups using the method of separation of harmonics (Johannessen and Swan, 2001). Baldock et al. (1996) super imposed many regular wave trains and investigated non-linearity of the wave-wave interaction on the structure of the one way directed wave groups and created group inversion concept. His concept of group inversion later used to develop separation of harmonics.

1.3 CFD and REEF3D

Representation of the extreme sea state into a three dimensional computer domain has enormous benefits in studying its kinematics and applying them in the coastal Engineering discipline because of its flexibility and easiness. There are so many numerical models available regarding Computational Fluid Dynamics (CFD), but the choice is completely dependence on the purpose and accuracy of the calculations needed. Physical, empirical and phenomenological are main kinds of numerical models on the basis of the philosophy they are developed. CFD is generally a physical model developed behind the real physics of the system. Solving Navier-Stokes equation in a three dimensional domain is very essential for studying the complex phenomena like focused wave structure interaction and to capture the flow and its kinematics details. CFD not only used in coastal engineering but also in many applications such as aeronautical and automobile engineering. REEF3D is an open source Computational Fluid Dynamics (CFD) code developed at NTNU to study coastal engineering aspects where Navier-Stokes equation is solved in a three dimensional discretized domain. So far many successful intensive investigations are done the the numerical wave tank using REEF3D regarding irregular waves (Aggarwal, 2015), breaking waves (Alagan Chella et al., 2015), and Focused waves (Bihs et al., 2016). Chen et al. (2014) carried out physical experiments with high steep waves with vertical cylinders to measure the forces. Ning et al. (2009) performed focused wave group laboratory experiments and compared it with numerical simulations using Higher Order Boundary Element Method (HOBEM). Localized wave group approach was used to generate focused wave groups in the laboratory. The simulated results were in good agreement with the experimental results.

Higher computer processing speed and accessibility to super computer server open the possibilities to run many simulations with finer grid sizes. Numerical model will be discussed in detail in chapter-2.

1.4 Motivation

Private and state investments on renewable energy have exponentially increased in the past decade(Bull, 2001). More awareness on the global warming in the third world countries has changed the phase in the investment on coal and fossil fuel industries. As a result; wind and solar energy became very obvious choices in these days. UK and Germany have planned to invest a lot in the offshore wind farms in the next decade (Ladenburg, 2008). So an intensive study is needed on the design of offshore wind turbines because interaction of the offshore structures with extreme waves can gather dangerous consequences such as ringing. They are difficult to model in the laboratory wave flume because of its non-linear kinematic nature and less probability of occurrence from its sea state. Predefined (where and when to focus) focused wave groups are used to generate high steep waves to study extreme wave kinematics. REEF3D CFD model is already validated for simulating and modeling focused waves and its interaction with structures. The main objective of the study is to investigate high steep waves using focused wave groups and its interaction with a vertical cylinder in REEF3D. Vertical cylinder resembles mainly a mono-pile substructure for offshore wind turbine.

1.5 Objective of the study

In the present master thesis, the extreme waves and their interaction with a vertical cylinder will be investigated using REEF3D. At the beginning the characteristics and kinematics of extreme waves will be investigated with focused waves. Then focused wave forces on vertical cylinder are investigated at the end.

- Primary scope:- The focused waves with a vertical cylinder for different wave and environmental conditions. This includes the analysis of wave forces from different focused wave steepness and the associated hydrodynamics around a cylinder will be studied.
- Secondary scope:- The convergence and spectral study of the focused waves, steepness and kinematic correlations, deviations of numerical model with intended focus point and time, spatial and temporal evolution of the focused waves and many more

Validation is necessary for any numerical model with experimental results to make them applicable in real life. Therefore all the investigations are validated with available experimental results.

Chapter 2

Numerical Model and Numerical Wave Tank

2.1 Numerical Model

2.1.1 Governing Equations

Navier-Stokes equation is one of the governing equation in the computational fluid dynamics. This is based on the conservation of mass and momentum balance which is very important in a fluid flow. Compressibility of water in room temperature is very small (Fine and Millero, 1973) and it is neglected.

$$\frac{\partial u_i}{\partial x_i} = 0 \tag{2.1}$$

So momentum conservation combined with continuity equation leads to generalized Navier-Stokes equation as follows (Chorin, 1968).

$$\frac{\partial u_i}{\partial t} + u_j \frac{\partial u_i}{\partial x_j} = -\frac{1}{\rho}\frac{\partial p}{\partial x_i} + \frac{\partial}{\partial x_j}\left[(\nu + \nu_t)\left(\frac{\partial u_i}{\partial x_j} + \frac{\partial u_j}{\partial x_i}\right)\right] + g_i \tag{2.2}$$

In this equations i & j are the indice in the X and Y plane, velocity u is averaged over time t, ρ is the density of the fluid, p is the pressure, ν is the kinematic viscosity, ν_t is the turbulent viscosity and g is the acceleration due to gravity.

The first term in the left hand side of this equation is the time rate of change of momentum, and the second in the left is net convective inflow rate of momentum from three dimensions which is the inertial force. In the right hand side first term stands for pressure force and the second term stands for the net diffusive inflow rate of momentum which is the viscous force and the last term stands for the gravitational force.

2.1.2 Discretization methods

To get an exact solution for a differential equation, one has to apply boundary condition and solve them analytically. There are many mathematical approaches to solve partial differential equations (PDE) but it is almost impossible to solve some of them analytically. Temporal and spatial dependency, non-linear relationship with variables and higher

order derivatives make them more complicated. Navier-Stokes equation is one of this kind which needs to be solved numerically. Partial differential equations are holding infinitely larger domains with infinite accuracy. It is impossible to preserve their infinite accuracy levels in computer because; computers are working in the limited calculation power and memory in the world of numbers. But a good numerical model should preserve the fundamental structure of the whole system and should converge to the real solution with required accuracy level.

The three most widely used numerical methods to solve PDEs are the finite element method (FEM), finite volume methods (FVM) and finite difference methods (FDM).

Finite Element Method

Elasticity and structural mechanics is the main application area of FEM (Wagner, 2004). Problems have to be solved in irregular geometries in this field. Main advantage of the FEM to finite difference method is of its flexibility regarding the geometry of the domain where the PDE has to be solved. Moreover the FEM is perfectly suitable as an adaptive method. Because, the local refinement in the solution can be easily done. PDE is transformed into equivalent weak forms and the method does not operate on the PDE itself (Hughes, 2012). FEM begins discretizing the domain with finite elements in which geometric shape is divided into a finite number of regions. The domain is split into regular intervals in a one dimensional PDE. In two dimensions the elements are usually of triangular or quadrilateral shape. In three dimensions tetrahedral or hexahedral forms are mostly used (Wagner, 2004).

Finite Volume Method

The finite volume method is a discretization method which is well suited for the numerical simulation of various types (elliptic, parabolic or hyperbolic, for instance) of conservation laws; it has been extensively used in several engineering fields, such as fluid mechanics, heat and mass transfer or petroleum engineering (Eymard et al., 2000). Some of the important features of the finite volume method are similar to those of the finite element method. It may be used on arbitrary geometries, using structured or unstructured meshes, and it leads to robust schemes. An additional feature is the local conservation of the numerical fluxes, which is conserved from one discretization cell to its neighbor. This is based on balanced approach; means local balance is written on each discretization cell called controlled volume, thus finite volume method is locally conservative. This makes finite volume method more preferable, when it comes to modeling in fluid mechanics (Eymard et al., 2000). Integral formulation of the fluxes over the boundary of the control volume is obtained from divergence formula. The fluxes on the boundary are discretized with respect to the discrete unknowns.

Finite Difference Method

The approach of finite difference method in general approximates differential operators constituting to the field equation locally (Smith, 1985).To execute this a grid frame in the

variable domain is necessary. Differential operators in the governing equation are rendered in a discretized equation for each nodes of the gridded domain. The number of nodes to be considered for each calculation step is governed by the order of the differential operator of the governing problem. Finite difference method is used in REEF3D with conservation as it is done in the finite volume method. For higher order schemes finite difference method is more convenient to apply as it is the case here. Finite difference method has less drawbacks compared to finite volume and finite element methods if it is applied with correct schemes. Values at the nodes of the grid are solved with linear combination of function values which is being approximated from the derivatives of the partial differential equations.

2.1.3 Boundary conditions

Numerical domain is always finite, so boundary conditions are needed at the beginnings and at the ends of the domain. These boundary conditions need to represent the influence of the outside world and in the other way around. Different kinds of the boundary conditions can be applied for the boundaries. The most common boundary conditions are Dirichlet, Neumann and Robin conditions (Engquist and Majda, 1977). On the physical understanding, a Dirichlet condition usually corresponds to setting the value, a Numann condition usually decides the flux in the boundary and a Robin condition generally represents a radiation condition.
Dirichlet condition provides a function of time $g(t)$, as the constraint on the solution at a specific boundary point $\vec{x_b}$,

$$u(\vec{x_b}, t) = g(t) \tag{2.3}$$

In the case of Neumann condition the flux of u normal to the boundary is specified by a given function $g(t)$ at a boundary point $\vec{x_b}$,

$$\frac{\partial u(\vec{x_b}, t)}{\partial \vec{\eta}} = g(t) \tag{2.4}$$

In which $\vec{\eta}$ is normal to the boundary. If $g(t) = 0$ then it is called an insulated boundary for which U can't have any vector across the boundary. The Robin conditioning is a combination of Dirichlet and Neumann conditions.

$$\alpha u(\vec{x_b}, t) + \beta \frac{\partial u(\vec{x_b}, t)}{\partial \vec{\eta}} = g(t) \tag{2.5}$$

Where α and β may in general depend on the position along the boundary. Boundary conditions can be classified into linear or non-linear and homogeneous or non homogeneous for PDE. The explanation given above is for linear cases.

2.1.4 Fundamental aspects of a numerical scheme

Grid Arrangement

There are two main kinds of grid arrangement. Collocated and staggered are those. In the collocated grid arrangement all variables (vectors and scalars) are defined in the same node of the grid. In the staggered grid arrangement vectors are defined at the cell face

while scalars are defined at the centers of the each cell volume. In the CFD flow simulations staggered grid arrangement is mainly used. Collocated grid arrangement can result in a weak coupling between pressure and velocity for many schemes. But, staggered grid arrangement can leads to higher degree of pressure-velocity coupling. Decoupling between variables can lead to vigorous discretization errors for some schemes (Bernardi and Maday, 1988). It is shown by Morinishi et al. (1998) that uniform Cartesian grid with staggered arrangement can preserve conservation for necessary parameters. But, collocated grid arrangement doesn't have the capability to do so.

For the validity of any numerical scheme three parameters 'stability, convergence and consistency' need necessarily to be satisfied.

Stability

Stability requires that the numerical scheme must remain bounded for amplitude error caused by any perturbation in the numerical solution. Numerical scheme must not diverge for any variable in the domain over the time.

Convergence

Assume domain grid sizes in the space and time are Δt and Δx. Assume a dependent variable C in the discretized domain at the space indice of m and at the time indice of n is called C_n^m in which time length $t = n\Delta t$ & space length $x = m\Delta x$. A numerical scheme is convergent if:$\lim_{\Delta x \to 0, \Delta t \to 0} C_n^m = C(x,t)$.

Consistency

In short consistency is the order of the accuracy of the scheme. If a scheme gets the higher order of consistency then the scheme will show lesser deviation from its real solution. The order of consistency can be generally found with Taylor expansion of the discretized term. To define the order of consistency first the scheme must be convergent. If a scheme is consistent and stable then the scheme is convergent.
$Consistency + Stability = Convergence$

2.1.5 Convection Discretization

Navier-Stokes equation consists of convective term. There are many discretization methods applicable to the convective terms. To get an accurate scheme the Courant conditioning must be satisfied and the stencil must be large enough and the scheme must be convergent (Courant et al., 1952). Stencil is a geometric representation of relation between discrete variables associated with the consecutive time steps at a nodal point. The CFL condition is a necessary condition for the convergence to any linear or nonlinear hyperbolic PDE in finite difference method. This condition was named after the publication by (Courant et al., 1928). This was considered as a very important milestone in the numerical solution of convective PDEs. For a convective equation associated boundary conditions are determined by number of characteristics entering the domain.

Preissmann scheme

A popular scheme for the convection equation is the so called Preissmann scheme or box scheme (Lyn and Goodwin, 1987). This scheme is constructed by applying trapezoidal rule both in time and spatial domains. This is sometimes called compact scheme because even though this schemes holds a small stencil but gives a second order consistency both in time and space domains. Computation in the Preissmann scheme is done explicitly. Discretization in space is shown below:

$$\frac{\partial u^n}{\partial x} = \frac{1}{2}\left\{\frac{(u_{m+1}^{n+1} - u_m^{n+1})}{\Delta x} + \frac{(u_{m+1}^n - u_m^n)}{\Delta x}\right\} \tag{2.6}$$

In which u is the flow speed, Δx represents the spatial discretization in the perpendicular direction of u, n & $n+1$ are time steps, m is the space step.

First order upwind schemes

First order upwind scheme is a one step method proposed by Courant et al. (1952). Convection equation is about characteristic propagation in a certain direction. This upwind scheme can direct the flow information in the direction of the flow propagation because it is sensitive to the flow direction. But this scheme can cause larger numerical diffusion if the gradients are large. Other negative side of this scheme is it has a first order accurate, and this is an implicit scheme thus needs more calculation in a single step. First order upwind discretization in space is shown below:

$$\frac{\partial u_m^n}{\partial x} = \frac{(u_m^n - u_{m-1}^n)}{\Delta x} \tag{2.7}$$

In which U is the flow speed and which is positive in this case; if it is negative then space step has to changed into other-way, Δx represents the spatial discretization in the perpendicular direction of u, n is the time step, m is the space step .

Central Differences

Central differences is a two step scheme. This is scheme has a second order consistency. This scheme needs less number of calculations to be performed in each step compared to first order upwind scheme. And numerical diffusion is less compared to first order upwind scheme. This scheme is conditionally applicable. In case of large gradients and undamped cases this scheme is unconditionally unstable and becomes not usable. Artificial dissipative term needs to be added to make them bounded. Lax-Wendroff scheme is an example for that (Kalita et al., 2002), but this increases the number of calculations to be performed in each step. Central differences space discretization is shown below:

$$\frac{\partial u^n}{\partial x} = \frac{(u_{m+1}^n - u_{m-1}^n)}{2\Delta x} \tag{2.8}$$

In which u is the flow speed , Δx represents the spatial discretization in the perpendicular direction of u, n is the time step, m is the space step.

High-Resolution schemes

High resolution schemes are efficient in avoiding spurious oscillations in the results. Sweby (1984) derived a scheme using a flux limiter in his search for the ultimate conservative difference scheme, and then Roe (1981) utilized flux limiting in his original monotonicity preserving second order scheme. Thereafter Chakravarthy (1983) have used limiters, as Harten (1983) who also introduced the notion of TVD (Total Variation Diminishing) to characterize oscillation free schemes. High resolution schemes work fine in overcoming wiggles which occur as a result of shocks or discontinuities in the spatial domain. Spatial derivatives are kept in the acceptable range of the solution using flux limiters. There are some drawbacks in applying this to higher order shallow water equation.

Weighted Essentially Non-Oscillatory (WENO) Scheme

In this study none of the previously explained scheme is not accurate enough or they are causing considerable amount of numerical errors thus Weighted Essentially Non-Oscillatory (WENO) scheme is used. Fifth order WENO scheme is used in discretizing the convective terms of the Reynolds-Averaged Navier-Stokes equation (RANS) (Jiang and Shu, 1995). Convective term is discretized as follows:

$$u_i \frac{\partial u_i}{\partial x_i} \approx \frac{1}{\Delta x}(\widetilde{u}_{i+1/2} u_{i+1/2} - \widetilde{u}_{i-1/2} u_{i-1/2}) \tag{2.9}$$

Here i stands for the spatial step and u is the flow velocity component in the x direction. $\widetilde{u}$ is the convection velocity which is obtained using the interpolation in the cell face. WENO procedure is used in reconstructing $u_{i+1/2}$ in the cell face $i + 1/2$.

$$U^{\pm}_{i+1/2} = \omega^{\pm}_1 U^{1\pm}_{i+1/2} + \omega^{\pm}_2 U^{2\pm}_{i+1/2} + \omega^{\pm}_3 U^{3\pm}_{i+1/2} \tag{2.10}$$

Upwind direction is indicated by $\pm$ sign, U^1, U^2 and U^3 represents three ENO stencils. Weight factors ω_1, ω_2 and ω_3 are determined for each ENO stencil and calculated explicitly based on the smoothness indicators(Jiang and Shu, 1995). Accuracy of the WENO scheme ranges from third to fifth order. Large smoothness indicators indicate a non-smooth solution in the ENO stencil. So largest weight of ω_n is assigned for the WENO schemes with smooth solution. WENO schemes can handle steep gradients without smearing unlike high resolution schemes till the shock. So convective terms in the RANS equation can be discretized with WENO scheme.

2.1.6 Time Discretization

Wave kinematics are highly sensitive to the discretized time scale of the numerical scheme because of the non-steady oscillatory nature of the waves. Time integration is necessary in the treatment of momentum and level-set equations. A third order accurate explicit TVD (Total Variance Diminishing) Runge-Kutta scheme is used in REEF3D which consists of three Eularian steps (Shu and Osher, 1988).

$$\begin{aligned} \phi^1 &= \phi^n + \Delta t L(\phi^n) \\ \phi^2 &= \frac{3}{4}\phi^n + \frac{1}{4}\phi^1 + \frac{1}{4}\Delta t L(\phi^1) \\ \phi^{n+1} &= \frac{1}{3}\phi^n + \frac{2}{3}\phi^2 + \frac{2}{3}\Delta t L(\phi^2) \end{aligned} \tag{2.11}$$

This scheme diminishes spurious oscillations by suppressing the local extrema (Harten et al., 1987). TVD properties express good numerical stability for the CFL values lesser than one.

2.1.7 Adaptive Time stepping

Primary purpose of the adaptive time stepping is to control the CFL number in order to avoid the exploding of the numerical scheme. Flow velocity (u), diffusion and other source terms (S) such as gravity (g) and water depth (h) are the control variables of the CFL number (Griebel et al., 1997). So adaptive time step size (Δt) is a function of these control variables as shown in the equation as follows:

$$\Delta t \leq 2 \left(\left(\frac{|u|_{max}}{dx} + D \right) + \sqrt{\left(\frac{|u|_{max}}{dx} + D \right)^2 + \frac{4\,|S_{max}|}{dx}} \right)^{-1} \tag{2.12}$$

D represents the contribution due to diffusion term. which is defined as follows:

$$D = max\,(\nu + \nu_t) \left(\frac{2}{(dx)^2} + \frac{2}{(dy)^2} + \frac{2}{(dz)^2} \right) \tag{2.13}$$

In which ν is kinematic viscosity, ν_t turbulent viscosity; dx, dy and dz are the magnitudes of the spatial discretization units. The diffusion part of the RANS equation is treated implicitly in the current numerical model thus it is being removed from the CFL criterion. The third order accurate TVD Runge-Kutta scheme is used for all transport equations except turbulence model in REEF3D.

2.1.8 Turbulence Modeling and RANS

All the aspects of a sea state is turbulent dominant with some exceptions. Acceleration and declaration nature of wave induced orbital motions and wave structure interaction give more rise to this turbulent nature. Turbulent flow vectors are uncertain in the time domain but they couldn't be explained by stochastic parameters. Turbulent induces efficient mixing and vortex shedding. This is a three dimensional and rotational phenomenon. Turbulent flows are dissipative which dissipate energy through the process of vortex shedding. Larger eddies transfer energy to smaller ones and finally they are dissipated as heat; this process is called energy cascading. Continuity of the energy is supplied by the mean flow. Molecules get exchanged between multiple flow layers with different speeds resulting in Reynold stresses. These stresses create momentum to rotate flow layers results in vorticity. All these turbulent nature has to be modeled in-order to study wave-structure interaction. To do so Navier-Stokes equation has to be solved and all the flow details must be represented to the smaller lengthy scales of the numerical solution. Direct Numerical Simulation (DNS) is usable for smaller Reynolds number and for the larger once this is not

so efficient because of its demanding for a higher number of grid points (Moser et al., 1999).

Reynolds-Average Navier-Stokes (RANS) equation approach is a feasible one. Sub-grid scale model is used to model small scale turbulence. This RANS approach is feasible with large scale turbulence processes because of the averaging philosophy (Menter, 1994). RANS equation with time averaging follows below:

$$\frac{\partial u_i}{\partial t} + u_j \frac{\partial u_i}{\partial x_j} = -\frac{1}{\rho}\frac{\partial p}{\partial x_i} + \frac{\partial}{\partial x_j}\left[(\nu + \nu_t)\left(\frac{\partial u_i}{\partial x_j} + \frac{\partial u_j}{\partial x_i}\right)\right] + g_i \tag{2.14}$$

In which u is the time averaged velocity, ρ is the density of the fluid, p is pressure, ν is the kinematic viscosity, ν_t is the eddy viscosity or it is called as viscosity by turbulent, g is the acceleration due to gravity. The eddy viscosity (ν_t) is calculated using $k-\omega$ model. In the current REEF3D model $k-\omega$ model proposed by Wilcox (1994) is being used combined with RANS model, and this is a two equation model based on the energy balance equations. This model is a balance between the turbulent kinetic energy (k) transported and the other one is the turbulent dissipation ω. So eddy viscosity or turbulent viscosity is being calculated as follows:

$$\frac{\partial k}{\partial t} + U_j \frac{\partial k}{\partial x_j} = \frac{\partial}{\partial x_j}\left[\left(\nu + \frac{\nu_t}{\sigma_k}\right)\frac{\partial k}{\partial x_j}\right] + P_k - \beta_k k\omega \tag{2.15}$$

$$\frac{\partial \omega}{\partial t} + U_j \frac{\partial \omega}{\partial x_j} = \frac{\partial}{\partial x_j}\left[\left(\nu + \frac{\nu_t}{\sigma_\omega}\right)\frac{\partial \omega}{\partial x_j}\right] + \frac{\omega}{k}\alpha P_k - \beta\omega^2 \tag{2.16}$$

$$\nu_t = min\left(\frac{k}{\omega}, \sqrt{\frac{2}{3}}\frac{k}{|S|}\right) \tag{2.17}$$

In which P_k is the production rate, $\sigma_k = 2, \sigma_w = 2, \alpha = 5/9, \beta_k = 0.09$ and $\beta = 0.075$ are closure coefficients. $|S|$ is the mean strain rate, k is the turbulent kinetic energy, ω is the turbulent dissipation. S can be large in case of oscillatory flow motion. The turbulent eddy viscosity ν_t is controlled by the equation 2.17 to avoid excess turbulence beyond the boundary layer in a highly strained flow (Durbin, 2009). On the vicinity of the free surface turbulence length scales have to be constrained which leads to increased turbulent dissipation. Turbulent fluctuations (eddies) perpendicular to the free surface are damped and they are redistributed parallel to the interface. But the RANS model doesn't catch these phenomenon well in-case of a two phase flow. Standard RANS over-predicts the maximum turbulence intensity at the free surface because mean strain rate (S) could be larger in the water air interface proximity. So an explicit additional turbulence damping scheme is necessary to achieve the free surface effect on the turbulence (Naot and Rodi, 1982).

$$\omega_s = \frac{c_\mu^{-\frac{1}{4}}}{\kappa} k^{\frac{1}{2}} \cdot \left(\frac{1}{y'} + \frac{1}{y^*}\right) \tag{2.18}$$

In which $c_\mu = 0.07$ and $k = 0.4$ are constants. $y^{'}$ stands for the turbulent length scale and it is being empirically proved to be $0.07\bar{h}$ by Hossain and Rodi (1980) in which $\bar{h}$ is the mean water depth. The transition between wall boundary value (ω) to free surface value is smoothed by an additional distance of y^* from the wall. The term for the specific

turbulent dissipation (ω_s) is activated around the interface Dirac delta function $\delta(\phi)$ as follows:

$$\delta(\phi) = \begin{cases} \frac{1}{2\epsilon}\left(1 + \cos\left(\frac{\pi\phi}{\epsilon}\right)\right) & if \ \ |\phi| < \epsilon \\ 0 & else \end{cases} \tag{2.19}$$

The fluid is assumed to be incompressible in this case. Chorin's projection method (Chorin, 1968) with staggered grid is used to model the pressure gradient in the RANS equation. Staggered grid arrangement is preferred over collocated grid arrangement as explained in Sec.2.1.4 to ensure a velocity-pressure coupling. Pressure gradient is explicitly treated and freed from momentum equation. Intermediate velocity u_i^* is updated after each adaptive time stepping. Thereafter the divergence of the intermediate velocity field calculation leads to the Poisson equation of the pressure gradient as follows:

$$\frac{\partial}{\partial x_i}\left(\frac{1}{\rho(\phi^n)}\frac{\partial P}{\partial x_i}\right) = -\frac{1}{\Delta t}\frac{\partial U_i^*}{\partial x_i} \tag{2.20}$$

Fully parallelized Jacobi-preconditioned BiCGStab algorithm is used to solve Poisson equation (Van der Vorst, 1992). Flow velocity is then corrected in the new time step from the old once by using the updated pressure gradient as follows:

$$u_i^{n+1} = u_i^* - \frac{t}{\rho(\phi^n)}\frac{\partial p}{\partial x_i} \tag{2.21}$$

2.2 Numerical Wave Tank

Numerical wave tank is used generally in Computational Fluid Dynamics (CFD) to study the propagation of waves, wave kinematics and forces. The results from numerical wave tank have to be validated experimentally for each wave phenomenon such as regular waves, irregular breaking waves, breaking waves, focused waves, wave-structure interaction, and many more. After validation the results from Numerical wave tank could be used in similar engineering application as a viable information source. Advanced computing capabilities with super computers have increased the demand for more sophisticated numerical wave tank models. There are many approaches used in setting-up the numerical wave tank. RANS with VOF, RANS with the LSM method and RANS with Potential theory are some of the approaches.

RANS with Volume of Fluid (VOF) approach is used in Open-FOAM CFD model. Finite volume method is used in the spatial discretization of this method (Choi and Yoon, 2009). RANS with LSM is used in the current study. In this approach wave tank is implemented with domain discretization method and Level Set Method (LSM) is used to capture the free surface (Yang and Stern, 2009). RANS and Potential theory combination is not yet well-developed so far.

2.2.1 Free Surface Capturing

Zero level set of the smooth signed distance function $\phi(\vec{x}, t)$ is used to seperate the interface between water and air in the spatial domain (Osher and Sethian, 1988). This conditional function distinguishes two mediums using the change in the sign.

$$\phi(\vec{x},t)\begin{cases} > 0 & if\ \vec{x}\ is\ in\ phase\ 1 \\ = 0 & if\ \vec{x}\ is\ at\ the\ interface(\Gamma) \\ < 0 & if\ \vec{x}\ is\ in\ phase\ 2 \end{cases} \tag{2.22}$$

Furthermore, the Eikonal equation $|\Delta\phi| = 1$ is satisfied. Following convection equation is used for the level set function if the the free surface (Γ) is dynamic due to forcing velocity field $\vec{u}$.

$$\frac{\partial\phi}{\partial t} + \vec{u}\nabla\phi = 0 \tag{2.23}$$

Hamilton-Jacobi version of the WENO scheme is used to solve this convection equation 2.23 as explained in Sec.2.1.5. Discretization in the time domain is done using third order Runge-Kutta scheme as explained in Sec.2.1.6. Distance value of the level-set function changes according to the dynamic evolution of the interface. After each time step level set function re-initializes for the purpose of mass conservation and to conserve level-set property. Numerical instability may occur due to the abrupt changes in the physical properties at the interface. Smoothening is done using Heaviside function $H(\phi)$.

$$\begin{aligned} \rho(\phi) &= \rho_1 H(\phi) + \rho_2(1 - H(\phi)) \\ \nu(\phi) &= \nu_1 H(\phi) + \nu_2(1 - H(\phi)) \end{aligned} \tag{2.24}$$

In which,

$$H(\phi) = \begin{cases} 0 & if\ \phi < -\epsilon \\ \frac{1}{2}\left(1 + \frac{\phi}{\epsilon} + \frac{1}{\pi}sin\left(\frac{\pi\phi}{\epsilon}\right)\right) & if\ |\phi| \leq \epsilon \\ 1 & if\ \phi > \epsilon \end{cases} \tag{2.25}$$

Densities of the two mediums are represented by ρ_1 and ρ_2. The interface thickness between ϵ is taken as 2.1 times grid size for the operation of the smoothening (Chella et al., 2016).The level set function in the cell-interface is calculated using simple interpolation (Croce et al., 2010). Density at the cell interface is calculated using modified single step approach with smoothed Heaviside function as follows:

$$\rho_{i+\frac{1}{2}} = \rho_1 H\left(\phi_{i+\frac{1}{2}}\right) + \rho_2\left(1 - H\left(\phi_{i+\frac{1}{2}}\right)\right), \tag{2.26}$$

Averaging of level set function:

$$\phi_{i+\frac{1}{2}} = \frac{1}{2}\left(\phi_i + \phi_{i+1}\right) \tag{2.27}$$

2.2.2 Wave generation and Absorption

At the one end, waves are generated with relaxation method and the other end waves are absorbed completely to avoid any reflection and standing waves in the numerical wave tank. Dirichlet boundary conditioning at the generation side is generally a choice for channel flows (Kim et al., 1987). Wave kinematics are oscillatory type, so a Dirichlet

boundary conditioning for wave generation is not a better choice. Relaxation method is used in REEF3D to generate waves (Mayer et al. (1998), Jacobsen et al. (2012)). In this method, waves are generated without any interferences to the free surface. In the numerical beach (wave absorption zone) relaxation method damps out velocity field smoothly and completely thus there is no reflection back to the domain of interest. Also in the numerical beach, pressure is damped reduced to the hydrostatic pressure caused by the still water level. The other good thing about relaxation method is that if any reflected wave travels back to the generation zone will be absorbed.

$$\begin{aligned} u(\widetilde{x})_{relaxed} &= \Gamma(\widetilde{x})u_{analytical} + (1-\Gamma(\widetilde{x}))u_{computational} \\ w(\widetilde{x})_{relaxed} &= \Gamma(\widetilde{x})w_{analytical} + (1-\Gamma(\widetilde{x}))w_{computational} \\ p(\widetilde{x})_{relaxed} &= \Gamma(\widetilde{x})p_{analytical} + (1-\Gamma(\widetilde{x}))p_{computational} \\ \phi(\widetilde{x})_{relaxed} &= \Gamma(\widetilde{x})\phi_{analytical} + (1-\Gamma(\widetilde{x}))\phi_{computational} \end{aligned} \tag{2.28}$$

The transformation from analytical to computational is gradual because the function $\Gamma(\widetilde{x})$ changes gradually depending on the zone. At the beginning (generation zone) analytical values of the velocity field and free surface are used to initiate the numerical computation. In the beach zone, the transformation of the values again takes place from the computational to the analytical values such that they become zero at the beach.

$$\Gamma(\widetilde{x}) = 1 - \frac{e^{(\widetilde{x}^{3.5})} - 1}{e - 1} \; for \; \widetilde{x} \in [0; 1] \tag{2.29}$$

The coordinate $\widetilde{x}$ is scaled to the length of the relaxation zone. The wave generation zone has about one length and wave dissipation zone is about two wave lengths.

Chapter 3

Focused Waves

Focused wave generation and the the theory behind first and second order wave component is explained in this chapter.

3.1 Focused Wave Generation

Wave generation and numerical beach boundary conditions are explained in the previous chapter. Simulation time and numerical wave tank spatial domain is set to be large enough to capture a focused wave group kinematics and its interaction with a vertical cylinder without much boundary effects.In this study relaxation method is used in the wave generation from the one end of the tank and in the absorption at the numerical beach in the other end. Focused waves are created by superimposing the regular linear wave components using the irregular wave groups generated in the wave tank. Wave group is directed to get focused at an intended location and time by tuning the initial phase angle of each component. Amplitudes of each wave component in a wave group is defined by the wave spectral parameters and number of waves in the group. Free surface elevation at a point in the spatial domain represents the preselected wave spectrum. In the present study JONSWAP spectrum is used to generate irregular waves.

Focused wave amplitude at the focus point is calculated upon spectral parameters. focused wave amplitude can be calculated using linear super positioning each wave amplitude and the spectrum:

$$A_f = A_i \frac{\sum_{i=1}^{N} S_i(\omega)\Delta\omega_i}{S_i(\omega)\Delta\omega_i} \tag{3.1}$$

In which A_f is the focused wave amplitude, A_i is the wave amplitude of the i^{th} wave component, $S(\omega)$ is the wave spectrum and $\Delta\omega_i$ is the corresponding angular frequency interval of the component. If the resulting wave steepness is higher; then the 2^{nd} order kinematic components become significant over the 1^{st} order kinematic components so that both have to be summed. Resulting particle velocity components (u, w) and free surface elevation (η) are calculated as shown below:

$$\eta = \eta^{(1)} + \eta^{(2)} \tag{3.2}$$

$$u = u^{(1)} + u^{(2)} \tag{3.3}$$

$$w = w^{(1)} + w^{(2)} \tag{3.4}$$

In which $\eta^{(1)}$, $u^{(1)}$, and $w^{(1)}$ are the first order kinematic components. $\eta^{(2)}$, $u^{(2)}$, and $w^{(2)}$ are the second order kinematic components. Analytical calculation of these components are explained in the upcoming section.

3.2 First and Second order Focused Waves

Linear wave theory and irregular wave theory (Krogstad and Arntsen, 2000) are not going to be discussed in detail here. Irregular surface elevation and other kinematics can be easily decomposed in case of a first order wave theory. So the first order wave theory can be written as a combination of N linear components.

$$\eta^{(1)} = \sum_{i=1}^{N} A_i \cos(k_i(x - x_0) - \omega_i(t - t_0) + \epsilon_i) \tag{3.5}$$

$$v^{(1)} = \sum_{i=1}^{N} A_i \frac{g A_i k_i}{\omega_i} \frac{\cosh\left[k_i(z+h)\right]}{\cosh\left[k_i h\right]} \cos(k_i(x - x_0) - \omega_i(t - t_0) + \epsilon_i) \tag{3.6}$$

In which g is acceleration of gravity, A is amplitude of the wave component, k is wave number, ω is angular frequency, z is height of the point of interest from the free surface, h is water depth, x horizontal distance to the point of interest, x_0 is the location of initialization, t is the time of interest, t_0 time of initialization, ϵ is the phase angle of the component.

The second order kinematics explained by Schäffer (1996) is used in the high steep wave cases to compare with the experimental focused wave cases (Sharma et al. 1981, Forristall 2000 and Dalzell 1999). Second order components of surface elevation ($\eta^{(2)}$) and the particle velocity in the wave propagation direction ($u^{(2)}$) are defined as follows according to Schäffer (1996) .

$$\begin{aligned}\eta^{(2)} = \sum_{i=1}^{N} \sum_{j>1} \Big\{ & A_i A_j H^{+} \cos[(k_i + k_j)(x - x_0) - (\omega_i + \omega_j)(t - t_0) + (\epsilon_i + \epsilon_j)] \\ & + A_i A_j H^{-} \cos[(k_i - k_j)(x - x_0) - (\omega_i - \omega j)(t - t_0) + (\epsilon_i - \epsilon_j)] \Big\} \\ & + \sum_{i=1}^{\infty} A_i^2 H^{+} \cos\{2(k_i(x - x_0) - \omega_i(t - t_0) + \epsilon_i)\}\end{aligned} \tag{3.7}$$

and

$$
\begin{aligned}
v^{(2)} = \sum_{i=1}^{N}\sum_{j>1}\Bigg\{ & (k_i+k_j)A_iA_j\frac{G^+(\omega_i,\omega_j)}{D^+(\omega_i,\omega_j)}\frac{\cosh[(k_i+k_j)(z+h)]}{\cosh[(k_i+k_j)h]} \\
& \times\cos[(k_i+k_j)(x-x_0)-(\omega_i+\omega_j)(t-t_0)+(\epsilon_i+\epsilon_j)] \\
& +(k_i-k_j)A_iA_j\frac{G^-(\omega_i,\omega_j)}{D^-(\omega_i,\omega_j)}\frac{\cosh[(k_i-k_j)(z+h)]}{\cosh[(k_i-k_j)h]} \\
& \times\cos[(k_i-k_j)(x-x_0)-(\omega_i-\omega j)(t-t_0)+(\epsilon_i-\epsilon_j)]\Bigg\} \\
& +\sum_{i=1}^{\infty}\Bigg\{k_iA_i^2\frac{G^+(\omega_i,\omega_j)}{D^+(\omega_i,\omega_j)}\frac{\cosh[2k_i(z+h)]}{\cosh[2k_ih]} \\
& \times\cos[2(k_i(x-x_0)-\omega_i(t-t_0)+\epsilon_i)]\Bigg\}
\end{aligned}
\tag{3.8}
$$

In which;

$$
D^{\pm}(\omega_i,\omega_j) = g(k_i\pm k_j)\tanh\{(k_i\pm k_j)h-(\omega_i\pm\omega_j)^2\} \tag{3.9}
$$

$$
\begin{aligned}
G^{\pm}(\omega_i,\omega_j) = -g^2\Bigg[& \frac{k_ik_j}{\omega_i\omega_j}(\omega_i\pm\omega_j)(1\mp\tanh(k_ih)\tanh(k_jh)) \\
& +\left(\frac{k_i^2}{2\omega_i\cosh^2(k_ih)}\pm\frac{k_j^2}{2\omega_j\cosh^2(k_jh)}\right)\Bigg]
\end{aligned}
\tag{3.10}
$$

$$
H^{\pm} = \frac{(\omega_i\pm\omega_j)}{g}\frac{G^{\pm}}{D^{\pm}}+F^{\pm} \tag{3.11}
$$

$$
F^{\pm} = -\frac{g}{2}\frac{k_ik_j}{\omega_i\omega_j}\frac{\cosh^2[(k_i\mp k_j)h]}{\cosh(k_ih)\cosh(k_jh)}+\frac{1}{2}(k_i\tanh(k_ih)+k_j\tanh(k_jh)) \tag{3.12}
$$

First and second order numerical results for steep wave cases are compared with the experimental results in chapter-04.

3.3 Wave Spectrum and FFT

JONSWAP spectrum is used in the present study to generate irregular wave groups. Irregular waves in a fully developed sea state is describe by Pierson-Moskowitz (PM) spectrum (Pierson and Moskowitz, 1964). This spectrum is validated with the North Atlantic sea state under unlimited fetch length with the fully developed local wind. But JONSWAP spectrum is developed for partially developed sea state. Actually PM spectrum is modified to JONSWAP spectrum with empirical adjustments. The inputs to the standard

wave spectrum are significant wave height (H_s), peak wave period (T_p) and the number of wave components (N).

$$S_{PM}(\omega) = \frac{5}{16} H_s^2 \omega_p^4 \omega^{-5} \exp\left\{\frac{-5}{4}(\frac{\omega}{\omega_p})^{-4}\right\} \tag{3.13}$$

$$\omega_p = \frac{2\pi}{T_p} \tag{3.14}$$

In which ω_p is the peak angular frequency of the spectrum and the range of the angular frequency is covered by ω. JONSWAP spectrum is defined as below from the PM spectrum:

$$S_{JW}(\omega) = S_{PM}(\omega) A_\gamma \gamma^{\exp\left\{-0.5\left[\frac{\omega-\omega_p}{\sigma\omega_p}\right]^2\right\}} \tag{3.15}$$

$$A_\gamma = 1 - 0.287 ln(\gamma) \tag{3.16}$$

In which $S_{PM}(\omega)$ is PM spectrum, γ is a dimensionless peak shape factor and its value is taken as 3.3 here, A_γ is the normalizing factor and σ is called as the spectral width parameter with the conditioning of the independent variable ω .
$\sigma = 0.07$; when $\omega < \omega_p$
$\sigma = 0.09$; when $\omega > \omega_p$

Angular frequency integral segment $d\omega$ is defined as follows:

$$d\omega = \frac{\omega_s - \omega_e}{N} \tag{3.17}$$

ω_e and ω_s are the upper and lower limits of angular frequency range.

Fast Fourier Transformation is the easier way with lesser computation to convert free surface elevation into spectrum. FFT is an algorithm to carry out Discrete Fourier Transformation. Refer Aggarwal (2015) for the detailed explanation on how FFT works. A predefined Matlab function '*pwelch* is used to transform discrete free surface elevation data into energy spectrum.

3.4 Wave Forces

In the numerical model wave forces on the cylinder are calculated by integrating the normal component of the viscous stress tensor τ over the surface Ω of the structural surface exposed to wave action. In a numerical model continuous integration is not possible thus the force vector is calculated from each grid point and cell face and then summed. Simplified integral function to calculate the total force is shown in the equation 3.18.

$$F = \int_\Omega (-np + n\tau) d\Omega \tag{3.18}$$

In which p pressure, τ is the viscous stress tensor and n is the unit normal vector to the surface which is in the outward direction to the body. Pressure component contains both hydrostatic and hydrodynamic terms.

Chapter 4

Focused Wave Kinematics

4.1 Introduction

It is essential to investigate the kinematics of the steep wave at the focus point to understand its nature. Parameters that are being correlated with each kinematic aspect needs to be defined. Focused wave amplitude at the focus point, temporal and spatial evolution and propagation of the wave group, geometrical aspects of the focused wave such as horizontal-vertical asymmetries, wave crest front, wave crest rear steepness and second and first order wave kinematic component are investigated. Simulation cases are defined in upcoming sections according to the choice of investigation. Results of numerical simulations are validated with available focused wave experimental results. Grid refinement study has to be done to find the largest possible validated grid size before begin the focused wave kinematic investigation cases.

4.2 Grid Refinement Studies

For a good convergence of the numerical scheme with experimental results, the grid sizes must be smaller as possible. But, the lower limit of the grid sizes are bounded by the time limit of the simulation. It is always efficient to pick the larger grid size which has a good agreement with experimental results. This study is called grid refinement study or convergence study. In the present study of convergence, second order wave theory of Schäffer (1996) has been used. For this study numerical wave tank is simulated in the two dimensional domain without wall and turbulence effects. Tank length of $15m$ and the simulation time of $20s$ are chosen. Grid sizes of $0.01m$, $0.015m$, $0.02m$, $0.025m$ and $0.035m$ are simulated to compare the wave surface elevation at the focus point with theoretical surface elevation. Later, experimental results of Ning et al. (2009) is discussed to find the appropriate grid size. Incident wave characteristics are set to focus at 7.5m from the generation side of the numerical wave tank at 10^{th} second of the simulation. In all these cases, JONSWAP spectrum is used with 20 waves to be focused with spectral parameters of significant wave height $0.04m$ and peak period of $1.25s$.

Fig.4.1 shows free surface elevation from the wave gauge at the focus point against the simulation time for all different grid sizes chosen. It clearly shows that the theoret-

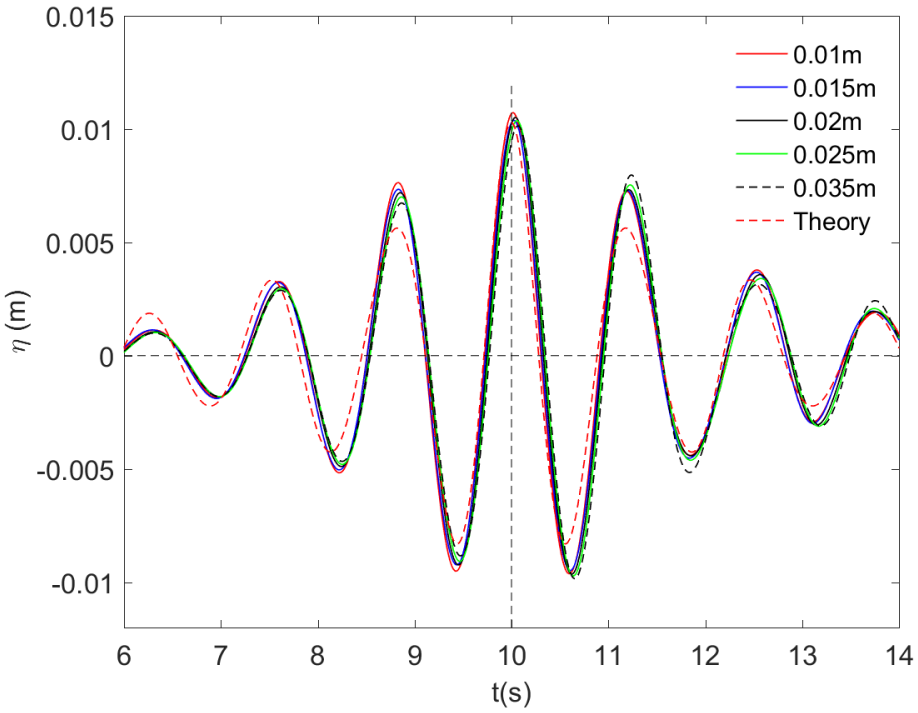

Figure 4.1: Free surface elevation (η) at the focus point of 7.5m for the different grid sizes chosen. ($H_s = 0.04m$, $N = 20$, JW spectrum, T_p=1.25s)

ical solution and the numerical results are in good agreement. The deviation from the numerical solution in this grid size range is not much significant compare to the order of the wave height.Numerical surface elevation exhibits some degree of deviation from the theory before and after the focus point. But, at the focus point and at the focus time this deviation diminishes sharply. The intended focus time in the numerical simulation is $10th$ second of the simulation, but it looks like there are some delays in the focus resulting greater focus times than 10 seconds. Assume numerical wave speed is $U^{'}$, theoretical wave speed is U, length both waves traveled before focus is L, Time taken to reach the focus point for the numerical wave is $t^{'}$ and time taken to reach the focus point for theoretical wave is t. Relative phase error (ϕ) is defined for a numerical scheme as the relative ratio between the wave speeds (Gresho et al., 1984).

$$\phi = \frac{U'}{U} - 1 = \frac{L/t^{'}}{L/t} - 1 = \frac{t}{t^{'}} - 1 \tag{4.1}$$

Actual focused times (t_f) and relative phase change (ϕ) for different grid sizes (dx) is plotted in Fig.4.2.

Fig.4.2(a) shows how the real focused time changes for different computational grid size choices while Fig.4.2(b) shows the relative phase change for different grid sizes chosen. From these plots it is obvious that the numerical focus is delayed and furthermore the delay is influenced by the grid size. The plot shows a trend of increasing negative phase change with increasing grid size. The delay in focusing is in the order of $0.01s$ which is small compared to the intended time of focus of 10 second.

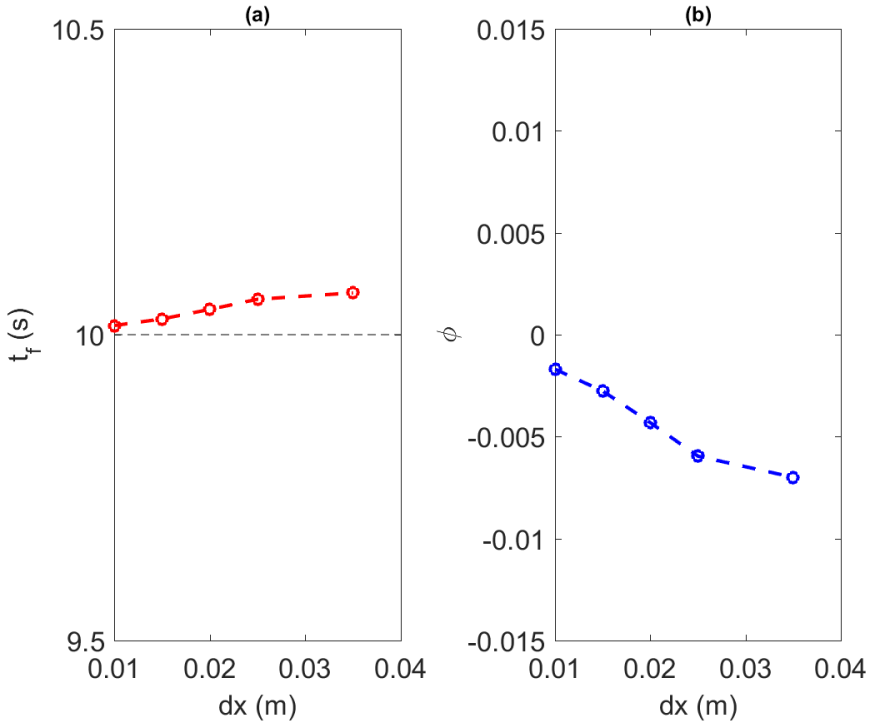

Figure 4.2: (a) focus time (t_f) and (b) relative phase change (ϕ) against grid sizes (dx). ($H_s = 0.04m$, $N = 20$, JW spectrum, T_p=1.25s)

Relative amplitude change (r) is defined as the relative ratio between the theoretical and numerical focus amplitudes at the focus point. Assume numerical focused wave height at the focus point is $A_f^{'}$, theoretical focused wave height is A_f.

$$r = \frac{A_f^{'}}{A_f} - 1 \tag{4.2}$$

Fig.4.3 shows relative amplitude change (r) plotted against different grid sizes chosen (dx). Relative amplitude change (r) holds both positive and negative values. According to this plot there is not any plane relationship between relative amplitude changes and varying grid sizes chosen. But there is clearly an influence and a milder decreasing trend in the focus amplitude. The order of amplitude changes are in the millimeter. So it can be concluded that different grid sizes in the spatial domain doesn't much influence the outcomes of the numerical focused wave amplitude at the focus point and the time of focus.

According to the input incident wave parameters in the numerical model, the waves have to focus at 7.5m (x_f) at 10th second (t_f) of the simulation. So the highest surface elevation in the whole domain must occur at the focus point (x_f) and at the focus time (t_p) theoretically. In order to check this aspect, the highest surface elevation in the whole domain out of time constraints is taken and it is compared with the peak surface elevation at the focus point for all different grid sizes. The highest surface elevation in the spatial and temporal domain is calculated by considering the maximum surface elevation for each time frame in 0.5 second interval. The peak surface elevation in the whole temporal and spatial domain (A_p) can be found by compiling and interpolating all those maximum

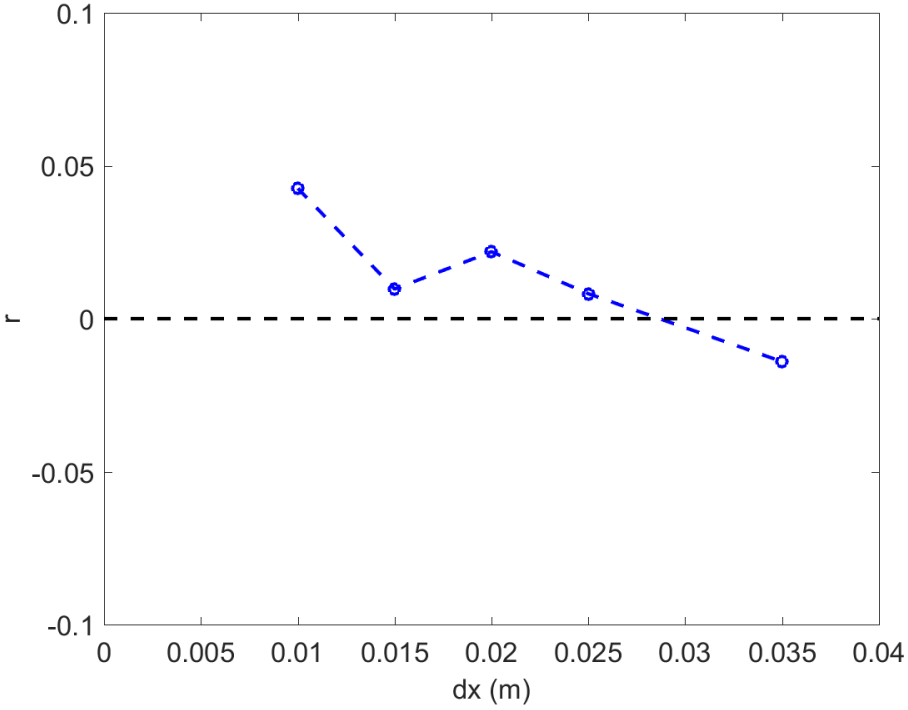

Figure 4.3: Relative focus amplitude change (r) at x_f for different grid sizes (dx). (Hs=0.04m, N=20, JW spectrum, Tp=1.25s)

values.

Highest amplitude in the domain (A_p) and focused wave height ($A_f^{'}$) are plotted for different grid sizes in Fig.4.4(a) and the magnitude different between A_p and $A_f^{'}$ is plotted in Fig.4.4(b). It is clear that the magnitude difference between A_p and $A_f^{'}$ lines increases with coarser grid sizes according to Fig.4.4(b). Another fact is that A_p is highly correlated to the $A_f^{'}$, because both lines follow the same pattern as shown in Fig4.4(a). After 0.025m of dx this difference in magnitude increases dramatically. But, this magnitude difference is in the $4th$ decimal order; so this parameter is not much influential in the selection of the grid size.
As a conclusive remark it can be stated that choices between 0.01m and 0.025m do not show-up any abrupt deviations from the theoretical solution. Relative phase and amplitude changes are also not much significant. Considering the simulation time of 0.025m could be an appropriate choice and this can be validated with the experimental results of Ning et al. (2009).

Ning et al. (2009) carried out experiments in a 69m long and 3m wide wave flume. Focus point (x_f) was 11.4m away from the wave generating paddle. A wave gauge was installed at this focus point to measure the free surface elevation. This experimental data is used in this grid refinement study to ensure the validity of the grid size of 0.025m. Ning et al. (2009) recorded four different experimental cases from the wave gauge as shown in Table 4.1. In the numerical model, a two dimensional wave tank with 15m length with the water depth of 0.5m is chosen. Focus point (x_f) is set at 7.5m from the wave gener-

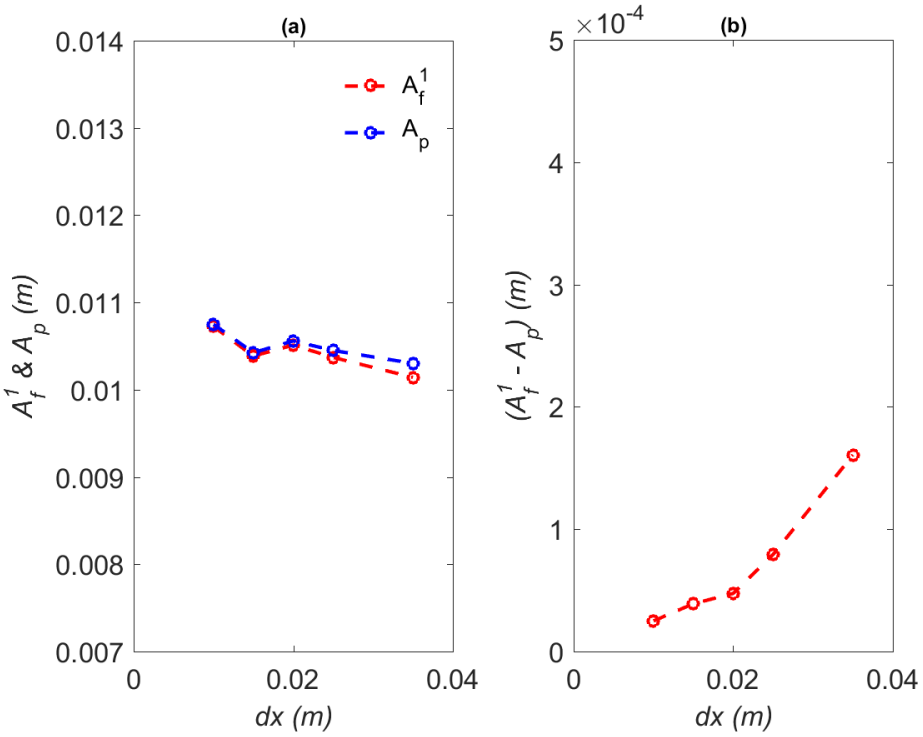

Figure 4.4: (a)A_p and $A_f^{'}$ Vs dx is plotted and (b) (A_p - $A_f^{'}$) Vs dx. ($H_s = 0.04m$, $N = 20$, JW spectrum, T_p=1.25s)

ation zone. Wave generation and dissipation zones are far enough from the focus point to avoid any influence from boundary effects. The real wave flume size is inefficient in the numerical model due to simulation time constraints thus this two dimensional wave tank is taken into consideration. Simulation time is 20s with the focusing time (t_f) of 10s. Schäffer's second order theory is used in the numerical simulation to capture second order components too, so that the numerical error could be narrow-down to convergence.

Case	$T_p(s)$	$A_f^{'}(m)$	$x_f(m)$	$h_s(m)$	$t_f(s)$
A1	1.20	0.0313	7.5	0.120	10.0
A2	1.20	0.0632	7.5	0.242	10.0
A3	1.25	0.0875	7.5	0.350	10.0
A4	1.25	0.1031	7.5	0.412	10.0

Table 4.1: Ning experimental cases and corresponding numerical cases.

Table 4.1 cases 01 and 02 are having lesser steepness than cases 03 and 04. Cases 01 and 03 are already validated by Bihs et al. (2016) for the grid size of 0.025m. Cases 02 and 04 are validated here with the experimental results by Ning et al. (2009).

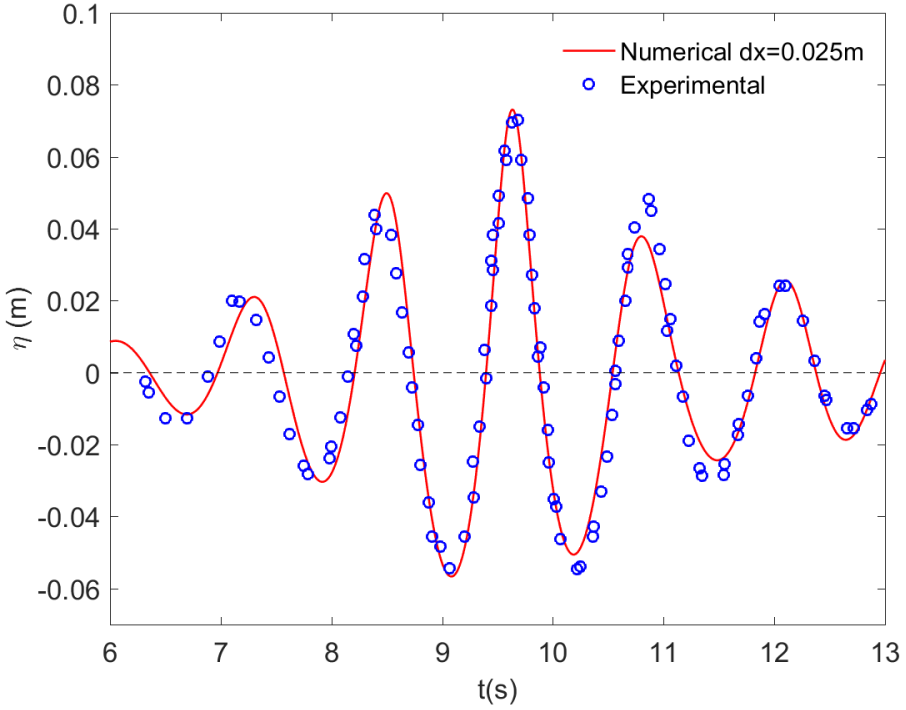

Figure 4.5: Numerical and experimental free surface elevation (η) at x_f against t for case $A2$ (Table 4.1). ($N = 20$, JW spectrum)

Fig.4.5 represents the comparison of simulated numerical results with the experimental data by Ning et al. (2009) for free surface elevation at focus point. It is clear that the numerical model captures the surface elevation of a focused wave group with enough accuracy for the grid size of $0.025m$ in the low steepness wave groups. Milder deviation is visible before and after the time of focus (t_f). But at the time of focus this milder deviation diminishes. Focused wave amplitude and the geometrical aspects of the focused waves are in good agreement.

Fig.4.6 shows the experimental and numerical free surface elevation of high steep case $A4$ at the focus point over the simulation time. Clearly they are in good agreement except some of the milder deviation at the beginning of the wave group. These variations could be a result of the experimental wave generation paddle as it generates a wave group with differing amplitudes instead of a wave group with the same amplitude. Anyhow there isn't any deviations at the focusing time of 10second. Numerical model predicts pretty well with the higher steep case $A4$ because second order wave theory is used here. As a conclusion it is found to be the numerical results converge with the experimental results at dx of 0.025m. So grid size of 0.025m can be used as a good choice for the study of focuses waves.

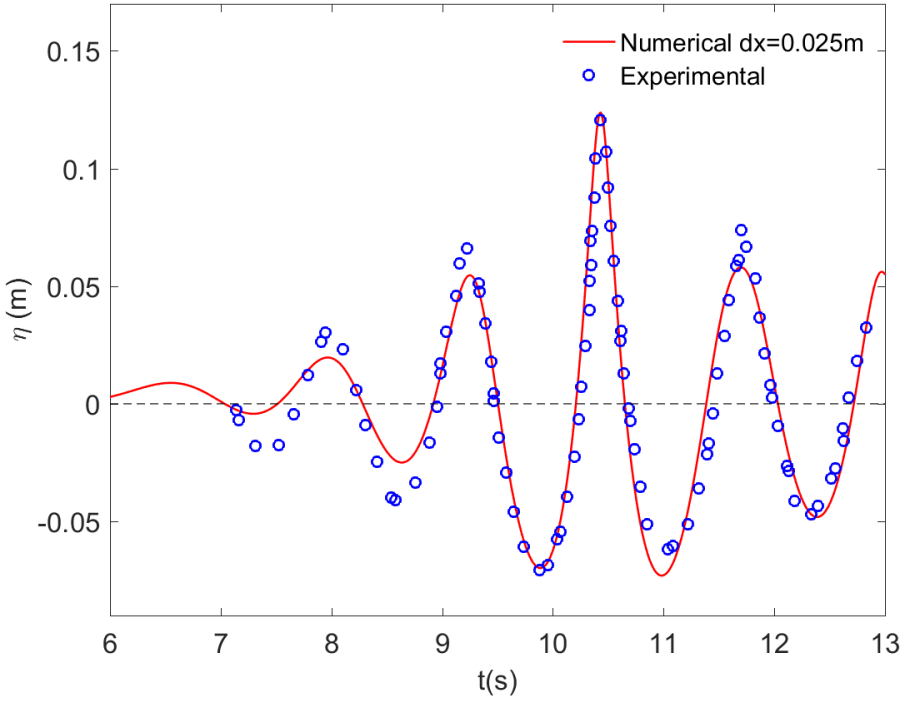

Figure 4.6: Numerical and experimental free surface elevation (η) at x_f against t for case $A4$ (Table 4.1). ($N = 20$, JW spectrum)

4.3 Influence of the number of waves

The choice of number of waves in a wave group must give an expected energy spectrum. Energy spectrum of the focused wave group in the domain could be investigated by changing the number of wave components (N) in the wave group. Three different steepness categories are taken into consideration for the investigation. Four different N values are chosen for each steepness category resulting in 12 different simulation cases as referred in Table 4.2. Other control variables are kept constant for all these 12 simulation cases. JONSWAP spectrum with $\gamma = 3.3$ is taken with spatial grid size $dx = 0.025$m. Relaxation method is used in wave generation and in numerical beach. Schäffer's second order theory is used for focused wave generation.

Fig.4.7 shows free surface elevation (η) at the focused point with the simulation time (t) for three different steepness categories. First category with the cases $B1, B2, B3$ and $B4$ holds the spectral steepness of 0.0164 shown in Fig.4.7(a). According to this Fig 4.7(a) focused wave amplitude is equal in all first four cases despite the changes in the number of wave components in the wave group. So focused wave amplitude is not being influenced by the number of wave components in the spectral representation. But there is a small difference in the surface elevation after $t = 13s$ in the case $B1$ ($N = 10$) where the low amplitude wave components which comes at the end have larger amplitudes than for cases $B2, B3$ and $B4$.

Case	$H_s(m)$	$T_p(s)$	N	S_p
B1	0.04	1.25	10	0.01640
B2	0.04	1.25	20	0.01640
B3	0.04	1.25	30	0.01640
B4	0.04	1.25	40	0.01640
B5	0.12	1.25	10	0.04920
B6	0.12	1.25	20	0.04920
B7	0.12	1.25	30	0.04920
B8	0.12	1.25	40	0.04920
B9	0.04	2.00	10	0.00641
B10	0.04	2.00	20	0.00641
B11	0.04	2.00	30	0.00641
B12	0.04	2.00	40	0.00641

Table 4.2: Numerical cases to study the influence of the number of waves on the focused wave generation.

This kinematic nature doesn't change for the spectral steepness 0.0492 at Fig.4.7(b). In Fig.4.7(c) for the cases $B9, B10, B11$ and $B12$ with the spectral steepness of 0.00641 smaller wave amplitude components deviate both at the end and at the beginning of the wave group for $N = 10$. In all three steepness categories $N = 20, 30$ and 40 gives the same results over the time domain but $N = 10$ shows deviation from other wave numbers.

Fig.4.8 shows the free surface elevation(η) at $t_p = 10$s along the numerical wave tank (spatial domain). Simulation cases with $N = 10$ clearly shows deviation in wave surface elevation in the wave generation zone for both high steepness cases in Figs.4.8(a) and (b). But a slight difference in free surface elevation near the dissipation zone is observed for cases $B9, B10, B11$ and $B12$ in Fig.4.8(c). Energy spectrum can explain which wave energy components are changing in the cases with $N = 10$.

Fig.4.9 shows the energy spectrum at the focus point for the first four cases with $H_s = 0.04$m, $T_p = 1.25$s and with differing N values. The energy spectrum for $N = 10$ differing from other cases as expected according to the Figs 4.8 and 4.7. All the wave number values give peak energy spectrum (S_{max}) at the peak frequency (f_p) of $0.8Hz$ which is correct ($f_p = \frac{1}{T_p} = \frac{1}{1.25} = 0.8Hz$). But the S_{max} magnitude shows a higher value than other three cases. Spectral distribution lies between $0.5Hz$ and $1.5Hz$ for all the

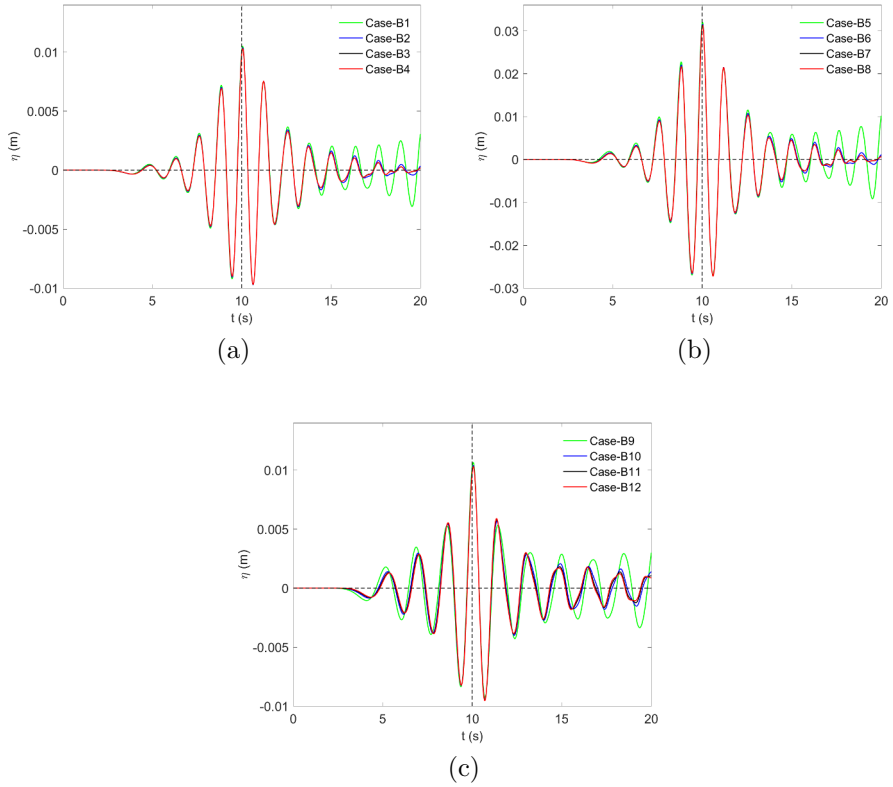

Figure 4.7: Free surface elevation (η) at $x_f = 7.5m$ against time (t) for all cases

cases. Spectral curves for $N = 20, 30$ and 40 overlaps on each other while the case with $N = 10$ doesn't show a smooth fit with other spectral curves. But a higher number of waves must approach the expected JONSWAP spectrum thus the cases with $N = 10$ do not have enough wave components in the wave group to resemble the expected energy spectrum.

Fig.4.10 shows the energy spectrum (S) for the cases $B5, B6, B7$ and $B8$ with $H_s =$ 0.12m and $T_p = 1.25$s. Maximum spectral energy increased from the order of 10^{-5} in Fig.4.9 to the order of 10^{-4} in Fig.4.9. This is due to the increase in the significant wave height from $H_s = 0.04$m to $H_s = 0.012$m, but $f_p = 0.8Hz$ remained unchanged for this case as before because of its unchanged T_p value. Case $B5$ with N=10 gives an increased spectral peak energy than other cases. The smoothness of the curve of $N = 10$ also doesn't fit with other spectral curves between the frequencies of $0.8Hz$ to $1.2Hz$. So the increased wave amplitude at the end of the wave group for the cases $B1$ and $B5$ according to the Figs.4.7 and 4.8 corresponding to the frequency of $0.8Hz$ with the wave periods of $1.25s$; because that is the only significant difference in the spectral curves.

Fig.4.11 shows the energy spectrum for the cases $B9, B10, B11$ and $B12$ with $H_s =$ $0.04m$ and $T_p = 2.00$s. The whole spectrum is shifted to the left compared to the earlier cases because spectral peak period is increased to $2.00s$. Spectral amplitude values remain the same with Fig.4.9 because $H_s = 0.04m$ for both categories. Maximum spectral energy (S_{max}) increases for the case with $N = 10$.

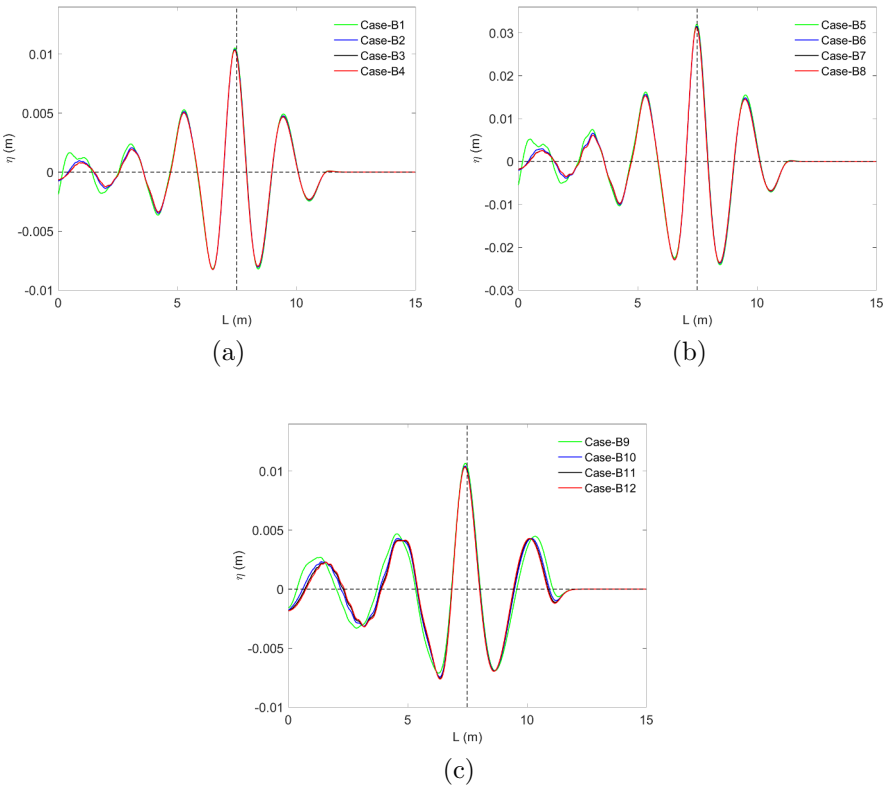

Figure 4.8: Free surface elevation (η) at $t_p = 10s$ along wave tank length (L) for all cases

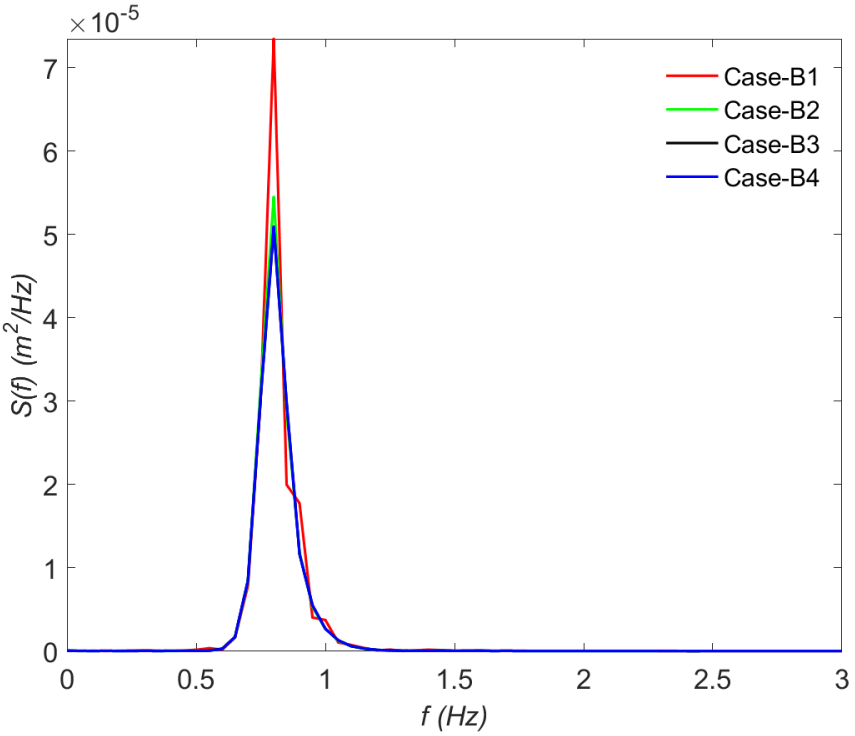

Figure 4.9: Energy Spectrum (S(f)) at focus point for cases $B1, B2, B3$ and $B4$

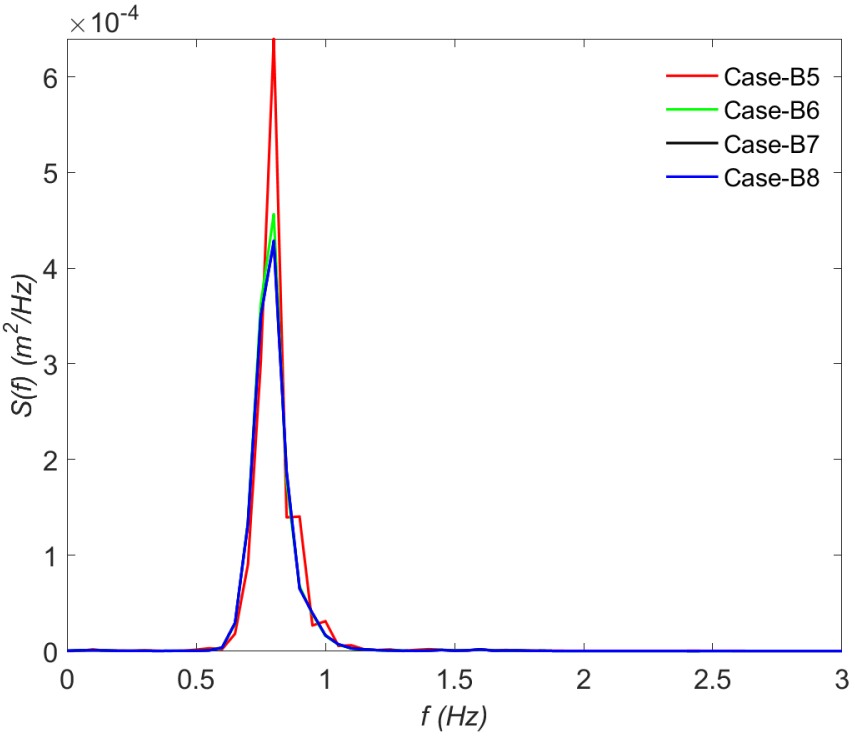

Figure 4.10: Energy Spectrum (S(f)) at focus point for cases $B5, B6, B7$ and $B8$

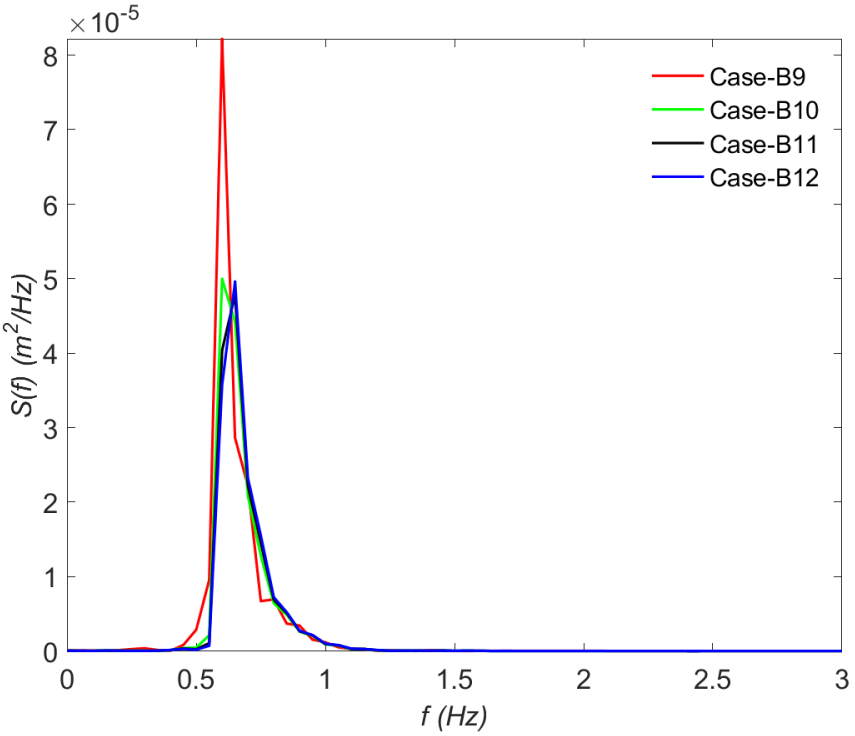

Figure 4.11: Energy Spectrum (S(f)) at focus point for cases $B9, B10, B11$ and $B12$

There is a milder shift in the magnitude of f_p between $N = 20$ and $N = 30$. Except these smaller changes N=20, 30 and 40 are in a good agreement.

As a conclusion the case with $N = 10$ does not have a good enough number waves to represent a smooth JONSWAP spectrum with predefined control parameters. But the number of incident wave components greater than 20 ($N \geq 20$) gives a good agreement with the spectral shape. In all the previous cases kinematic study is done with $N = 20$, thus they are valid upon spectral constraints.

4.4 Steepness study of focused waves

It is very essential to investigate the kinematic parameters which can be influenced by the steepness of the focused wave group. focused wave amplitude at the focus point, wave steepness at the focus point, spatial and temporal evolution of the focused wave group, geometrical aspects such as vertical and horizontal asymmetries, wave crest front and rear steepness, wave length, peak and trough of the wave, relative phase and amplitude changes are the aspects of a focused wave investigated in this with differing steepness of the wave. To do so nine different wave cases are taken into consideration. Different steepness is achieved by changing the significant wave height (H_s) and the peak period (T_p) of the spectrum. Standard JONSWAP spectrum is used with 20 waves to get focused at the focus point of $7.5m$ from the one end which is in the middle of the wave tank. In all these cases second order Schaäffer theory is used. Simulation time is $20s$ and intended focus time (t_f) is 10^{th} second. All of the study in this section is done with the two dimensional wave tank with the water depth of $0.5m$ as shown in the Fig.4.12.

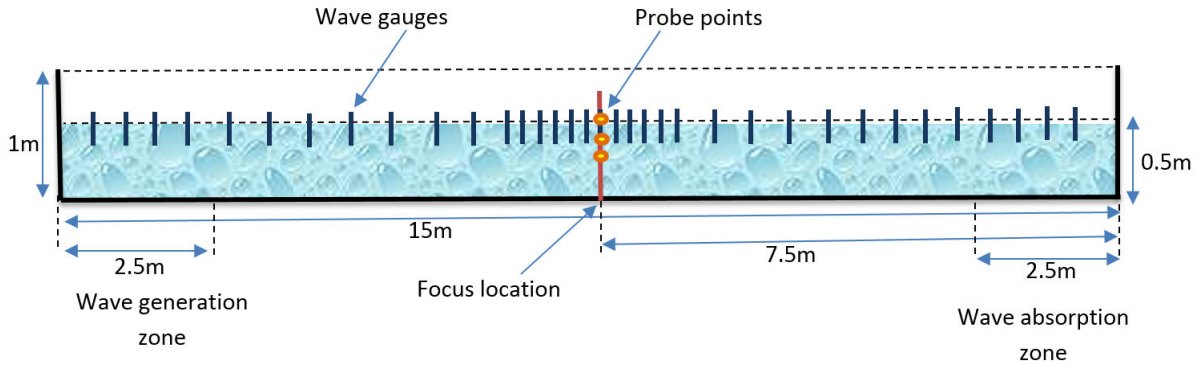

Figure 4.12: Schematized section of the numerical wave tank for the steepness investigation.

As shown in Fig.4.12 intended focus point (x_f) is in the middle of the tank to avoid boundary effects. Incident wave steepness has to be defined to correlate the influence on the kinematics of the focused wave. But incident wave characteristics are controlled by spectral parameters. So steepness of the incident wave must be a function of the spectral parameters. Steepness (S_p) based on the peak period of the spectrum (T_p) and significant wave height (H_s) is defined as below (Forristall, 2000). This can be called as spectral steepness.

$$S_p = \frac{2\pi}{g}\frac{H_s}{T_p^2} \tag{4.3}$$

This parameter is widely used to correlate spectral steepness to the wave kinematics. Higher spectral steepness will result in components with higher wave amplitudes in a group thus higher focused wave amplitudes.

4.4.1 Effect of Spectral steepness on Focused wave Kinematics

Case	$H_s(m)$	$T_p(s)$	$S_p \times 10^{-3}$
C1	0.02	1.25	8.17
C2	0.04	1.25	16.40
C3	0.08	1.25	32.86
C4	0.12	1.25	49.20
C5	0.16	1.25	65.60
C6	0.04	1.00	25.64
C7	0.04	1.50	11.37
C8	0.04	1.75	8.36
C9	0.04	2.00	6.41

Table 4.3: Numerical cases to study influence of the steepness in focused wave groups.

In the first five cases steepness of the incident wave is changed by altering the significant wave height (H_s). In the last four cases, steepness is changed by changing the peak period (T_p) of the spectrum. Higher spectral peak periods increase the wave length of each wave components due to dispersion relation. Case-$C2$ being kept as the base case. Cases $C1, C3, C4, C5$ are formed by changing the significant wave heights from the base case thus steepness changes. Cases $C6, C7, C8, C9$ are formed by changing the wave period from the base case thus steepness changes.

Fig.4.13 shows the free surface elevation from the wave gauge at the focus point for the wave cases $C1, C2, C3, C4$ and $C5$. It is obvious that none of the wave is breaking at the focus point. Each wave group got focused at the 10^{th} second of the simulation as predicted. It can be assumed that the numerical scheme captures the surface elevation well, because all the steepness of the cases are lesser than the steepness of the experimental case-$A4$ thus non-linearity of the steep waves are captured well with Schäffer's second order wave theory. Another important fact is that the free surface elevation crosses the mean water level exactly at the same time for each cases, because peak period (T_p) is equal in all the five cases so wave length is same for all cases. In all these cases waves are focused in the crest but not in the trough as intended.

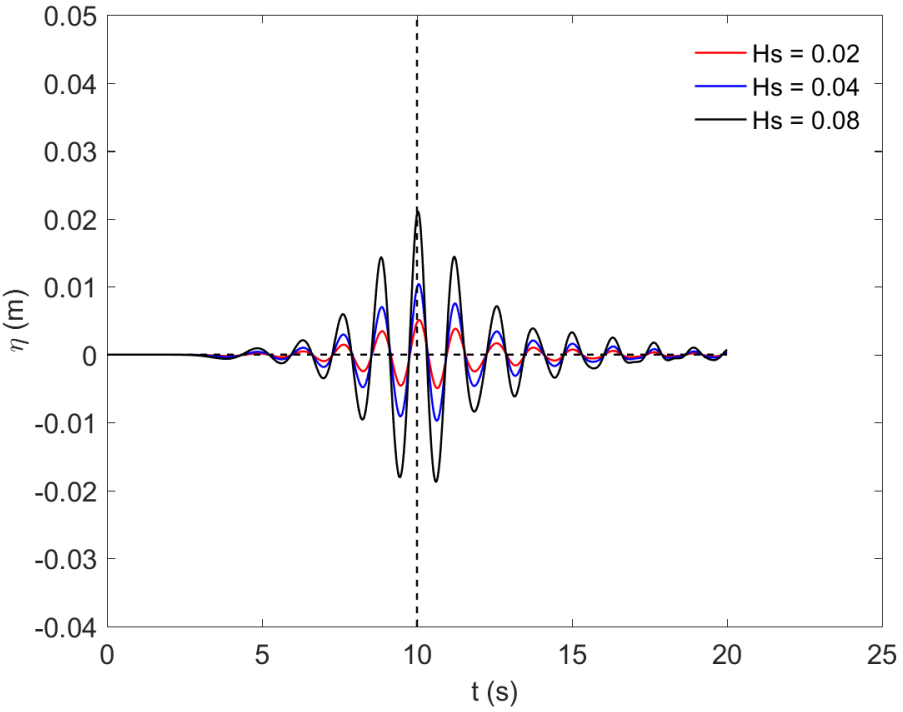

(a)

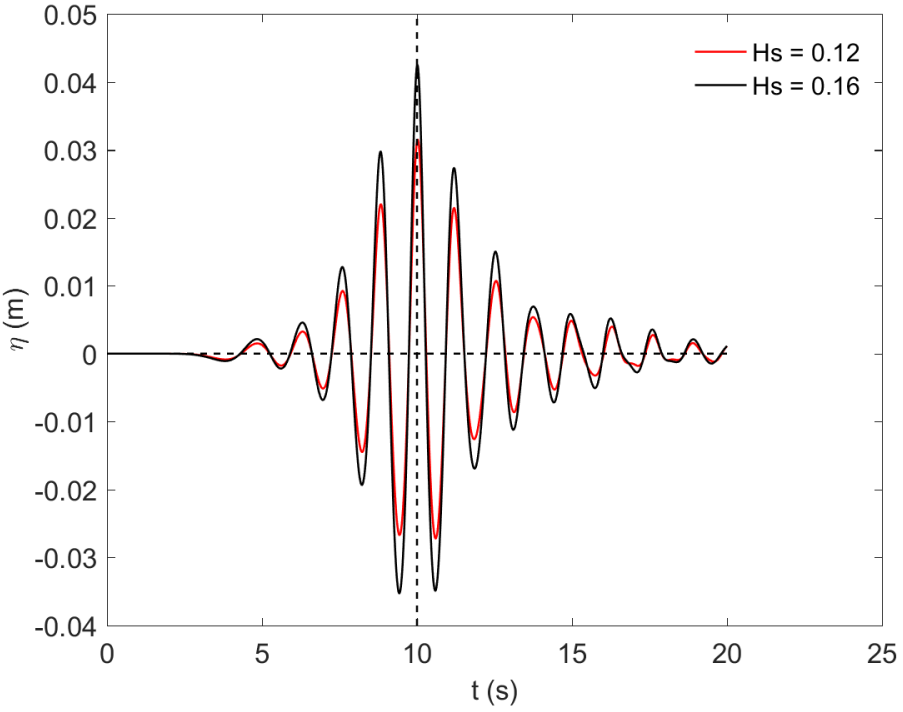

(b)

Figure 4.13: Free Surface elevation (η) at the focus point for cases $C1, C2, C3, C4$ and $C5$.

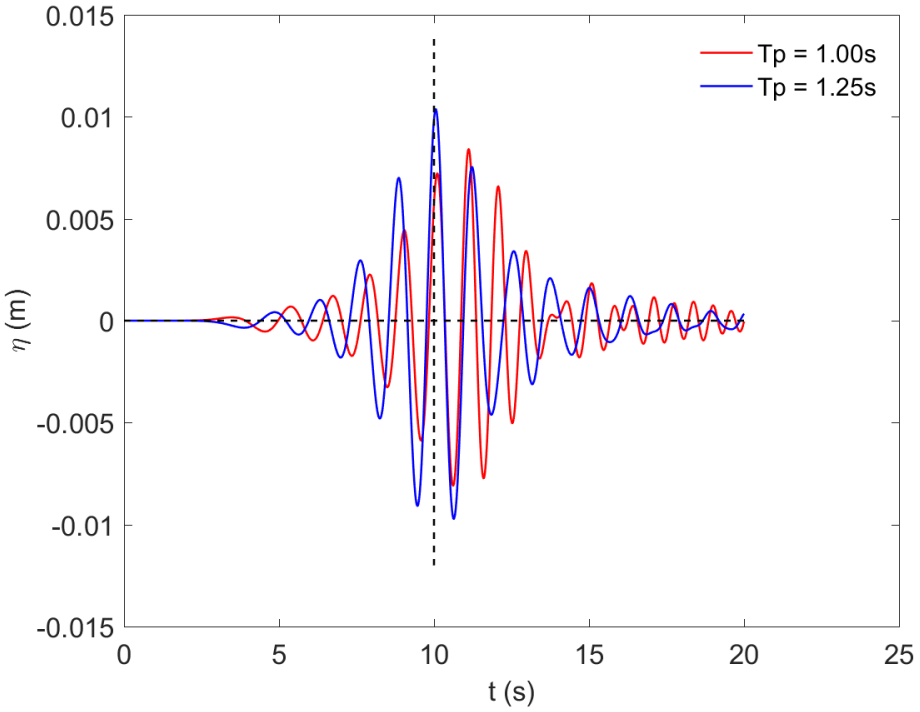

(a)

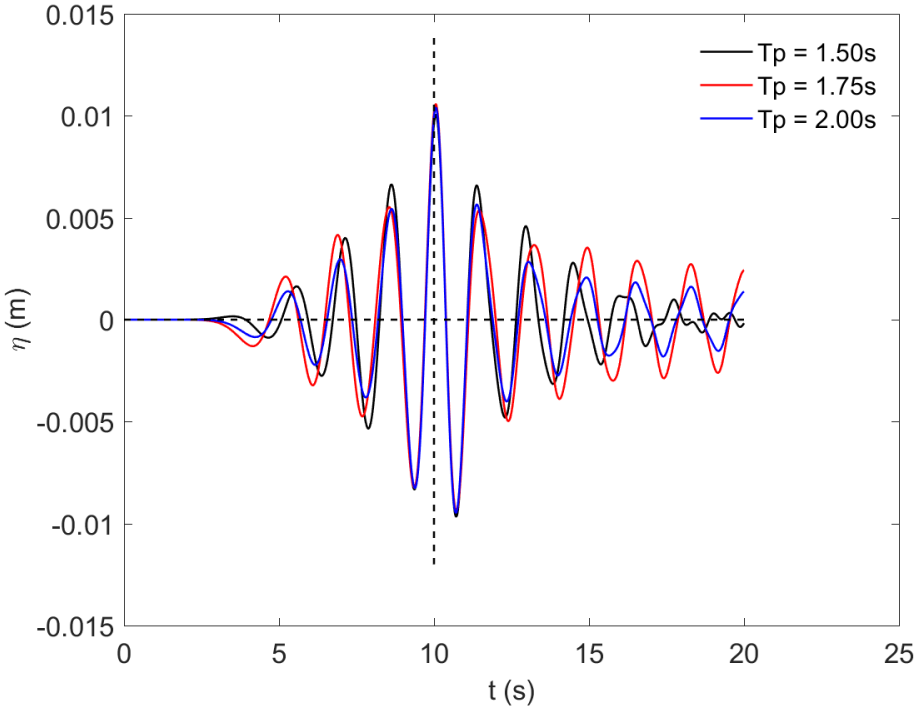

(b)

Figure 4.14: Free Surface elevation (η) at the focus point for cases $C2, C6, C7, C8$ and $C9$.

Fig.4.14 shows the surface elevation (η) at the focus point of the wave group for the wave cases $C2, C6, C7, C8$ and $C9$. Base case $C2$ is again included in this comparison because it serves for $T_p = 1.25s$. These Figs.4.14(a) and (b) look a bit messy but there are no breaking waves in these cases too. The reason is in all these cases surface elevation crosses mean water level in different time intervals due to differing peak periods. But all the wave groups arrange themselves to get focused around 10^{th} second except case-$C6$. Case-$C6$ gives a higher focused wave amplitude ($A_F^{'}$) after 12^{th} second of the simulation. But spectral steepness of the incident wave group for case-$C6$ is not higher than that of cases-$C3, C4$ and $C5$. Hence the non-linear effects caused by the higher steepness are not the reason. The reason is due to small peak period of 1s which is not a common ocean wind wave case (Hasselmann et al., 1973). So in the upcoming investigations case-$C6$ shouldn't be considered in the kinematic study.

4.4.2 Focused wave height ($A_f^{'}$)

Wave height and other kinematic parameters of a wave group at the focusing location can be calculated as explained in Chapter 03. Focusing wave height ($A_f^{'}$) is positively correlated to the significant wave height (H_s) of the spectrum. This can be checked with cases $C1, C2, C3, C4$ and $C5$.

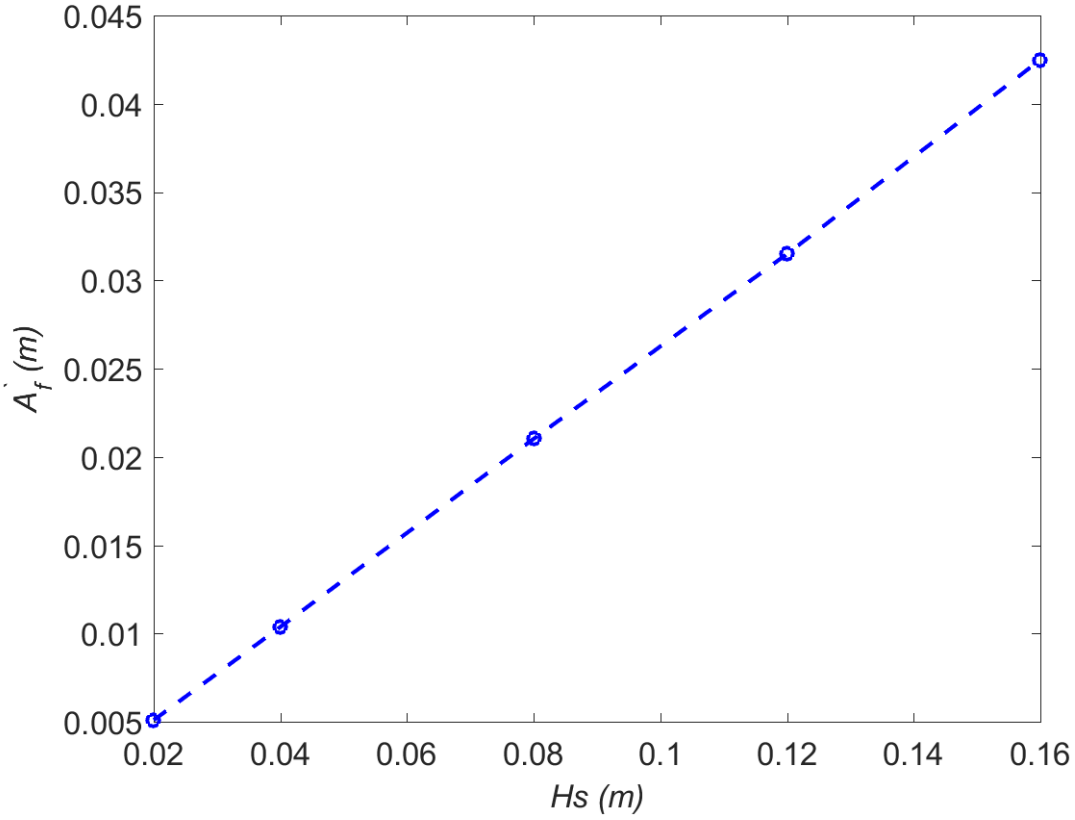

Figure 4.15: Focusing wave height ($A_f^{'}$) at the focus location ($x_f = 7.5m$) versus H_s

Fig.4.15 shows focused wave amplitude ($A_f^{'}$) for cases $C1, C2, C3, C4$ and $C5$ against

the significant wave height (H_s) of the cases. It is clear that the relationship is linear between these two parameters under the constrain of equal T_p and the relation stands $H_s \approx 4A_f^{'}$. For the non-breaking cases, this can be used as a viable relationship to calculate the focused wave height using JONSWAP spectrum in REEF3D. Second order components in Schäffer's wave theory for surface elevation as expressed in the equation 3.7 has a function of angular frequency (ω). Therefore second order component of the surface elevation (η^2) could be influenced by the the peak period (T_p) of the spectrum. So focused wave amplitude ($A_f^{'}$) could be influenced by the the peak period (T_p) for the high steep cases where second order components are significant.

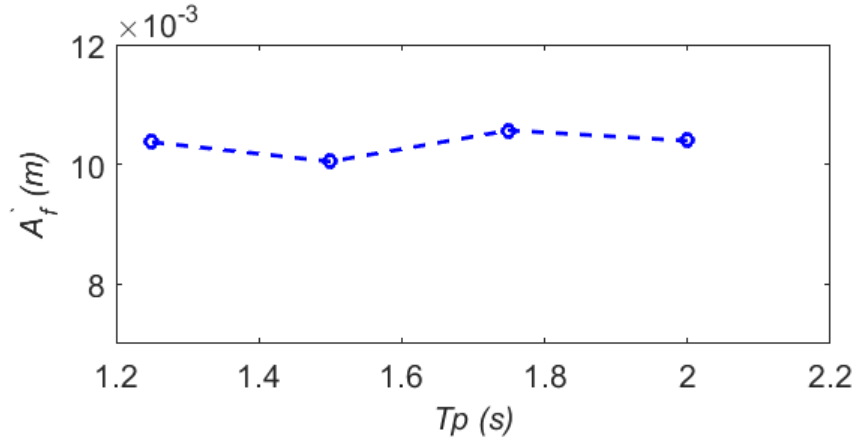

Figure 4.16: Focusing wave height ($A_f^{'}$) at the focus location ($x_f = 7.5m$) versus T_p

Fig.4.16 shows the focused wave amplitude ($A_f^{'}$) plotted against varying peak period (T_p) while significant wave height ($H_S = 0.04m$) is being kept constant. According to this Fig.4.16 there is not much changes in the amplitude of the focused wave at the focusing point corresponding to the spectral peak period. Here H_s is $0.04m$ and the spectral steepness changes from 0.00641 to 0.01640 which may be not enough to make the second order effects more significant on the free surface thus the amplitudes remain unchanged. To increase the steepness further T_p couldn't be reduced further because wave grouping at focused point doesn't occur as expected and explained in Sec.4.4.1. But H_s could be increased and all the simulation for differing T_p could be performed and investigated further. So any changes in the focused wave amplitude ($A_f^{'}$) is only correlated to the single parameter of the spectrum which is the significant wave height of the incident wave group for steepness cases lesser than 0.01640.

4.4.3 Wave group in the numerical tank

In the previous section, focused wave kinematics are discussed in the time domain. Surface elevation in the numerical wave tank at a specific time gives the physical appearance of how a focused wave generated and absorbed (dissipated) at the numerical beach in the spatial domain.

Fig.4.17 is plotted for surface elevation (η) over the wave tank length (L) at the time of focus ($t_f = 10s$) for cases $C1, C2, C3, C4$ and $C5$. Wave generation and wave dissipation

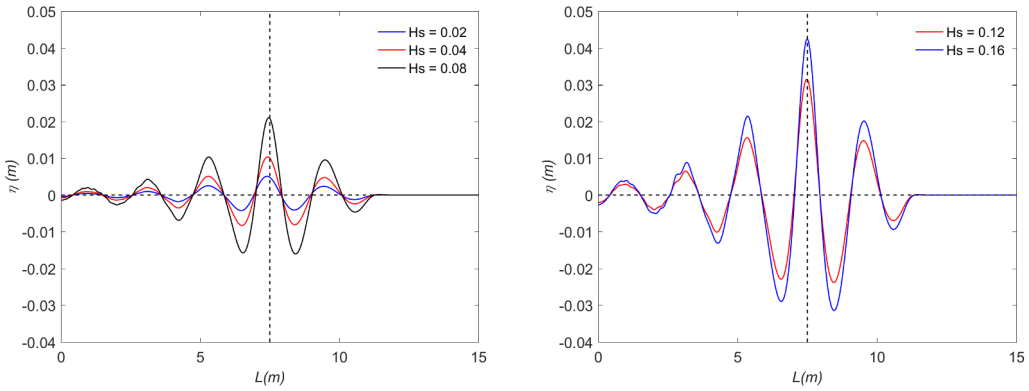

(a) (b)

Figure 4.17: Free surface elevation (η) in the wave tank (L) at the time of focus $t_f = 10$ second for the cases $C1, C2, C3, C4$ and $C5$

zones of the wave tanks are identifiable from its free surface elevations. Dissipation of the waves at the numerical beach begins exactly at the same location despite the differences in the significant wave height (H_s) thus relaxation method damps out waves properly. In the wave generation zone, wave group is generated with differing wave amplitude components. Some wiggles are visible on the free surface in the generation zone but the wiggles are damped because they are not observed in Fig.4.13. Furthermore wavelength of each wave component is equal because they cross the mean still water level at same location. In Fig.4.17(a) there is a milder delay in focusing is visible because the peak amplitude still didn't reach the intended focus point of 7.5m. Any how this delay disappears for cases $C4$ and $C5$ in Fig.4.17(b).

Fig.4.18 is plotted for case $C5$ and the free surface elevation (η) is captured in a second interval over the domain length (L) to see the propagation of the wave component which get focused at the 10^{th} second (t_f) of the simulation. The intended focus location ($x_f = 7.5m$) is marked with the vertical dashed black line. The wave component which get focused released from the wave generation zone at $t = 6s$. At the time of release the wave amplitude of the component is not larger than the other wave components in the domain. But as the time goes the wave component gains amplitude and propagates in the spatial domain. Wave component's amplitude reaches a peak value at $t = 10s$ and $x = 7.5m$, which is the intended focus time(t_f) and location (x_f) of the wave group. Furthermore after $t = 10s$ amplitude of the focused wave component starts to decrease because of the super positioning of the other wave in the wave group starts to deviate. The wave component which get focused completely vanishes in the wave dissipation zone at $t = 14s$.

Fig.4.20 shows the free surface elevation (η) over the numerical wave tank length (L) at the focus time ($t_f = 10s$) for the wave cases $C2, C7, C8$ and $C9$. All these simulation cases have the same significant wave height (H_s) but differing T_p. Therefore each wave group shows different wave lengths and different propagation speeds. In Fig.4.20(a) and (b) free surface elevation amplitudes don't coincide in the horizontal axis except the focus location (x_f). In Fig.4.20(b) amplitudes of the different wave components also changes except the focusing component. In both Figs.fig:914(a) and (b) wiggles (not breaking)

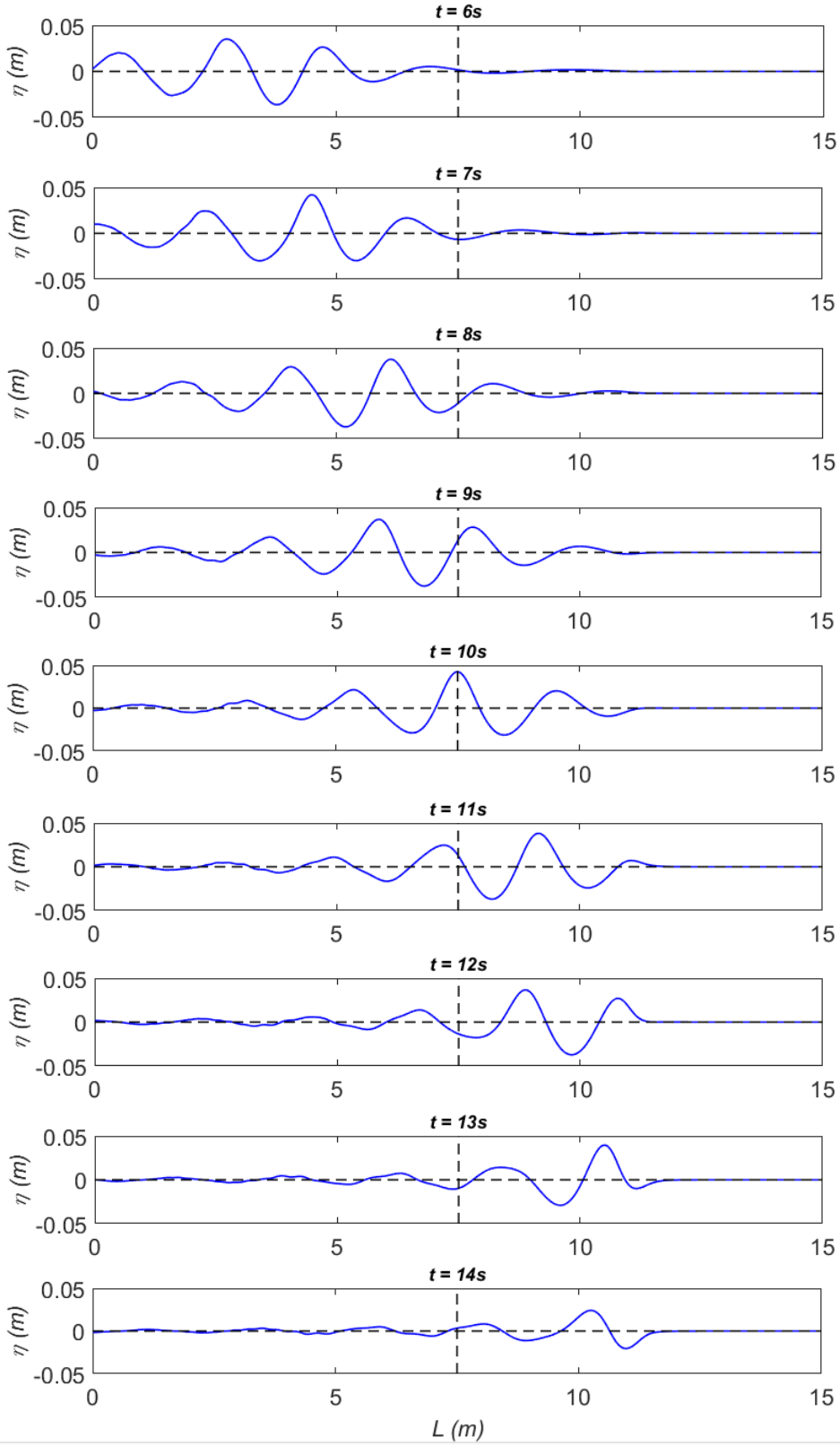

Figure 4.18: Propagation of the focusing wave group for case-C5. Free surface elevation (η) is captured in a second interval in the domain (L)

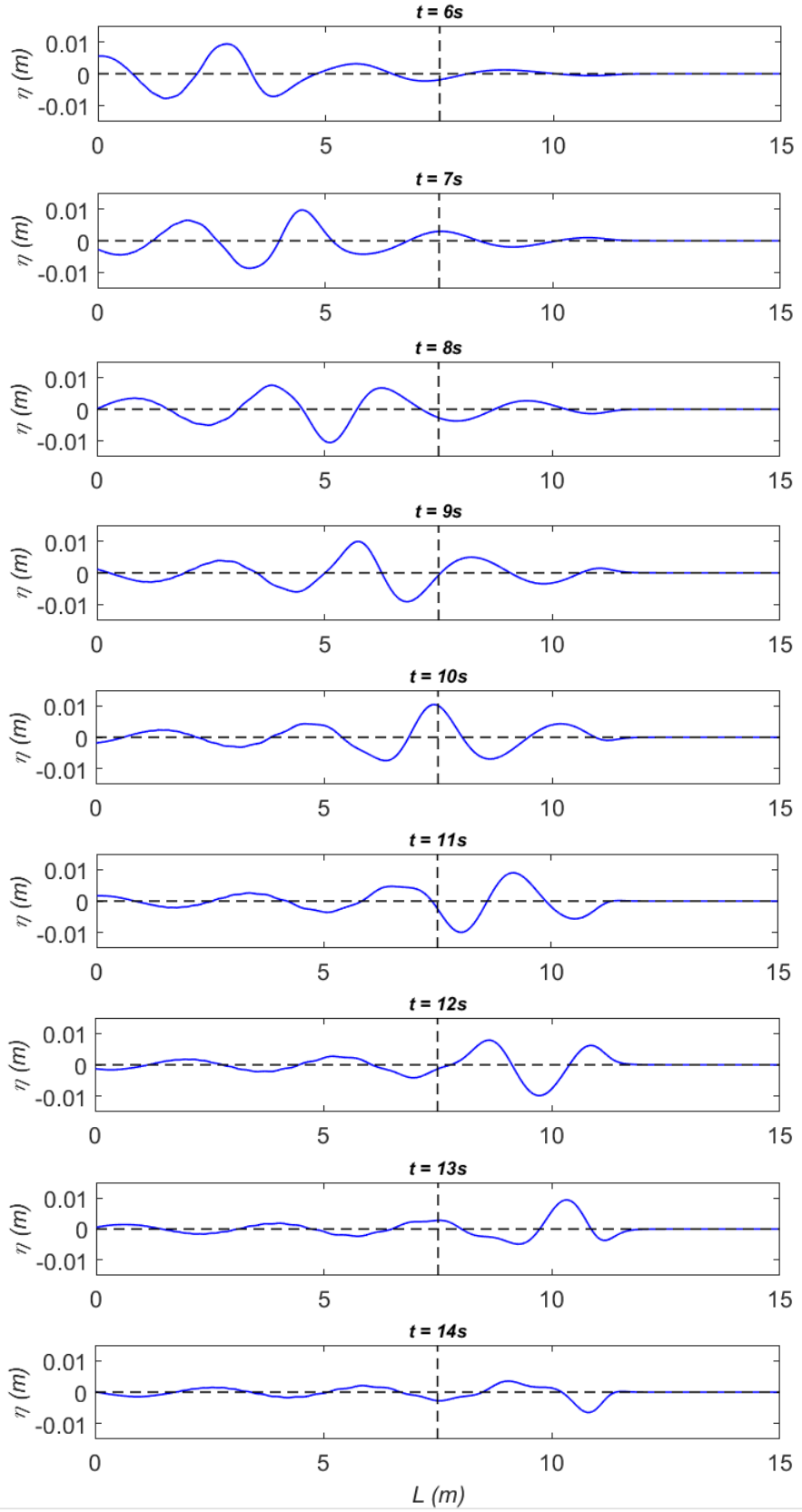

Figure 4.19: Propagation of the focusing wave group for case-$C9$. Free surface elevation (η) is captured in a second interval in the domain (L)

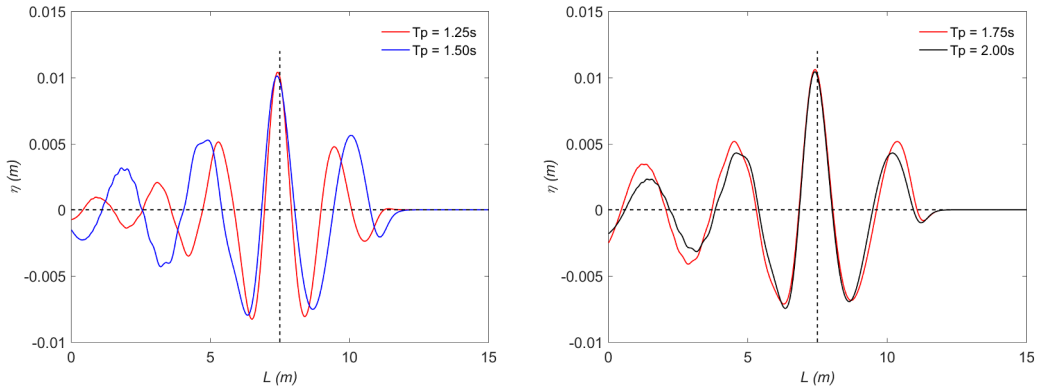

(a) (b)

Figure 4.20: Free surface elevation (η) in the wave tank (L) at $t_f = 10s$ for the cases $C2, C7, C8$ and $C9$

are visible in the free surface inside the generation zone. But wiggles disappear near the focus location. In Fig.4.20(b) amplitude of the wave components start damping out in the dissipation zone at the same location. But in Fig.4.20(a) beginning of the damping out location slightly differs. But none of these changes do not influence the kinematics at x_f.

Fig.4.19 shows free surface elevation (η) in the numerical wave tank domain length (L) at one second interval for case $C9$. Case $C5$ and case $C9$ are the higher and lower steep cases among other cases respectively. Lowest steep case $C9$ shows the same nature of propagation as case $C5$ except some of the geometrical nature of the focused wave. Wave generated at $t = 6s$ get focused at $t = 10s$ and dissipated at $t = 14s$ at the numerical beach. There are only four fully developed wave components are in the numerical wave tank in this case $C9$ at the time of focus; while five fully developed waves are visible in Fig.4.18 for case $C5$. This is due to the changes in the wave length. Crest of the wave components are not sharper but they are very gentle except the focused wave component at $t = 10s$. All these geometrical features are discussed at Sec.4.4.5.

4.4.4 Spatial and Temporal evolution of the focused wave

Spatial evolution of the wave group tells how the amplitude of the focused wave component changes over the numerical tank length while the wave group propagates. Temporal evolution of the wave group tells how the amplitude of the focused wave component changes over time.

Fig.4.21 shows the spatial evolution of the wave amplitude of the particular wave component which got focused at $t = 10s$ at the focused point. This wave amplitude evolution is tracked along the numerical wave tank length (L) in a Lagrangian perspective at 0.5s interval. Each black curvilinear line indicate the position of the wave component's location at 0.5s interval. The red dashed line is drawn through the crest of the wave component. It can be observed from Fig.4.21 that the wave component don't increase its

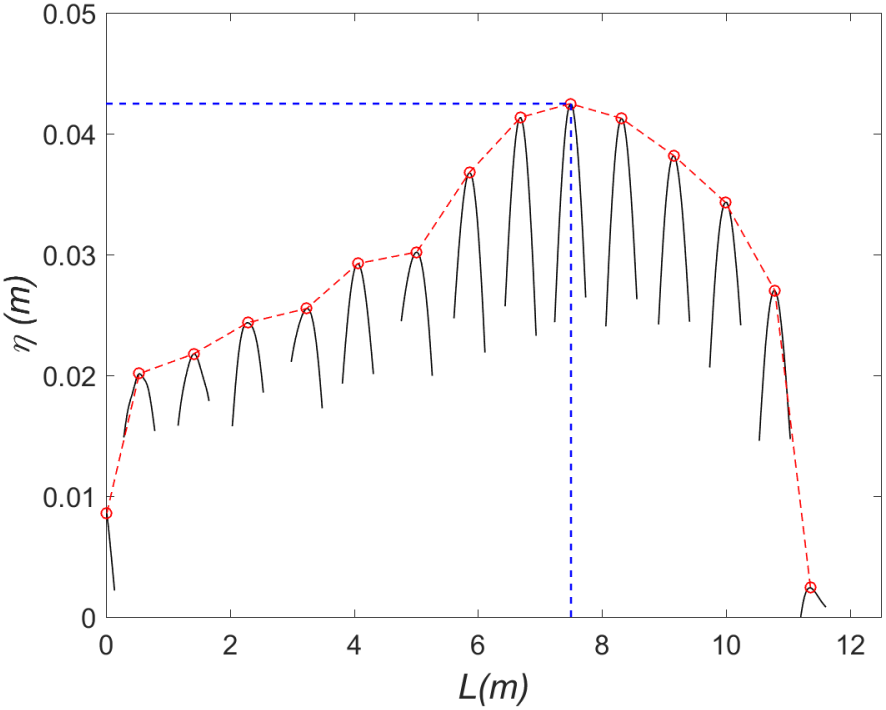

Figure 4.21: Spatial evolution of the focused wave group Wave case $C5$

height in a regular manner because the red dashed line is not a smooth polynomial line. The reason is focusing and de-focusing (super-positioning of other wave components in the group) doesn't happen in a regular interval. But the peak focused wave amplitude $(A_f^{'})$ is achieved at $x = x_f = 7.5m$ as intended. After $L = 10m$ amplitude of the wave component drops rapidly which is not because of de-focusing but because of the numerical beach damping.

Fig.4.22 shows the temporal evolution of the wave amplitude of the particular component which got focused at at $t = 10s$ as intended for case $C5$. Position of the wave gauges in the numerical wave tank are shown in Fig.4.12. The calculated free surface changes from each wave gauge is used to capture the time at which the wave component has passed the particular gauge location. A Matlab algorithm combined with wave speed is used to accomplish this task. The black curvilinear lines indicate the temporal evolution of the crest of the wave component which get focused at the intended time. The red dashed line is drawn by connecting the wave crests. Here again it is clear by observing Fig.4.12 that the amplitude gain of the wave component is not uniform over the time. Because focusing of other wave harmonics of the wave group over this wave component is not occurring at a regular interval thus amplitude gain isn't regular over the time. Even though the peaked value of the focused wave amplitude $(A_f^{'})$ is gained at $t = t_f = 10s$ as intended.

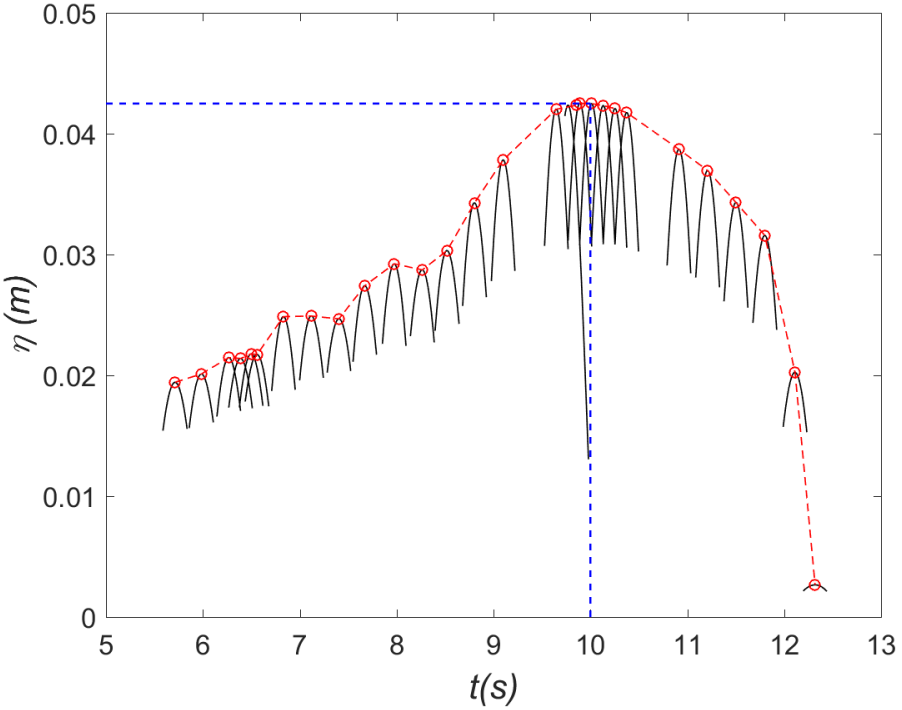

Figure 4.22: Temporal evolution of the focused wave group, Wave case $C5$

4.4.5 Geometrical Properties of the Focused waves

Wave steepness parameter is a good measure for a symmetric linear wave. But in these focused wave cases waves are not symmetric due to the influence of the second and third order harmonics. Investigation on geometrical aspects of high steep waves are done by many scholars (Miller and Zeigler 1964, Iwagaki and Sakai 1972, Ippen and Kulin 1954, Adeyemo 1968, Myrhaug and Kjeldsen 1986). There is limited amount of study specifically on the focused wave geometry. Relationship between wave geometrical parameters such as wave crest front and rear steepness, vertical and horizontal asymmetries with incident wave characters are investigated here.

Defining geometrical properties

A previous study by Kjeldsen and Myrhaug (1978) on the breaking wave geometrical aspects have used in this study to standardize the definitions of the geometrical properties.

Dimensions of a wave free surface is shown in the Fig.4.23. Parameters for the investigation are defined below (Kjeldsen and Myrhaug, 1978):

Crest front steepness:

$$\epsilon = \frac{\eta^{'}}{L^{'}} \tag{4.4}$$

Crest rear steepness:

$$\delta = \frac{\eta^{'}}{L^{"}} \tag{4.5}$$

Vertical asymmetry:

$$\lambda = \frac{L^{"}}{L^{'}} \tag{4.6}$$

Horizontal asymmetry:

$$\mu = \frac{\eta^{'}}{H} \tag{4.7}$$

With these geometrical properties wavelength at focus point (λ_w), wave amplitude ($A_f^{'}$) and relative phase change (ϕ -defined in Sec.4.2) also investigated.

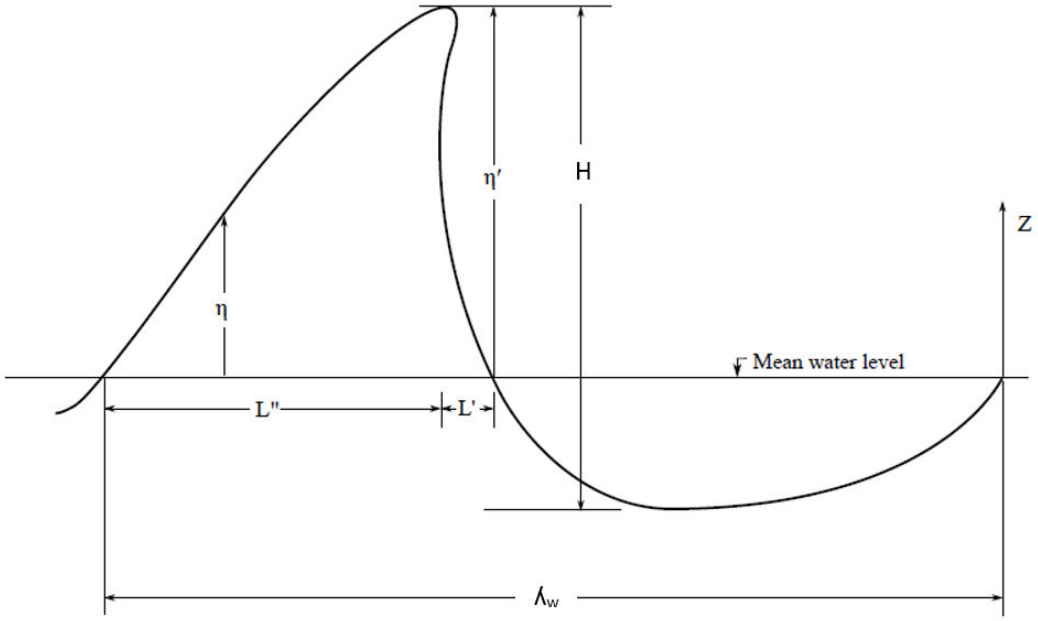

Figure 4.23: Wave geometric parameters Kjeldsen and Myrhaug (1978); $\eta^{'}$-wave amplitude, λ_w-wave length, H-wave height, $L^{'}$ and $L^{"}$ are wave crest front and rear portions of half wave length.

Focused wave geometry correlations

Free surface elevation (η) at the time of focus in the wave tank domain is plotted in the Fig.4.24. Fig.4.24(a) shows with varying H_s and Fig.4.24(b) shows with varying T_p, so

case $C2$ becomes common in both plots.

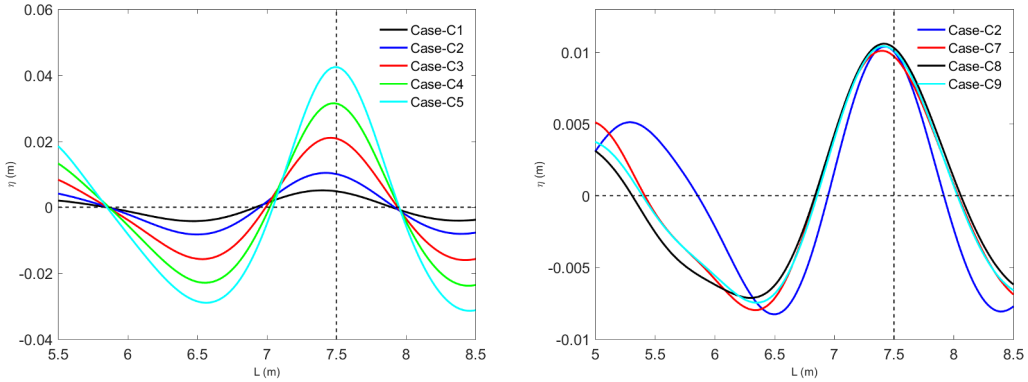

(a) (b)

Figure 4.24: Focused wave geometry at the focus time (t_f)

From these above graphs geometric dimensions are measured using Matlab tools. Refer Table 4.4 for these values.

Case	$\lambda_w(m)$	$A_f^{'}(m)$	$T_r(m)$	μ	λ	δ	ϵ	ϕ
C1	2.05	0.00511	0.00422	0.5477	0.9520	0.010735	0.01022	-0.01664
C2	2.05	0.01039	0.00826	0.5571	1.0274	0.021335	0.02192	-0.009983
C3	2.08	0.02105	0.01573	0.5723	1.0021	0.04422	0.04432	-0.006655
C4	2.09	0.03150	0.02290	0.5790	1.0065	0.06745	0.06789	-0.003461
C5	2.10	0.04248	0.02895	0.5947	0.9634	0.09503	0.09155	-0.003461
C7	2.63	0.01010	0.00797	0.5589	0.9072	0.01781	0.01616	-0.013443
C8	2.75	0.01060	0.00712	0.5982	0.8817	0.01846	0.01628	-0.013443
C9	2.64	0.01043	0.00745	0.5833	0.8932	0.01889	0.01688	-0.013443

Table 4.4: Geometrical characteristics of all focused wave cases

Each of these geometrical properties from Table 4.4 could be correlated to three incident wave parameters which are significant wave height of the spectrum (H_s), peak period of the spectrum (T_p) and the spectral steepness (S_p).
Fig.4.25 shows how relative phase is being influenced by the incident parameters (S_p, H_s, T_p) of the wave wave group.

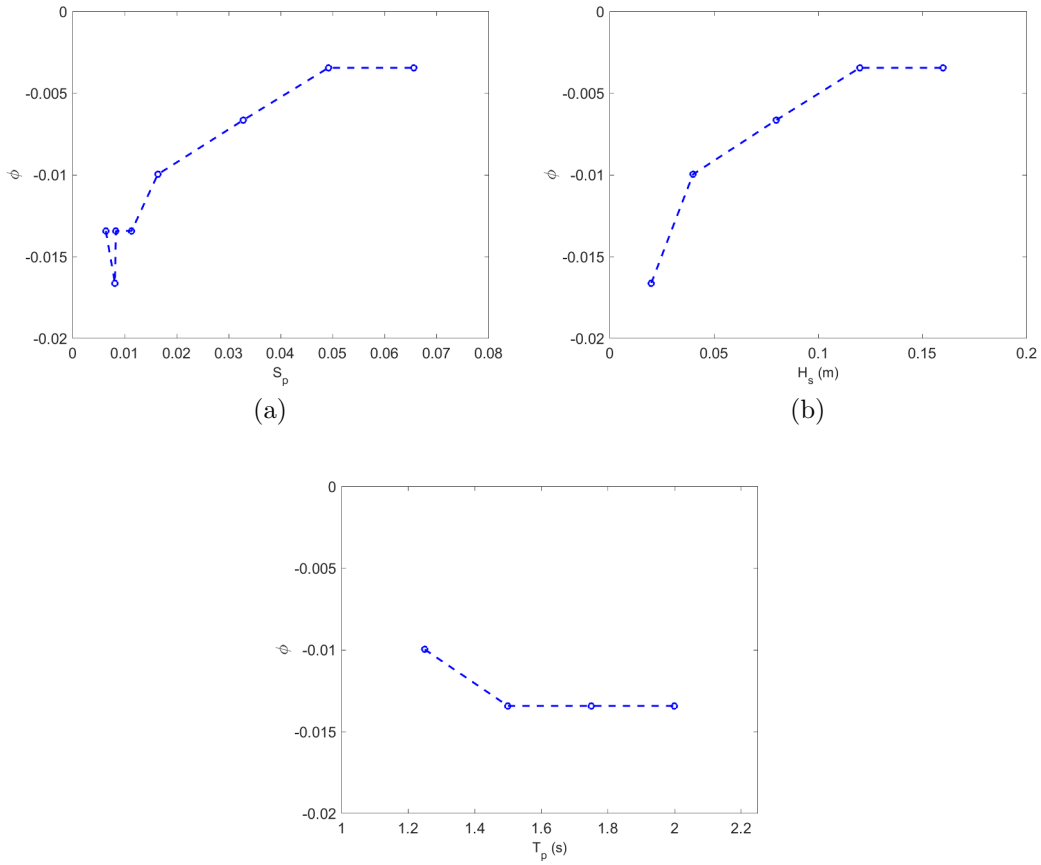

Figure 4.25: Relative phase change (ϕ) with (a) spectral steepness (S_p), (b) significant wave height (H_s) and (c) peak period (T_p)

Relative phase change (ϕ) exhibits a negative value in all three sub-figures. It means that the wave propagation speed is numerically damped by the scheme for all nine cases of investigation, therefore wave propagation is slower in the numerical wave tank rather than an experimental case. In Fig.4.25(a), relative phase change ϕ show a trend of approaching zero with increasing spectral steepness but it has some uncertainty at low steepness cases. Steady parabolic profile is observed with varying H_s from Fig.4.25(b). Relative phase change almost remains unchanged with changing T_p from Fig.4.25(c). So it is evident that relative phase change parameter is highly influenced by significant wave height and spectral steepness but not peak period. But spectral steepness is dependent on H_s and T_p. Therefore relative phase change is only correlated to the significant wave height.

Wave length (λ_w) is plotted for incident wave parameters in Fig.4.26. Spectral steepness doesn't show any strong correlation to the wave length from Fig.4.26(a). From Fig.4.26(b) Wave length is almost constant with increasing significant wave height but there are some milder changes caused by higher order non-linear wave components. Wave length increases and then stabilizes with increasing T_p at the focused point from Fig.4.26(c). Wave length is strongly correlated to peak period.

Fig.4.27 illustrates horizontal asymmetry with incident wave parameters.

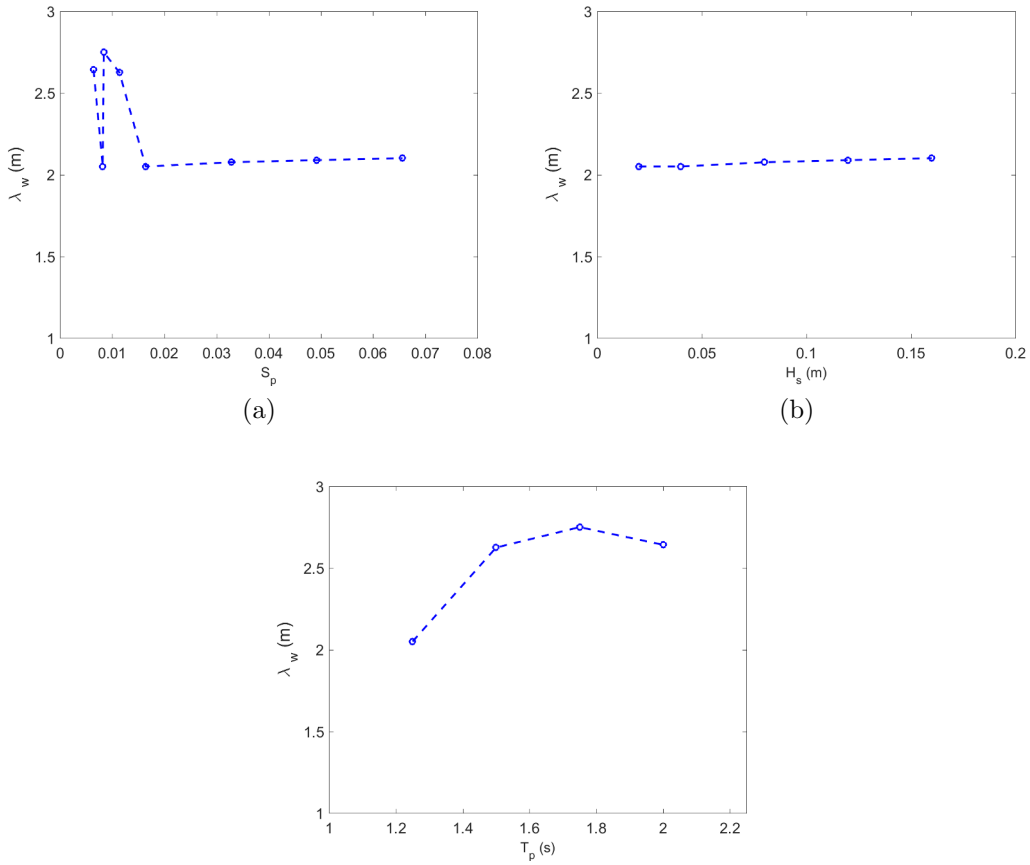

Figure 4.26: Wave length at focus point (λ_w) with (a) spectral steepness (S_p), (b) significant wave height (H_s) and (c) peak period (T_p)

Magnitude of $\mu = 0.5$ is a horizontally symmetric wave which has the crest and trough in equal distances from the mean water level according to the definition from eq.4.7 for horizontal asymmetry. Horizontal dashed black lines in Figs.4.27(a),(b) and (c) show horizontal symmetric reference for comparison. Spectral steepness doesn't show a solid correlation with vertical asymmetry but there is a milder increasing trend according to Fig.4.27(a) but all the cases show a μ value greater than 0.5 thus all cases have a flatten trough. All these waves are in intermediate water depth ($\frac{1}{20} \prec \frac{h}{\lambda_w} \prec \frac{1}{2}$)(Arntsen Ø.A, 2000) thus the trough is flatten out by higher order harmonic components. According to Fig.4.27(b) this vertical asymmetry increases almost linearly with increased H_s, therefore highly correlated with H_s. There is no strong trend visible of μ with T_p. So horizontal asymmetry is strongly correlated with H_s.

Vertical asymmetry (λ) is plotted with incident wave parameter in Fig.4.28. If λ is greater than one then the wave is pitched forward and if the λ is lesser than one then the wave is pitched backward according to the definition of λ from eq.4.6.

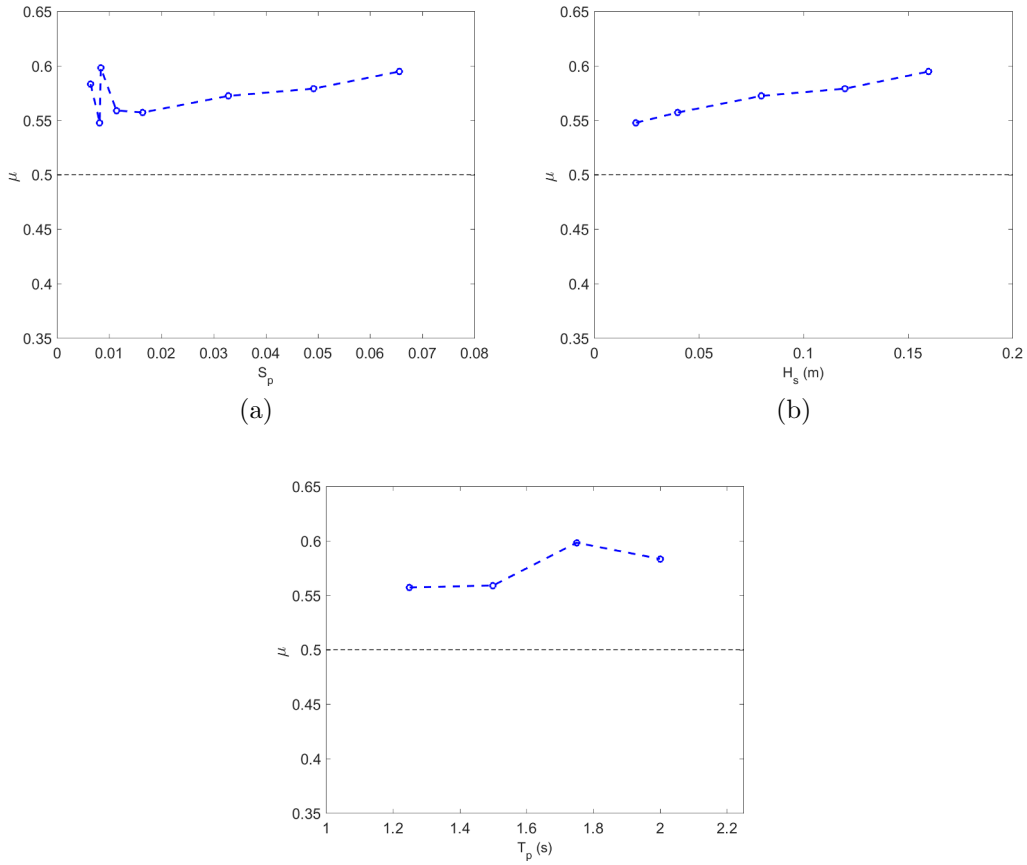

Figure 4.27: Horizontal asymmetry (μ) with (a) spectral steepness (S_p), (b) significant wave height (H_s) and (c) peak period (T_p)

From Fig.4.28(a), the wave geometry shifts from pitched backward shape to pitched forward and then back again to pitched backward thus there isn't ant strong correlation with spectral steepness but a milder increasing trend can be noticed. Same story holds with significant wave height according to the Fig.4.28(b). From Fig.4.28(c) it is clear that increasing peak period changes the shape from pitch forward to pitch backward thus strongly correlated with T_p.

Fig.4.29 shows the relationship of crest front steepness (ϵ) at the focusing point with incident wave parameters. There is a relation between spectral steepness with the crest front steepness of the focused wave according to the Fig.4.29(a). At the beginning the relation is not consistent but as a whole the correlation is very clear. Forward steepness gives a linear and strong relationship with significant wave height from Fig.4.29(b). But crest front steepness is not influenced by the peak period according to Fig.4.29(c). Therefore crest front steepness is only correlated with significant wave height.

Fig.4.30 shows crest rear steepness with incident wave parameters. These plots have the same trend as crest front steepness . With the same arguments it can be concluded that the crest rear steepness is strongly and linearly correlated with significant wave height. As a summary, crest front steepness, crest rear steepness, horizontal asymme-

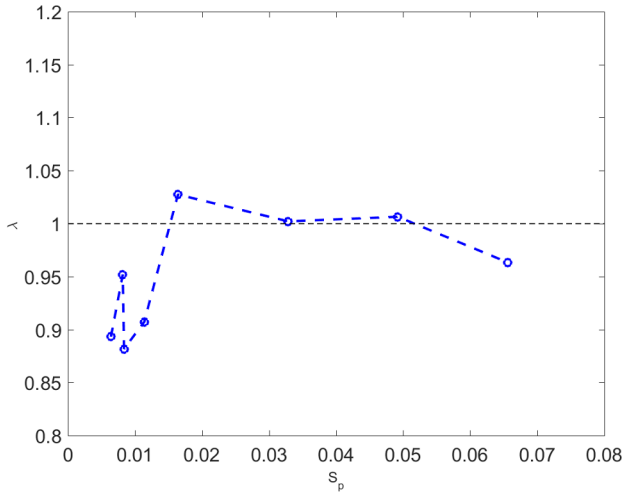

(a)

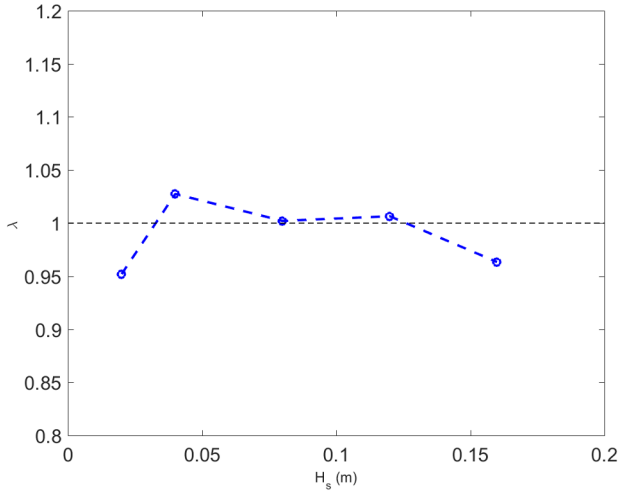

(b)

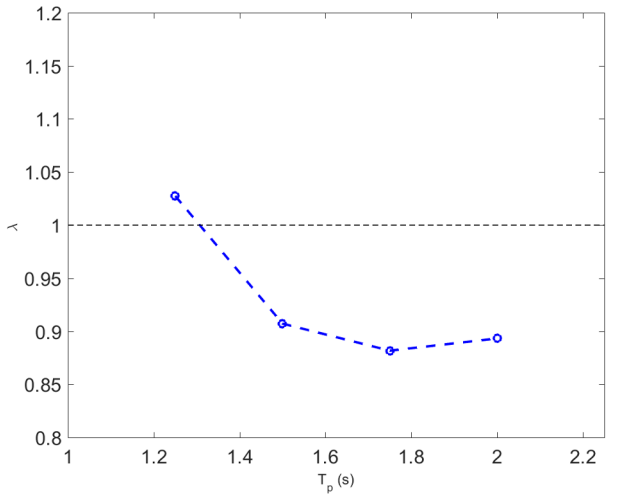

(c)

Figure 4.28: Vertical asymmetry (λ) with (a) spectral steepness (S_p), (b) significant wave height (H_s) and (c) peak period (T_p)

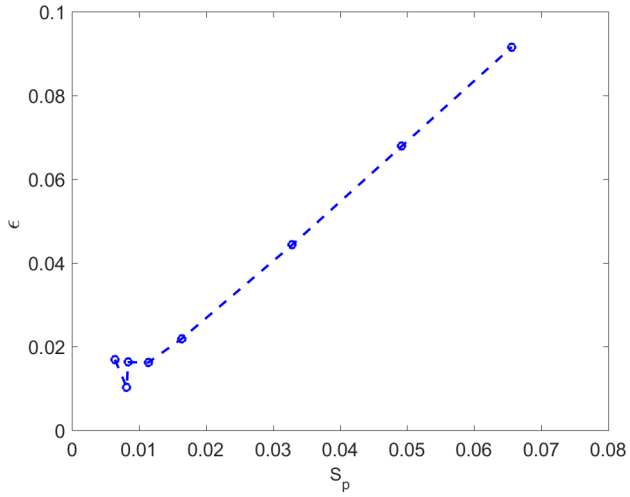

(a)

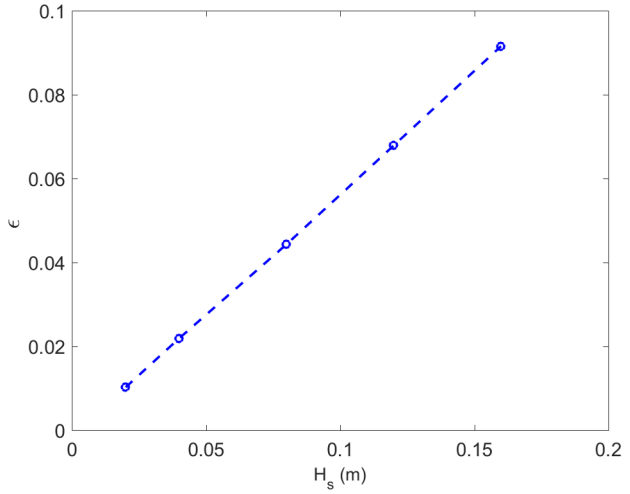

(b)

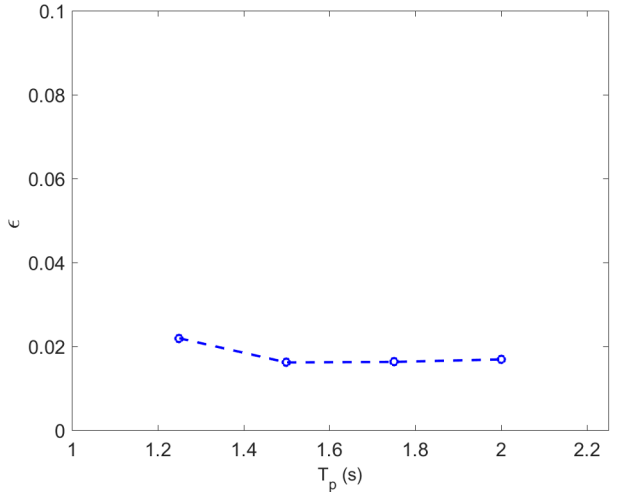

(c)

Figure 4.29: Wave crest front steepness at the focusing location (ϵ) with (a) spectral steepness (S_p), (b) significant wave height (H_s) and (c) peak period (T_p)

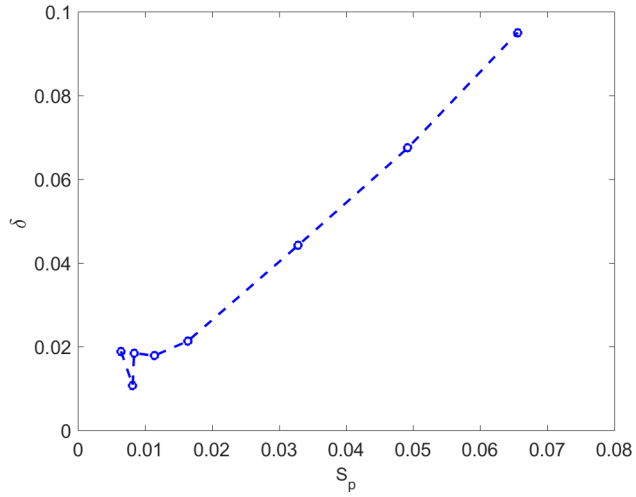

(a)

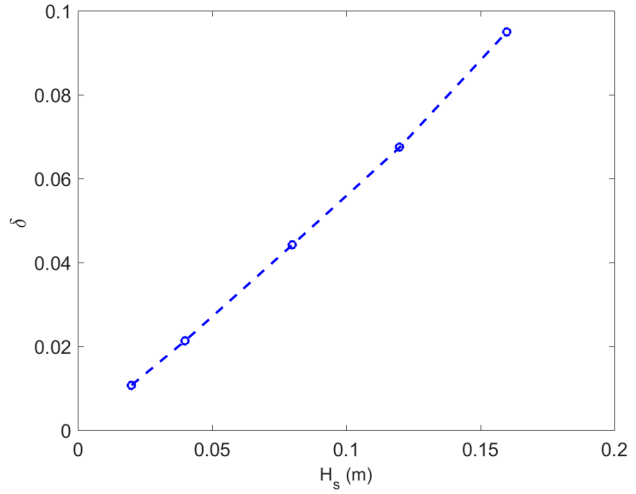

(b)

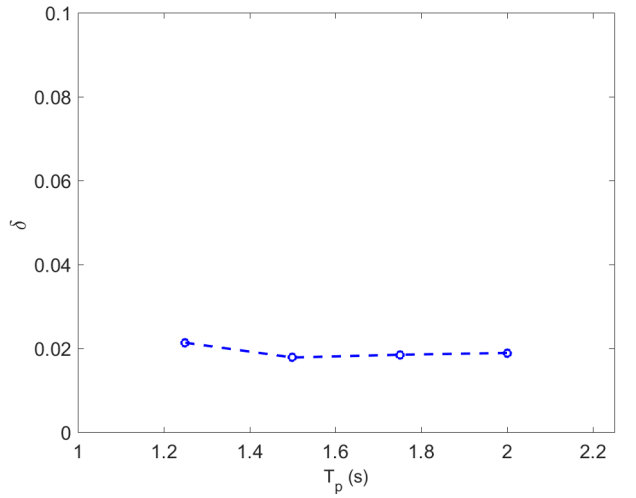

(c)

Figure 4.30: Wave crest rear steepness (δ) at the focusing location with (a) spectral steepness (S_p), (b) significant wave height (H_s) and (c) peak period (T_p)

try and relative phase change are strongly correlated to significant wave height; vertical asymmetry and wave length are related to peak period.

4.5 Wave Theories with Experimental results

Different wave theories are tested for generating focused waves in the numerical wave tank. It is vital to check whether the used wave theory satisfies the basic conditions of application such as wave height, water depth, wave length and (or) wave period. Numerical model could be validated with experimental results for each wave theories used in the numerical model. Three focused wave theories are used in the numerical model; to first order focused waves, Schäffer's second order focused waves version-1 (Schäffer$-v^{(1)}$) and Schäffer's second order focused waves version-2 (Schäffer $-v^{(2)}$). (Scäffer's second order theory $v^{(1)}$ and $v^{(2)}$ are not different second order theories, indeed they are just two different mathematical approaches used in formulating the second order components.) Actually these are not specific focused wave theories instead they are different wave theories implemented over the super-positioning concept of focused waves as explained in chapter-03. Fist order theory captures primary kinematic components while second order theory captures primary and higher (second) order kinematic components. Second order focused wave theory should capture the free surface elevation well than the first order wave theory in the high steepness focused wave cases when comparing with relevant experimental results; because higher order harmonics are significantly larger with higher wave steepness. Ning et al. (2009) experimental cases mentioned in the Table 4.1 is used to validate this different focused wave theories.

Fig.4.31 shows the free surface elevation at the focus point for the experimental result and numerical result with different focused wave theories for the case-$A1$. Case $A1$ has experimental focused wave amplitude ($A_f^{'}$) of $0.0313m$ and it has a $H_s = 0.12m$ and $T_p = 1.20s$ as the input to the numerical model. In this case both first order and second order theories are in good agreement with the experimental result as shown in the Fig.4.31.

Fig.4.32 shows the surface elevation (η) at the focusing point with time (t) for experimental and numerical results with different wave theories. Experimental focused wave amplitude is $0.0632m$. Control variables for numerical simulation are $H_s = 0.242m$ and $T_p = 1.20s$. Experimental results are well represented in the numerical simulation by both first order and second order wave theories for this steepness case. But the variation between first and second order theory has been increased compared to Ning case $A1$. In the Fig.4.32 and at $t = 11s$ second order theory is clearly separated from the first order theory. However the focused amplitude is correctly predicted by both theories well at the time of focus for this steepness case.

Free surface elevation at the focused point for experimental Ning case $A3$ with corresponding numerical results with different wave theory is presented in the Fig.4.33. Experimental focused wave amplitude is $0.0875m$ with $Hs = 0.35m$ and $Tp = 1.25s$. Harmonic separation between the first and second order wave theory is visible. At $t = 11s$, the calculated η by second order wave theory is more accurate than the first order wave the-

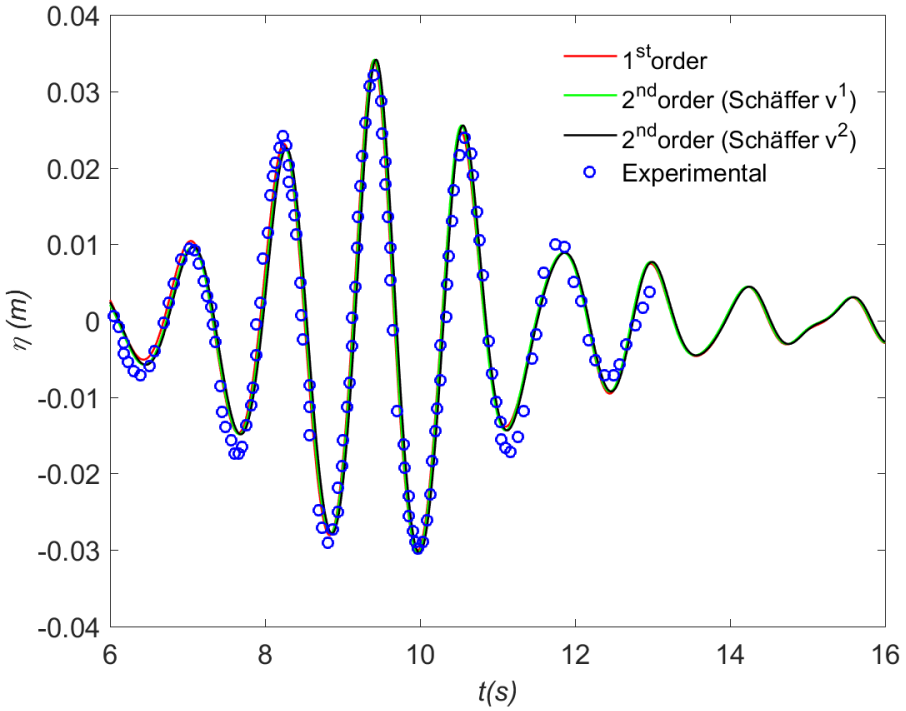

Figure 4.31: Ning Experimental case $A1$ ($H_S = 0.12$m, $T_p = 1.20$s) free surface elevation (η) at the focus point for different wave theories

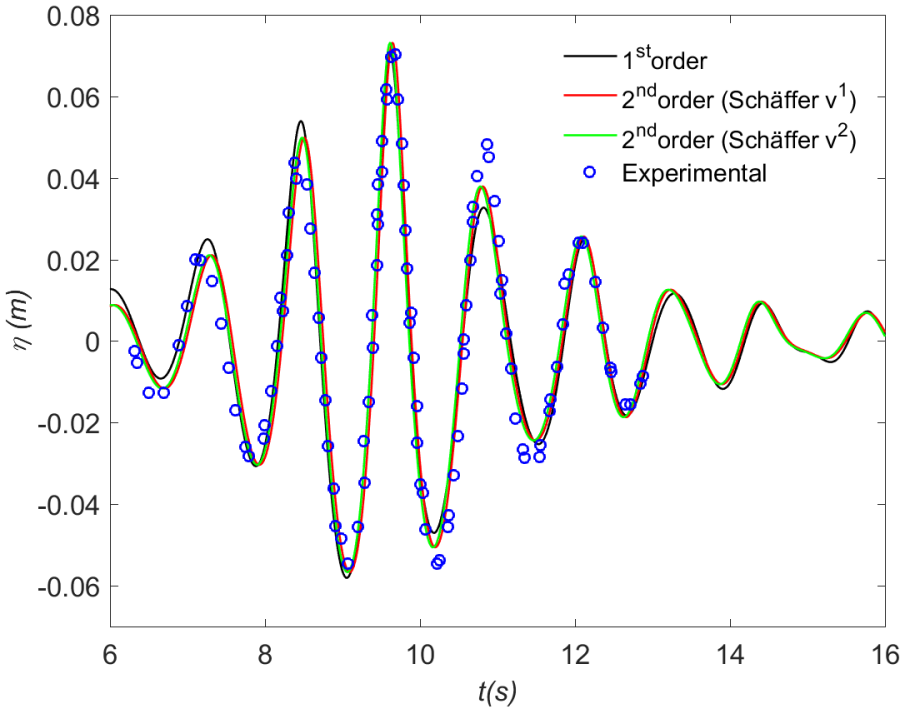

Figure 4.32: Ning experimental case $A2$ ($H_S = 0.242$m, $T_p = 1.20$s) free surface elevation (η) at the focus point with different wave theories

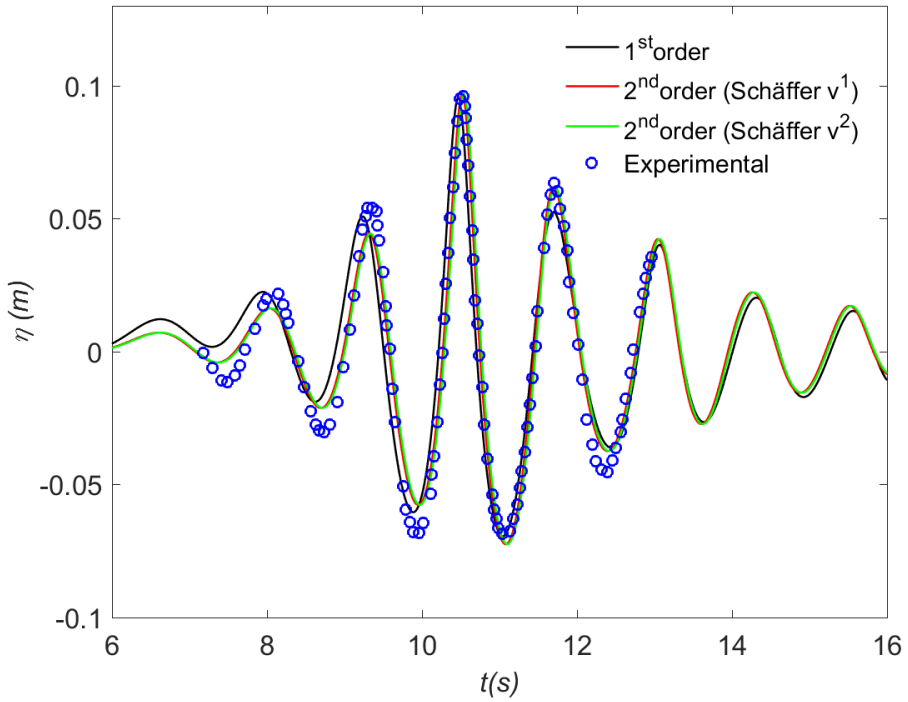

Figure 4.33: Ning experimental case $A3$ ($H_S = 0.350$m, $T_p = 1.25$s) free surface elevation (η) at the focus point with different wave theories

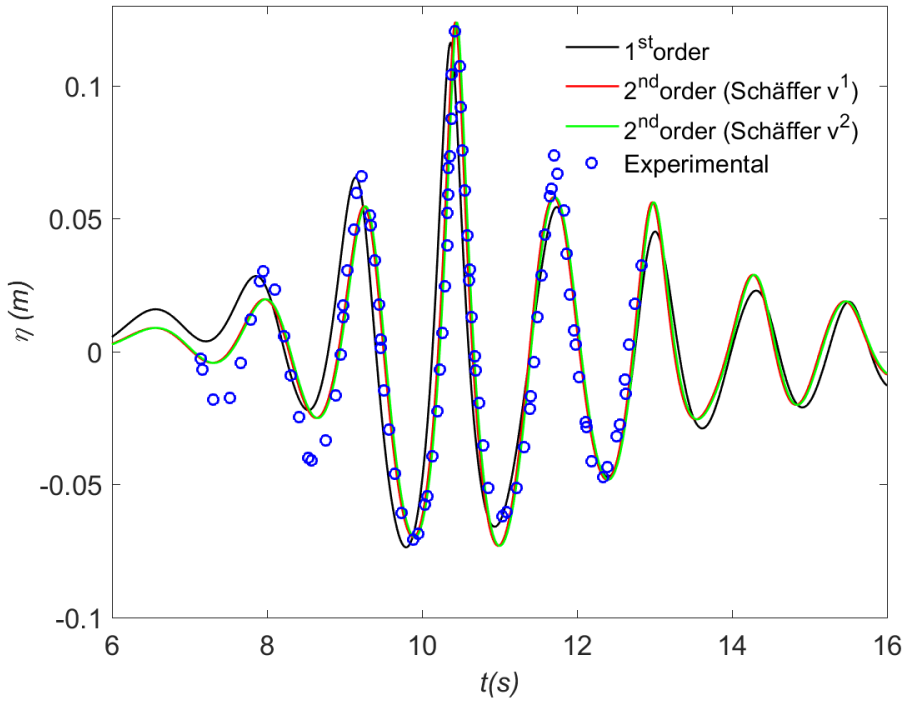

Figure 4.34: Ning case $A4$ ($H_S = 0.412$m, $T_p = 1.22$s) free surface elevation (η) at the focus point with different wave theories

ory. Experimental $A_f^{'}$ value is achieved in both but there is a small difference in the magnitude.

Free surface elevation at the focus point using different wave theories with Ning experimental case $A4$ is shown in Fig.4.34. Experimental focused wave amplitude is $0.1031m$ with $fp = 0.8Hz$. To achieve this amplitude $Hs = 0.412m$ and $Tp = 1.25s$ are used as the input variables to the numerical scheme. The results are showing significant difference within different wave theories used in the numerical model. According to Fig.4.34 both second order wave theories gain the focus amplitude at the time of focus but the focus amplitude of the first order wave theory is slightly lower than that of the experimental results. This variation precedes through all over the simulation time. Higher order kinematic components become very important for the higher steepness cases. In all these four different cases ($A1, A2, A3$ and $A4$) JONSWAP spectrum is used with 20 number of waves in the wave group to focus. As a conclusive remark the choice of the wave theory is dependent upon the incident wave parameters. But it is always a safe approach to stick with the second order wave theory for any steepness case

Chapter 5

Wave Interaction with Vertical Cylinder

Focused wave interaction on cylindrical column and the associated kinematic changes are investigated in this chapter. Available experimental results in the paper by Chen et al. (2014) are validated with numerical results. Some of the cases which get investigated in chapter 4 with two dimensional kinematic study are again used in three dimensional wave-structure interaction. Standard numerical wave tank setup for structure interaction must be done in a three dimensional domain. All the numerical cases are run with the shorter simulation time of $t = 16s$ which is enough to let a focused wave group pass the numerical tank domain. Numerical wave tank length is chosen as $L = 10m$ to minimize the computational time but this length is enough to avoid generation and dissipation boundary effects at the focused point. Width of the tank is chosen as $2m$ with water depth of $0.5m$. Cylindrical diameter of $0.25m$ is taken for all the additional investigation cases. All the three dimensional investigation is done for crest focused waves. Schäffer's second order ($v^{(1)}$) wave theory is used in the numerical simulation with JONSWAP spectrum which contains 20 wave components. Grid size of $0.025m$ is chosen in the spatial discretization as it is validated in the grid refinement study. This grid size applies to all three direction in the domain.

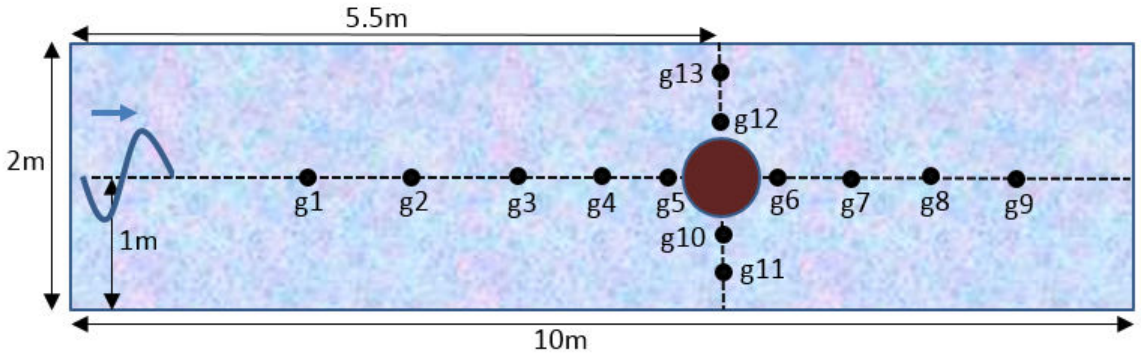

Figure 5.1: Schematized plan view of the numerical wave tank

Plan view of the numerical wave tank is shown in the Fig.5.1. Wave gauges are marked with the name 'g'. The wave propagation is from left to right in the numerical wave tank. Wave forces on the cylinder is calculated as explained in the chapter -2. Simulation cases

are shown in the Table 5.2. First five cases of two dimensional kinematic investigation is selected for the study. Additionally, the numerical model is validated for four different experimental cases listed in Table 5.1.

5.1 2D and 3D kinematic comparison

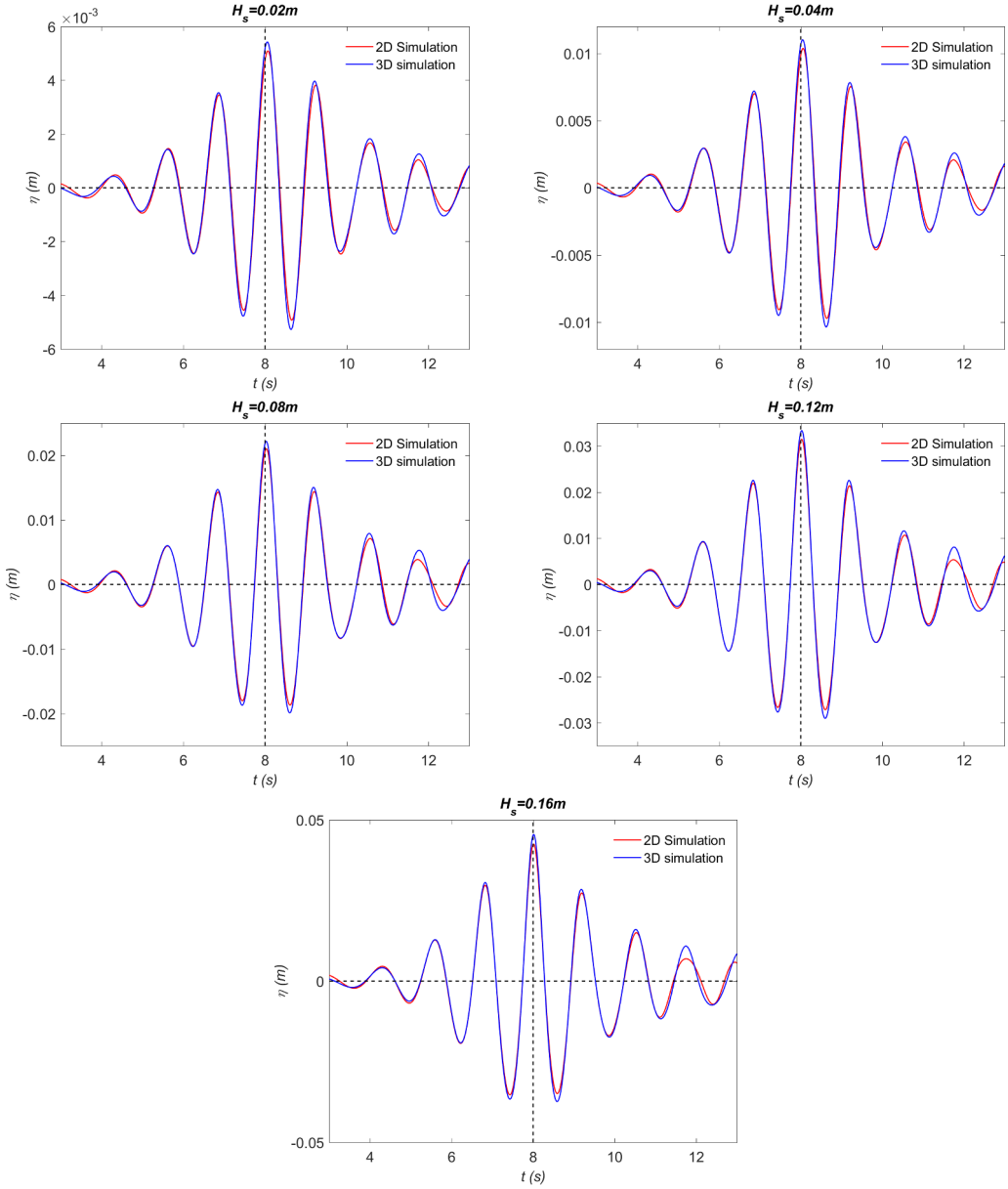

Figure 5.2: Comparison of $2D$ and $3D$ free surface elevation (η) at the focus point.

All the earlier kinematic study was done with the two dimensional spatial domain. Therefore it is very important to know changes on the kinematics due to the conversion from $2D$ to $3D$ spatial domain. To do so; all the cases in Table 5.2 simulated without cylinder in the numerical tank. Focused point is set at $x_f = 5m$ and $t_f = 8s$. Free surface elevation at the focus point in $2D$ for the first five cases in Table 4.3 is compared with the cases in

Table 5.2.

Fig.5.2 shows the comparison between free surface elevations at the focused point for $2D$ and $3D$ cases. According to the Fig.5.2 there is not much change in the free surface elevation, but the changes do exist. The change is caused only by the boundary effects (friction and turbulence) because any other input parameter doesn't change. But the change doesn't get influenced by the effect of the wave steepness or wave height because the difference doesn't grow exponentially. The change is proportional to the order of wave amplitude. This change is negligible compared to the magnitude order of the wave height. So all the kinematic study done so far with $2D$ spatial domain is valid in $3D$ spatial domain of $REEF3D$.

5.2 Benchmark cases for Wave structure Interaction

Validating the numerical model for the focused wave-structure interaction is essential to investigate the wave forces and the resulting flow features. Chen et al. (2014) performed laboratory experiments with focused wave structure interaction in the DHI shallow water basin. Dimension of the shallow water basin is $35m \times 25m$ with the water depth of $0.505m$. A vertical cylinder with the diameter of $0.25m$ is placed in the wave tank at $7.8m$ away from the wave generation paddles. Focused wave location is exactly at the upstream edge of the cylinder. This shallow water basin is larger to simulate in the numerical model due to time constraints. But it is very important to replicate the physical environment in the numerical wave tank as it is in the experimental cases. From the previous section it has been found that the numerical wave tank size of $10m \times 2m$ is enough to avoid boundary effects at the center line of the tank. So this tank size is used for the numerical simulation of experimental cases by Chen et al. (2014). The cylinder is placed $5.5m$ from the wave generation side. Intended focus point in the numerical model is adjusted in order to get the actual focusing exactly at the upstream edge of the cylinder.

Case	$T_p(s)$	$A_f^{'}(m)$	$x_f(m)$	$h_s(m)$	$t_f(s)$
D1	1.22	0.035	5.0	0.144	8.0
D2	1.22	0.070	5.0	0.300	8.0
D3	1.63	0.060	5.0	0.240	8.0
D4	1.63	0.120	5.0	0.480	8.0

Table 5.1: Simulation cases of Chen et al. (2014).

Table 5.1 shows the experimental cases with relevant numerical input values. Numerical simulation time is set to be $16s$ with the focusing time $t_f = 8s$. Readings from experimental wave gauge ($WG9$ of Chen et al. (2014)) and numerical wave gauge ($g5$

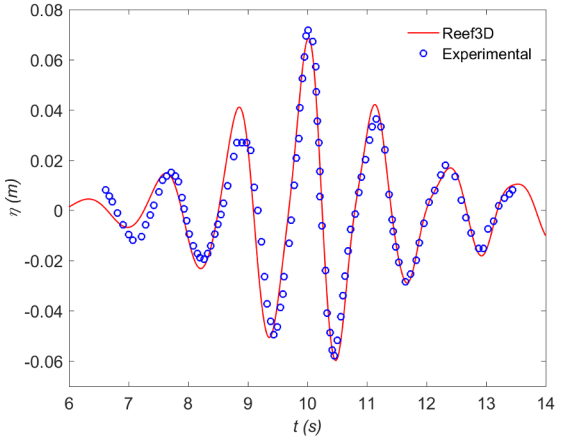

(a) Free surface elevation

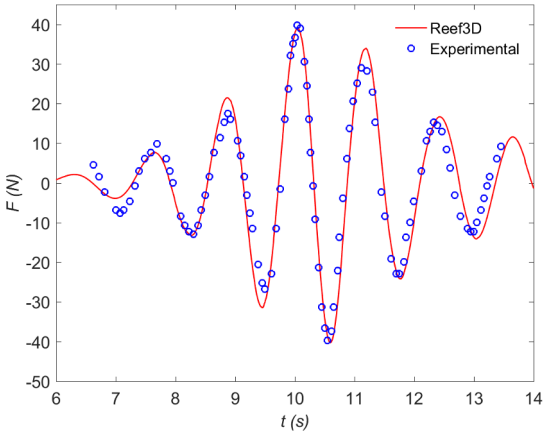

(b) Force on the cylinder

Figure 5.3: Validation of forces and surface elevation for case-$D1$

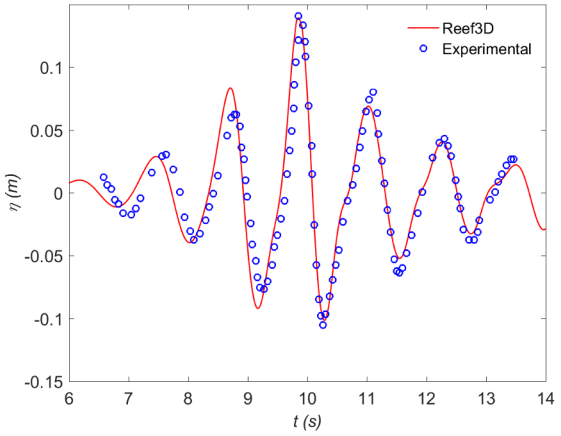

(a) Free surface elevation

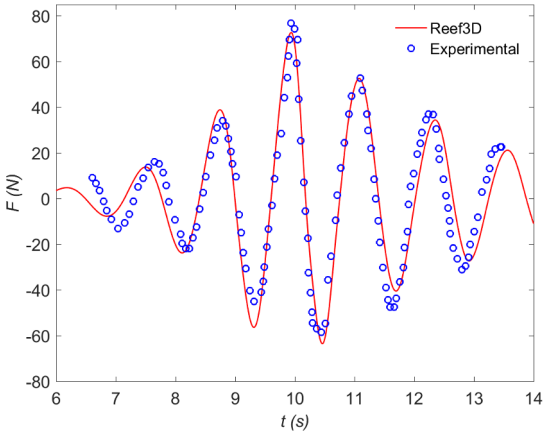

(b) Force on the cylinder

Figure 5.4: Validation of forces and surface elevation case- $D2$

of Fig.5.1) are used to compare the free surface elevation; both gauges are at the same position from the cylinder.

Fig.5.3 shows the free surface elevation and the wave force on the cylinder for the experimental case $D1$. Good agreement between force and free surface elevation is found. Steepness is lower in this cases, thus low steepness makes non-linear terms less significant.

The experimental case $D2$ with higher steepness also agrees well with the measured free surface elevation and wave force according to Fig.5.4. There are some marginal deviations in the free surface elevation before and after the focus point but at the time of focus the deviation vanishes. The numerical model predicts the free surface elevation and the wave force well for both cases. These cases have already been validated by Bihs et al. (2016).

Horizontal force on the cylinder for Experimental case $D3$ is presented in Fig.5.5.

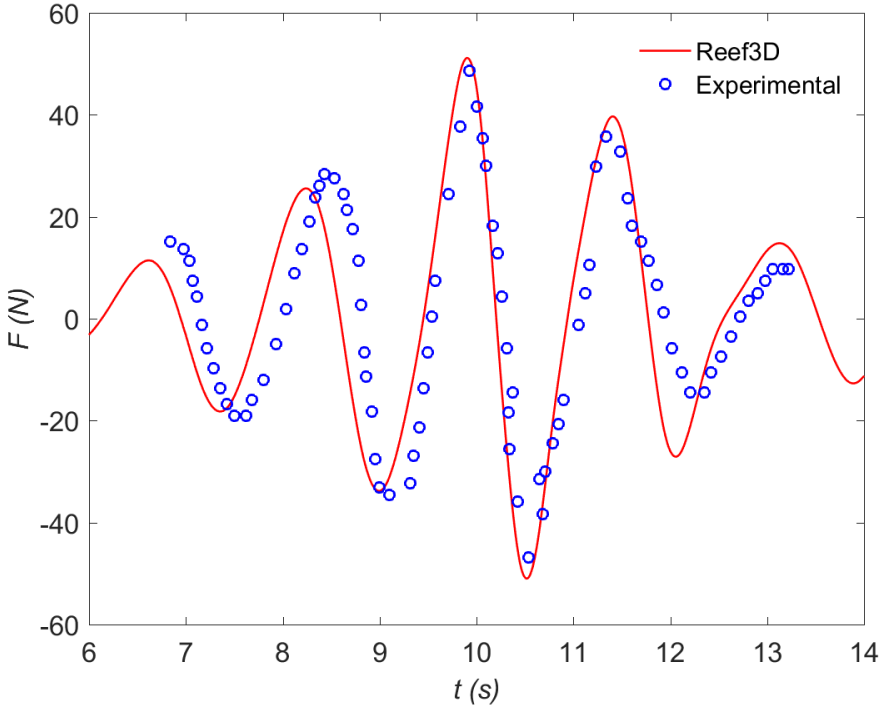

Figure 5.5: Comparison of force on the cylindrical for case-$D3$.

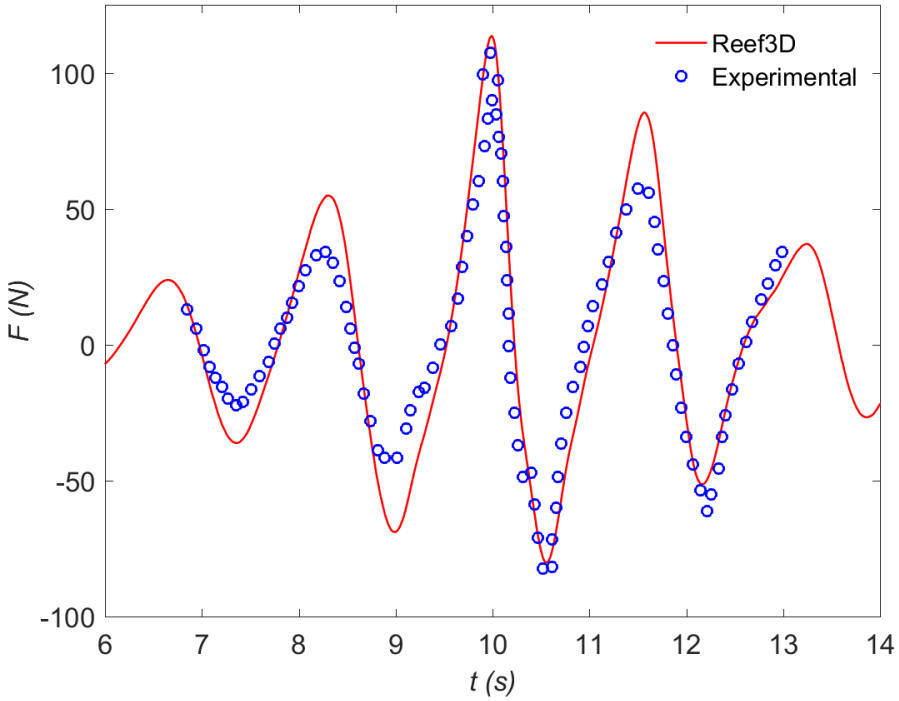

Figure 5.6: Comparison of forces on the cylindrical for case-$D4$.

There are some small amplitude changes in the force but overall the results are fine.

Fig.5.6 shows the horizontal force on the cylinder for the highest steepness case $D4$. The second order components give a higher contribution in this case thus the vertical asymmetry is larger which reflects in the force spectrum. Experimental wave forces are well agreeing with the numerical wave loading in these cases too. The force curve is slightly over predicted before and after the focused wave crest passes the cylinder, though the peak force value is predicted well. As a conclusion, the numerical model REEF3D could be used as an efficient tool for simulating high and low steep focused wave structure interaction cases.

5.3 Kinematic Changes due to interacting with Cylinder

The study of steep wave structure interaction can be done easily through focused wave groups. Many researchers have investigated steep wave-structure interaction using focused wave groups numerically (Ma et al. 2001, Chen et al. 2014). Table 5.2 presents a list of simulations for the cases with cylinder of diameter $0.25m$ and without cylinder. Waves are generated with JONSWAP spectrum of 20 wave components. Hydrodynamic features such as wave loading, diffraction, wave run-up and wave run-down and free surface flow features when wave interacts with the vertical cylinder (Clauss, 2002), (Sumer et al., 1997). These aspects could be investigated with REEF3D as well.

Case	$H_s(m)$	$T_p(s)$
E1	0.02	1.25
E2	0.04	1.25
E3	0.08	1.25
E4	0.12	1.25
E5	0.16	1.25

Table 5.2: Numerical cases to study wave-structure interaction with and without cylinder.

Figs.5.8 and 5.7 is drawn from the free surface elevation in the tank domain for case $E5$ in $0.5s$ interval. The line of this free surface elevation is chosen to be in the longitudinal direction along the middle of the tank ($1m$ from side of the tank). This longitudinal section passes through the cylinder which is in the middle of the tank. Cylinder is shown in the figures with correct dimensions. Free surface elevation is then compared in the figures with the case without cylinder so that the temporal changes in the wave characteristics can be observed separately. Here case $E5$ is chosen because it has the higher significant wave height thus the changes in the kinematics are significant. At $t = 6.0$s (Fig.5.7(a)) the wave group starts to interact with the cylinder. Wave group is moving from the left to right. Therefore the free surface elevation which interact at $t = 6.0s$ dropping down. The case with cylinder shows some additional drop in η than the case without cylinder.

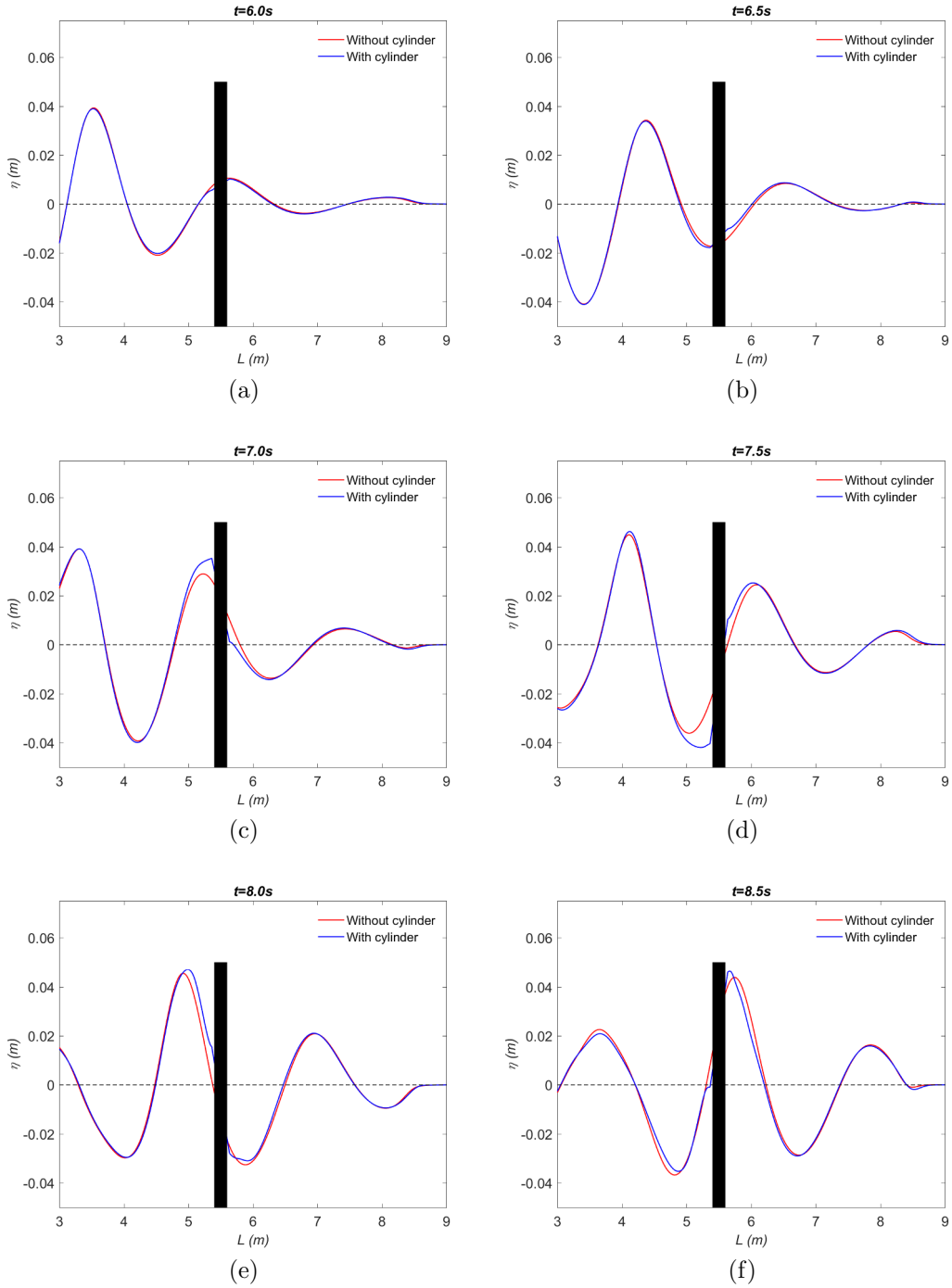

Figure 5.7: Comparison of free surface elevation (η) in the wave tank (L) (t = 6.0s to 8.5s) with and without cylinder for case $E5$

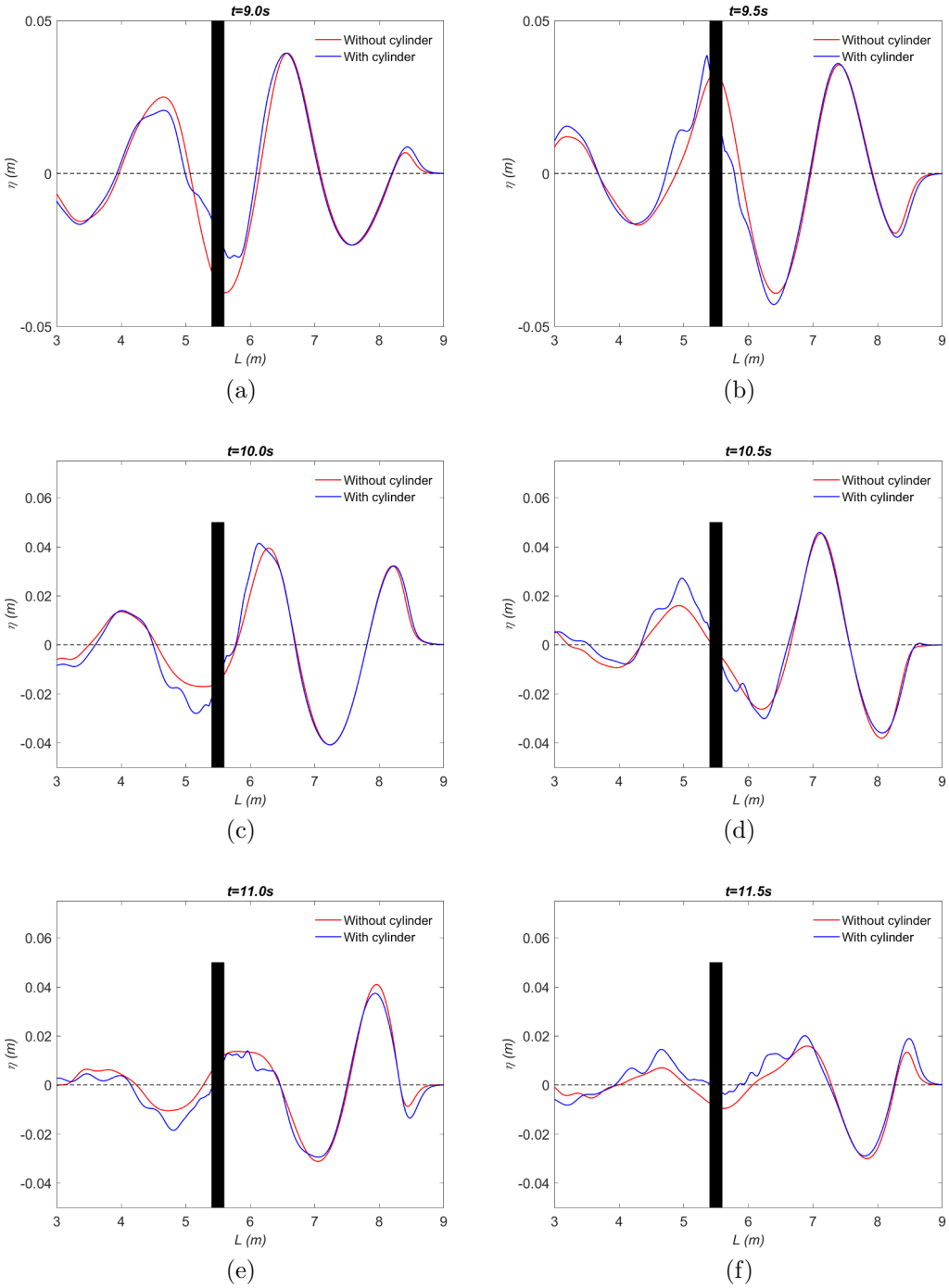

Figure 5.8: Comparison of free surface elevation (η) in the wave tank (L) (t = 9.0s to 11.5s) with and without cylinder for case $E5$

Another fact is that the presence of the cylinder doesn't create any other influence in the numerical tank at $t = 6.0$s and $t = 6.5$s. It is also observed that there is no change in η in the upstream side of the cylinder at $t = 6.5s$. But there is a slight surge in the free surface elevation at the downstream of the cylinder due to diffraction.

At $t = 7.0$s η rises in-front of the of the cylinder. The rise in water level is clearly visible with the value of 0.004m for the wave component's amplitude of 0.02m order. At $t = 7.5$s fall in water level is seen with the same order of value as run-up. Wave kinematics is disturbed by the cylindrical interaction to the extent of 0.7m in the upstream direction from the surface of the cylinder edge. As well the wave kinematics is disturbed to the downstream direction of 0.7m from the cylinder edge. Between $t = 8.0$s and $t = 8.5$s the peak focused wave crest passes the cylinder. At $t = 9.0s$ fall in water level is limited by the cylinder. Now the free surface elevation is distributed for a length of 1.2m in the upstream direction from the cylinder. At $t = 9.5s$ fall in water level is visible and η is influenced in the domain from $L = 3$m to $L = 6.5$m. Ripples and wiggle formations are observed in the free surface after $t = 10s$ till $t = 11.5s$ through which the energy of the focused wave group is dissipated by the structure.

Flow velocity near the cylinder caused by focus wave interaction for the numerical case $E5$ is shown in Fig.5.9 and 5.10. At $t = 6.5$s focused wave begins its interaction. There is a flow velocity of of 0.23m/s around the cylinder at $t = 7.0$s and at $t = 7.5$s even before focused wave crest begin iteration with the cylinder. At $t = 8.0$s peak focused wave crest interacts with the cylinder increasing the magnitude of the flow filed around the cylinder. Returning flow around the cylinder caused by diffracted waves are clearly visible at $t = 8.5$s and at $t = 9.0$s. Reflected wave energy causing a weak flow field with the magnitude of 0.15m/s in the upstream side of the cylinder after focused wave group passed the cylinder, which is clearly visible in Fig.5.10 at $t = 9.5$s and at $t = 10.0$s. This reflection and diffraction phenomenon causing wave group to dissipate its energy as explained by the Figs.5.7 and 5.8.

Free surface elevation from the wave gauge '$g5$' (Fig.5.1) is used to compare the influence of the cylinder and plotted in Fig.5.11 for all the five cases mentioned in the Table 5.2. In all the cases the peak and trough magnitudes are exceeded at the cylindrical surface at the upstream side. This clearly shows the amount of rise and fall in free surface heights with associated wave amplitudes. This excess amount of run-up and run-down make the dynamic wave loading efficient thus this factor influences the ringing effect (Zang et al., 2010).

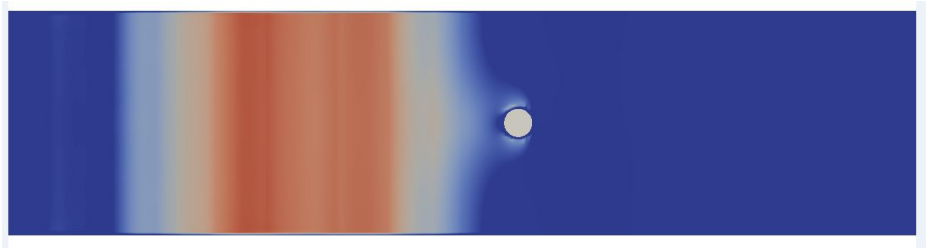

(a) t=6.5s

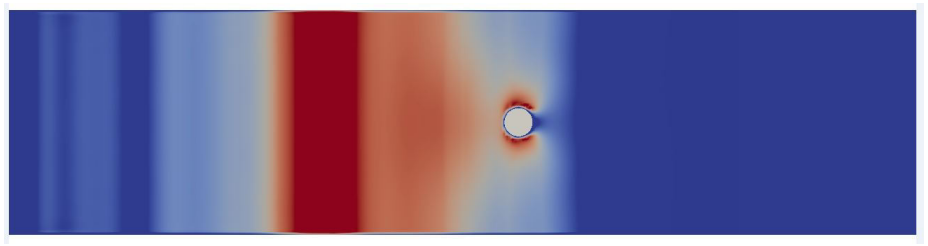

(b) t=7.0s

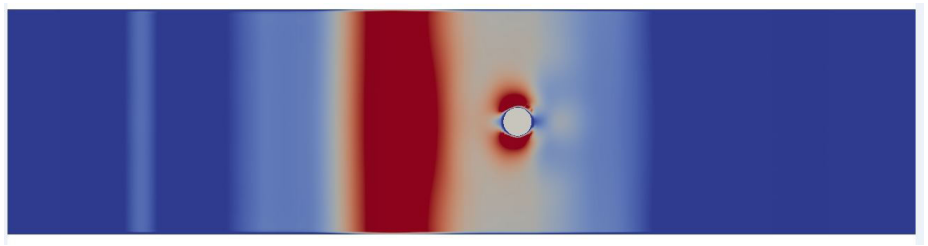

(c) t=7.5s

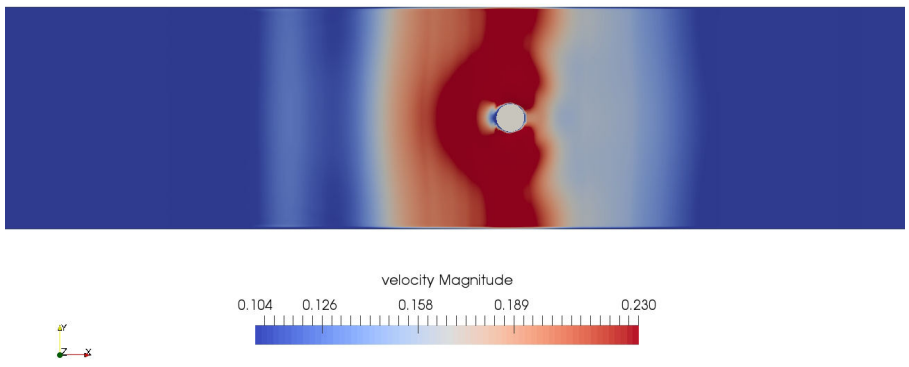

(d) t=8.0s

Figure 5.9: Flow velocity near the cylinder ($t = 6.5$s to 8.0s) for case $E5$

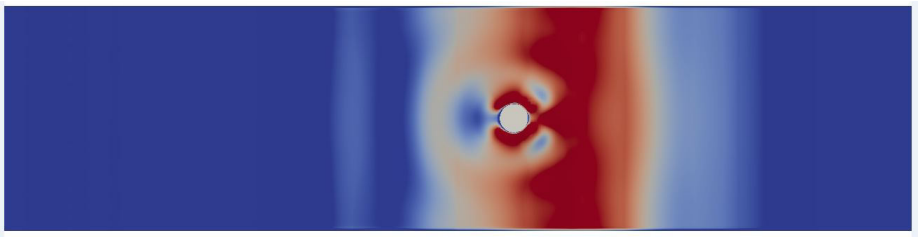

(a) t=8.5s

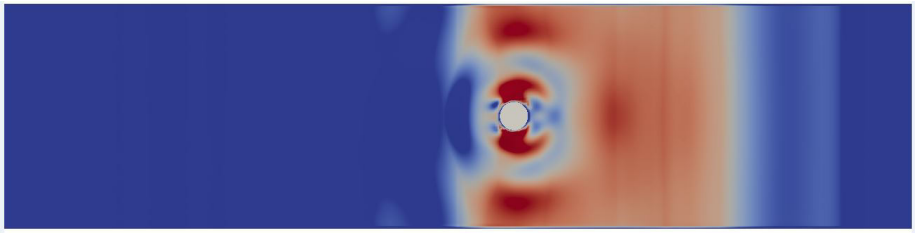

(b) t=9.0s

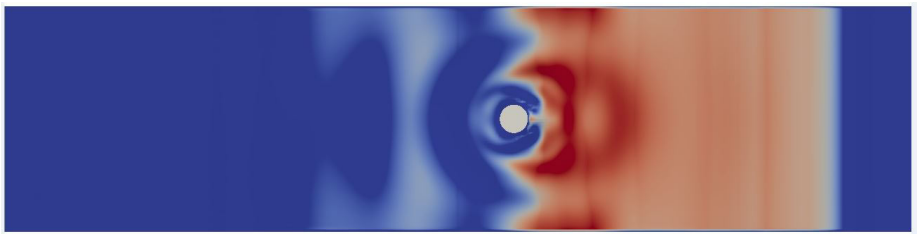

(c) t=9.5s

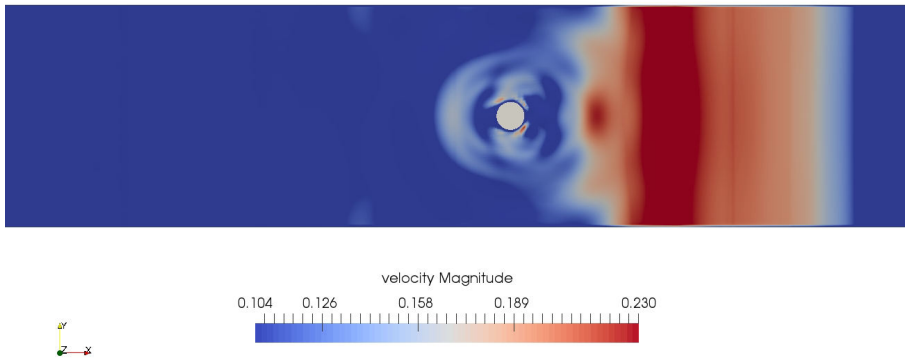

(d) t=10.0s

Figure 5.10: Flow velocity near the cylinder ($t = 8.5$s to 10.0s) for case $E5$

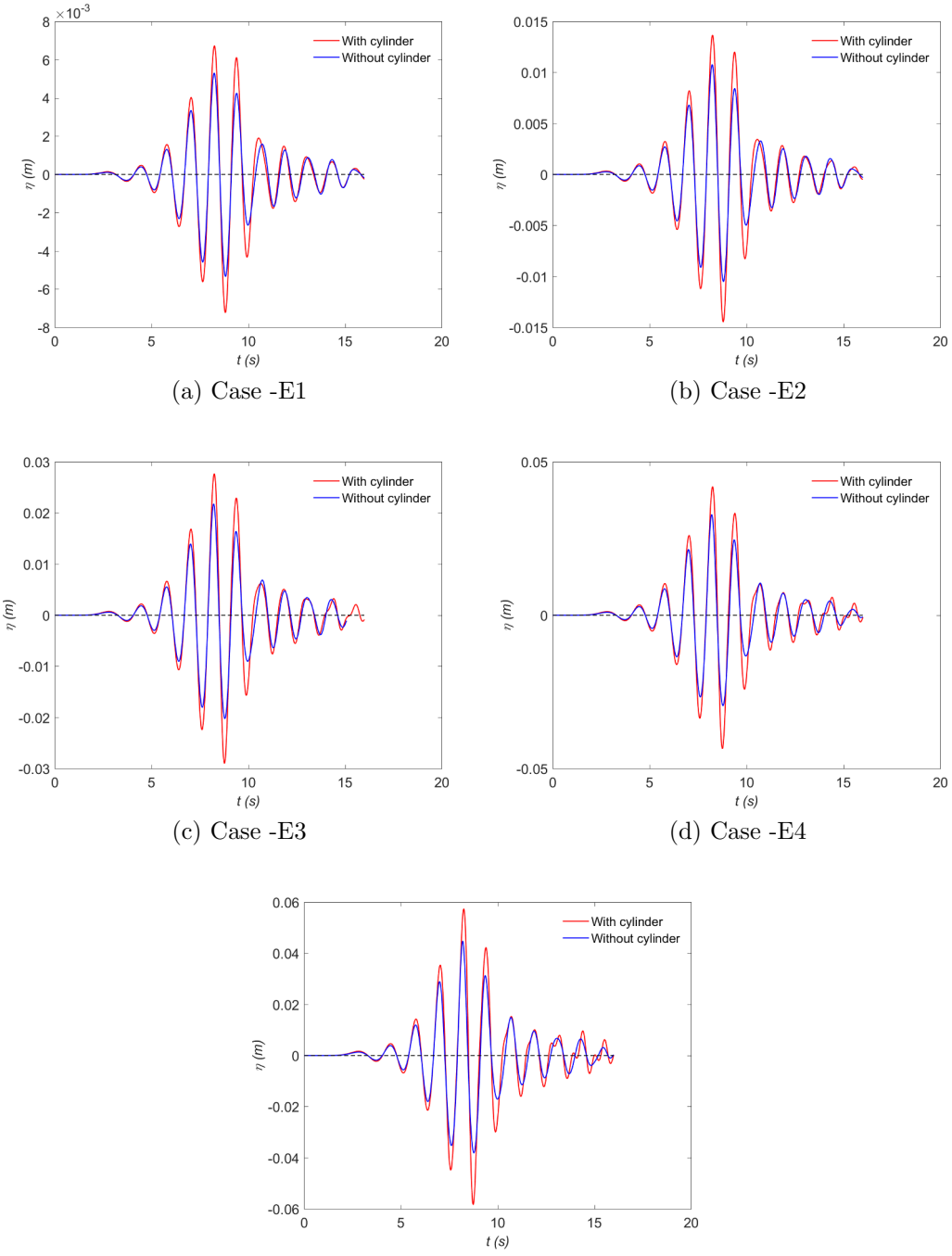

(a) Case -E1

(b) Case -E2

(c) Case -E3

(d) Case -E4

(e) Case -E5

Figure 5.11: Free surface elevation (η) from wave gauge $'g5'$ (Fig.5.1) with and without cylinder for cases -$E1, E2, E3, E4$ and $E5$

5.4 Wave forces and kinematic correlations

Wave forces are associated with drag, shear and inertial components (MacCamy and Fuchs, 1954). All these components of wave loading is correlated with the free surface height from the still water level and the flow velocity. But in waves flow velocity is also associated with the wave height. Therefore wave amplitude and wave period is the defining control parameters in wave loading on vertical cylinders. Numerically calculated wave force on the cylinder and the free surface elevation from the wave gauge '$g5$' are normalized with their peak values. These normalized values are plotted in Fig.5.12 for all the wave cases in the Table 5.2.

Both normalized curves shpwn in Fig.5.12 follow the same oscillation pattern over the time. In all these cases there is a milder time delay in gaining the corresponding wave force on the cylinder. In Fig.5.12(a) this time lag is about $0.2s$. The reason is that the wave loading is a perfect quasi-static (not instantaneous) process. It consumes time in mobilizing the pressure over the surface of the body (Koliopulos, 1988). The other interesting phenomenon is that the peak wave force doesn't come from the peak focused wave component in the wave group. The peak wave force is obtained from the next wave crest after the focused wave crest passes the cylinder. In Fig.5.12(a), the peak wave crest is recorded at $t = 8$s while the peak force (F) is recorded at $t = 9.5$s. This is happening in all five cases. This time lag in force recording disappears after $t = 11s$ and both peak curves are coinciding in the time domain. After $t = 10s$ free surface elevation tends to show deflection in the cases with higher H_s value in Figs.5.12(c),(d) and (e) due to reflection and diffraction caused by the cylinder. But these deflected free surface elevation has no influence on the shape of the force curve. This can be seen clearly in Fig.5.12(e), in which at $t = 13s$ free surface elevations are not keeping a sinusoidal shape but, forces do keep a near sinusoidal shape. This is because the shorter time duration at which the deflection of η from the sinusoidal shape occurs is not enough to fully mobilize the pressure profile over the cylindrical surface thus this changes are not captured in the force curve.

Figs.5.13 and 5.14 show the horizontal wave forces on the cylinder and the corresponding force spectrum for all the simulation cases as listed in Table 5.14. Maximum force in each cases increases with increasing significant wave height. In all these cases, peak period is 1.25s according to Table 5.14 which gives a peak frequency $f_p = 0.8Hz$. Peak frequency of the force spectrum is also $0.8Hz$ in all the cases from Figs.5.13(b),(d) and (f) and from Figs.5.14(b) and (d). This confirms the fact that both wave loading and free surface elevation have almost the same shape of curves as explained by the normalized values in Fig.5.12. The spectral curves are smoother after $f = 1.5Hz$ for low steep cases $E1, E2$ and $E3$. But there are some force components in the order of 2N to 3N after 1.5Hz of frequency in the force spectrum for the cases $E4$ and $E5$. This is due to diffraction because there is no wave component in the wave group containing a wave period lesser than $0.67s$ (wave period $T = \frac{1}{f} = \frac{1}{1.5} = 0.67s$). So higher steep wave cases $E4$ and $E5$ exerts a high frequency low magnitude wave loading on the cylinder.

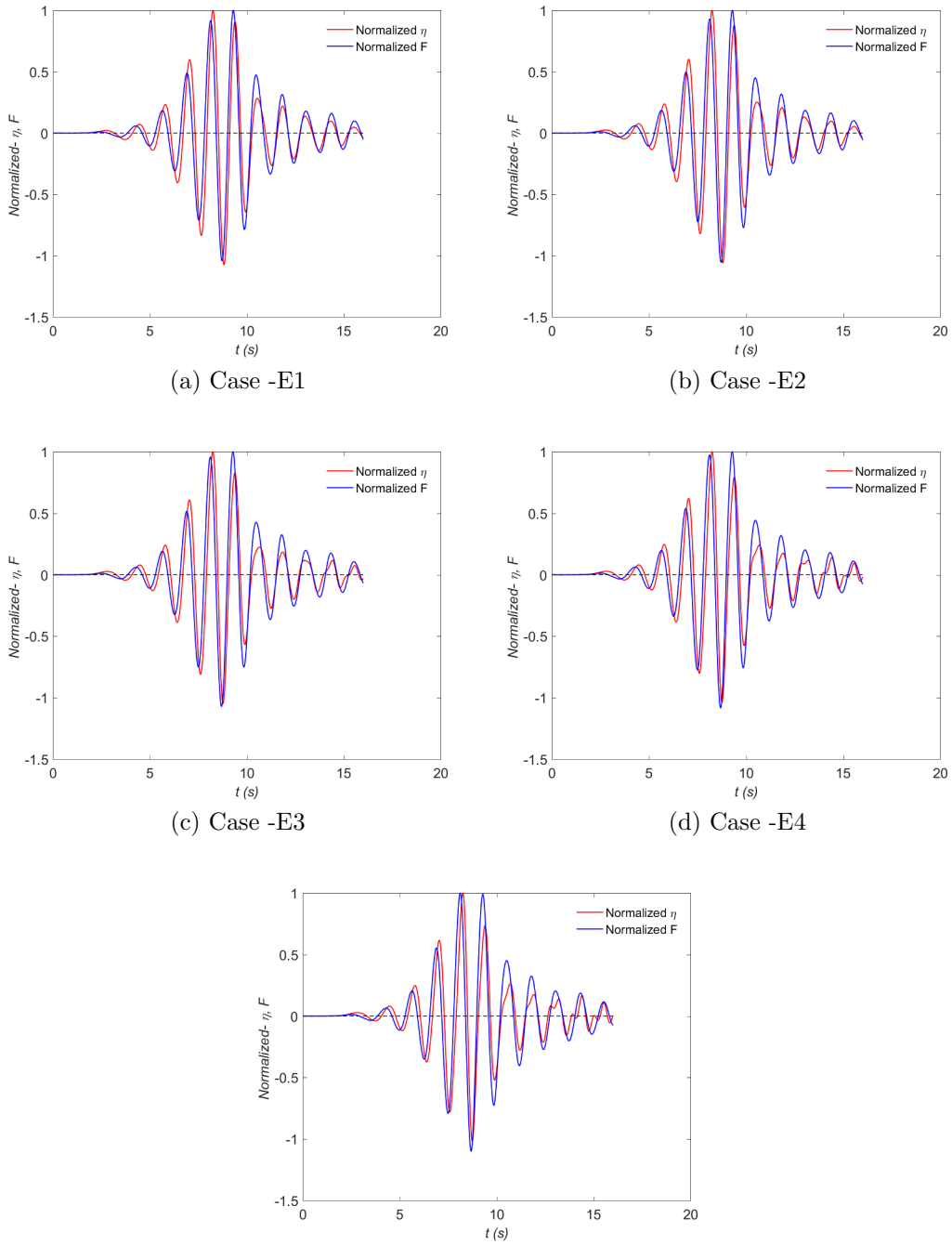

(a) Case -E1

(b) Case -E2

(c) Case -E3

(d) Case -E4

(e) Case -E5

Figure 5.12: Normalized free surface elevation (η) from wave gauge $'g5'$ with normalized force (F) on the cylinder for cases -$E1, E2, E3, E4$ and $E5$

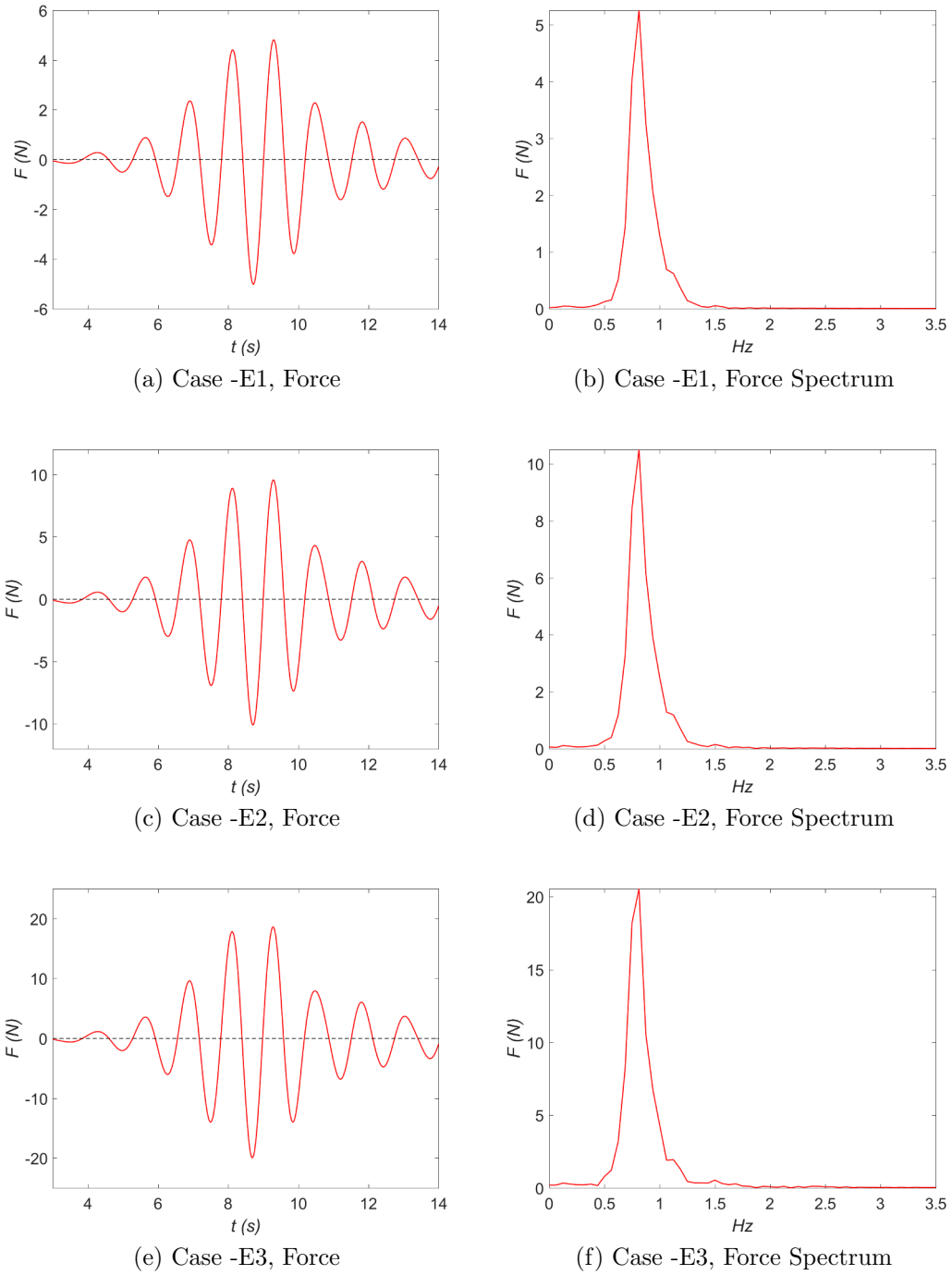

(a) Case -E1, Force

(b) Case -E1, Force Spectrum

(c) Case -E2, Force

(d) Case -E2, Force Spectrum

(e) Case -E3, Force

(f) Case -E3, Force Spectrum

Figure 5.13: Horizontal wave loading on the cylinder (F) and force spectrum for cases -$E1, E2$ and $E3$

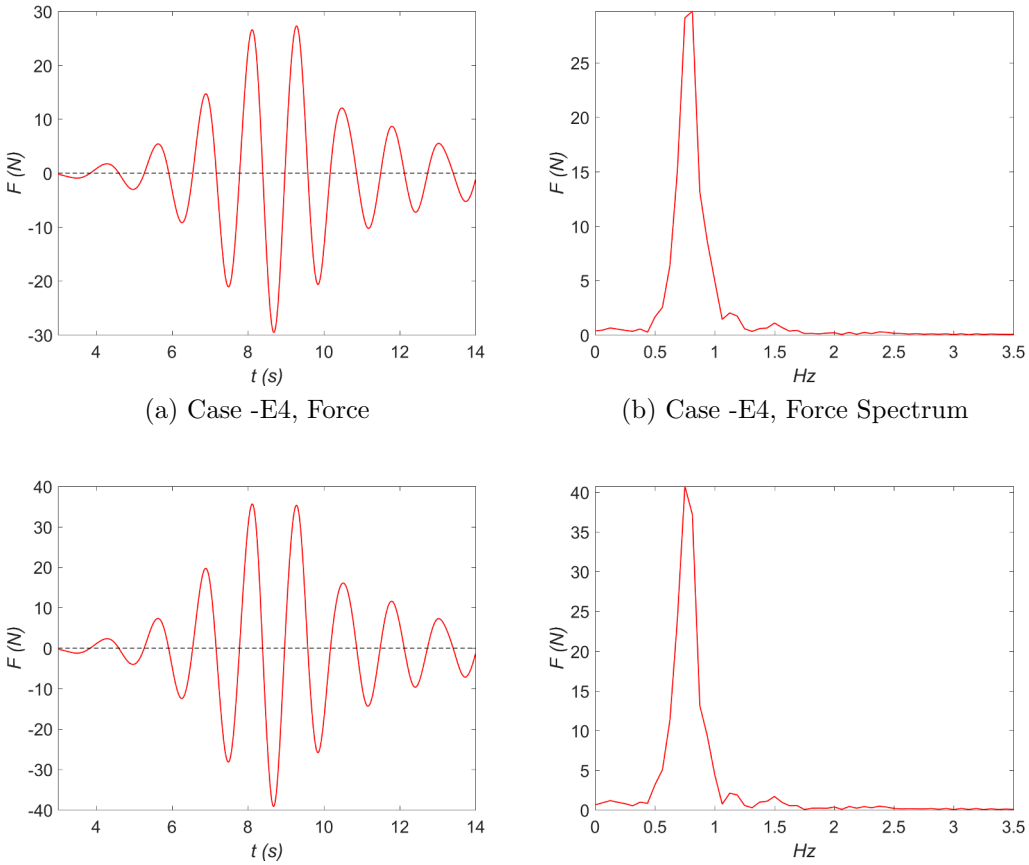

(a) Case -E4, Force

(b) Case -E4, Force Spectrum

(c) Case -E5, Force

(d) Case -E5, Force Spectrum

Figure 5.14: Horizontal wave loading on the cylinder (F) and force spectrum for cases -$E4$ and $E5$

Fig.5.15 shows the free surface elevation for the cases $E1, E2, E3, E4$ and $E5$ at the time of focus while it interact with the cylinder. None of the waves are of breaking type in this study which can be confirmed from this figure.

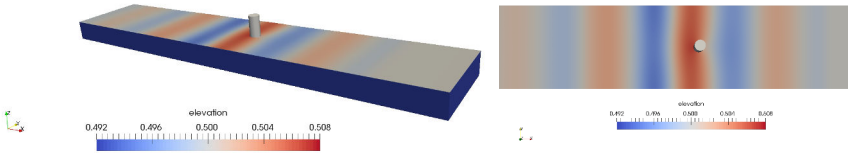

(a) Case-E1 (b) Case-E1

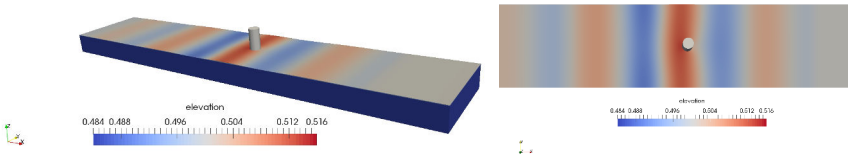

(c) Case-E2 (d) Case-E2

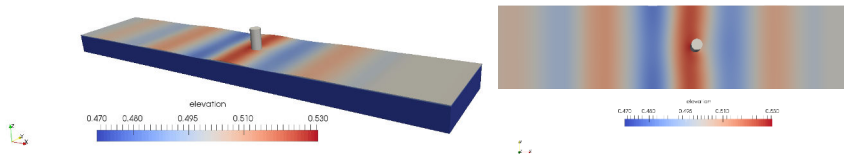

(e) Case-E3 (f) Case-E3

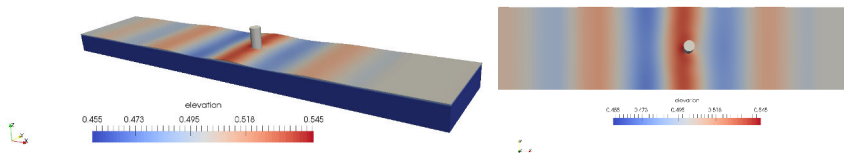

(g) Case-E4 (h) Case-E4

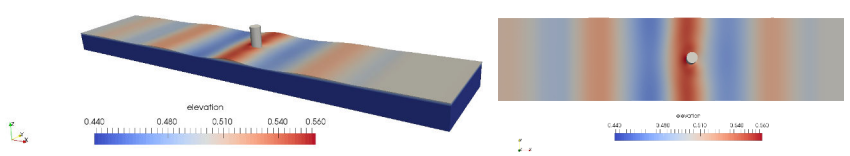

(i) Case-E5 (j) Case-E5

Figure 5.15: Free surface elevation for case $E1, E2, E3, E4$ and $E5$ at the time of focus

Chapter 6

Conclusions, Recommendations and Future works

6.1 Conclusions

In this thesis kinematic nature of the focused wave groups are studied with REEF3D numerical model and validated with available experimental results. Later the focused wave interaction with a vertical cylinder is validated with experimental data and studied further. At first, the grid refinement study was carried-out to find the suitable grid size for the simulation of the focused waves. Several properties of a numerical scheme such as relative phase and amplitude changes and expected focus amplitude with varying grid sizes are investigated. Grid size of $0.025m$ was chosen as a good estimate. At the end, the experimental data by Ning et al. (2009) from laboratory results are used in order to validate that the grid refinement study outcome of $0.025m$ is correct. Influence of the number of wave components (N) used in the wave generation is studied for three steepness cases with spectral steepness 0.0164, 0.0492 and 0.00641. There isn't any different in the free surface elevation both in time and spatial domains except $N = 10$. All three steepness cases give a smooth spectrum with $N = 20$ or above. $N = 20$ is considered as the minimum number of waves to numerically generate a Jonswap spectrum and this number is used in all other investigations. Then incident wave spectral steepness (S_p) is defined and used as an input control parameter to study the kinematics correlated to the incident wave group steepness. Nine wave cases with differing amplitude and wave period is used in the simulation in studying the steepness nature of the focused waves. At first free surface evolution of focused wave is compared in both time and spatial domains. Propagation, spatial and temporal evolution of the waves are studied for varying steepness cases.

Geometrical aspects such as crest front and crest rear steepness, vertical and horizontal asymmetries, wave length and many other kinematic characters are investigated with varying control parameters such as significant wave height, peak period and spectral steepness. Some of the geometrical aspects are highly influenced by significant wave height but some are with peak period. focused wave groups can be generated with different first and second (high) order wave theories. First order, Schäffer's second order $v^{(1)}$ and $v^{(2)}$ theories are used in the focused wave generation in REEF3D. All these theories are validated with experimental results and their application limits are found.

At the beginning kinematic studies are performed with $2D$ simulations. The results from 2D simulations and 3D simulations are compared to understand the necessary numerical wave tank dimension to avoid boundary effects. Numerical wave forces exerted on a vertical cylinder and the associated free surface elevation in the upstream side of the cylinder are validated with four experimental cases. These four experimental cases were performed by Chen et al. (2014) with varying wave steepness. All the experimental cases give a good agreement with the numerical results. Additionally, five more three dimensional simulation cases are performed with REEF3D with varying significant wave heights. Cylindrical diameter of $0.25m$ is used in all the cases. Rise, fall and other changes in the free surface elevation is investigated. The correlation between free surface elevation and wave force on the cylinder is investigated through normalized terms of both η and F. Some of the findings of this study is given below:

- Grid size of $0.025m$ is fine enough to simulate the focused wave group and focused wave-structure interaction in REEF3D.
- A negative relative phase change is present between the numerical scheme and the expected propagation speed.
- There is a larger wave amplitude in the spatial and temporal domain than the intended focused wave amplitude.
- Higher steep Ning case $A4$ also gives a good validation with the numerical scheme.
- Focused wave height linearly increases with incident significant wave height.
- Focused wave height doesn't show significant changes with spectral peak period.
- Vertical asymmetry and wave length of a focused wave is correlated with spectral peak period.
- Crest front and rear steepness, horizontal asymmetry and relative phase change are highly correlated with significant wave height but not with spectral steepness.
- Twenty is the minimum number of waves necessary resemble JONWAP spectrum in a focused wave case.
- Wave structure interaction is validated with the high steep non-breaking experimental cases.
- There is a time lag of around 0.2s between the free surface elevation and the corresponding wave loading
- The peak wave force is not corresponding to the focused wave crest in the wave group according to the normalized value investigation.
- Force spectral analysis shows that higher significant wave height cases induce high frequency low magnitude wave loading on the cylinder.

This study concludes focused wave generation, propagation, interaction with structure and calculation of wave forces can be successfully numerically modeled using REEF3D. REEF3D focused wave simulation results are validated using experimental results for free surface elevation and force calculations. REEF3D can be used as a tool in investigating focused wave groups and this interaction with structure in practical applications.

6.2 Recommendations and Future works

Study shows REEF3D is a promising tool in simulating focused wave group and the interaction with cylindrical structure. This is effective in the small spatial and temporal domains. Study can be further expanded in many directions. All the cases studied so far in focused wave groups are non-breaking. Focused peak amplitude wave component can be made broken by increasing the spectral steepness further and can be investigated for breaking kinematics of focused waves. Location of the vertical cylinder can be adjusted away from the focus location and changes in the wave loading could be analyzed. A numerical wave tank with sloping bed can be used to study shoaling and breaking kinematics of a focused wave group which resembles a surf zone in a coast. Effects on coastal dynamic processes such as cross shore, long shore current and sediment transport capabilities can be studied with the focused wave groups. Different shapes and characters of structures such as tripods, sills, abutments and combination of these structures can be used to study focused wave structure interaction. Focused wave harmonic decomposition study can be performed both on forces and kinematics by signal processing techniques. These are some of the possible future scopes of the study with the focused wave groups.

It is recommended to begin the focused wave study in the future with the breaking focused wave groups. REEF3D needs to be further enhanced with the validation of future studies.

Bibliography

Adeyemo, M., 1968. Effect of beach slope and shoaling on wave asymmetry, in: Proc. 11th Conf. Coastal Eng, pp. 145–172.

Aggarwal, A., 2015. Numerical modelling of irregular waves and irregular wave forces with reef3d .

Alagan Chella, M., Bihs, H., Myrhaug, D., Muskulus, M., 2015. Breaking characteristics and geometric properties of spilling breakers over slopes. Coastal Engineering 95, 4–19.

Arntsen Ø.A, Krogstad, H., 2000. Linear wave theor; part a regular waves. Department of Civil and Transport Engineering, NTNU Trondheim 1.

Baldock, T., Swan, C., Taylor, P., 1996. A laboratory study of nonlinear surface waves on water. Philosophical Transactions of the Royal Society of London A: Mathematical, Physical and Engineering Sciences 354, 649–676.

Bernardi, C., Maday, Y., 1988. A collocation method over staggered grids for the stokes problem. International journal for numerical methods in fluids 8, 537–557.

Bihs, H., Alagan Chella, M., Kamath, A., Oivind, A., 2016. Wave-structure interation of focused waves with reef3d. OMAE2016-54917 1.

Bull, S.R., 2001. Renewable energy today and tomorrow. Proceedings of the IEEE 89, 1216–1226.

Chakravarthy, S.R., 1983. High resolution applications of the 83-1 943 osher upwind scheme for the euler equations .

Chella, M.A., Bihs, H., Myrhaug, D., Muskulus, M., 2016. Hydrodynamic characteristics and geometric properties of plunging and spilling breakers over impermeable slopes. Ocean Modelling 103, 53–72.

Chen, L., Zang, J., Hillis, A., Morgan, G., Plummer, A., 2014. Numerical investigation of wave–structure interaction using openfoam. Ocean Engineering 88, 91–109.

Choi, J., Yoon, S.B., 2009. Numerical simulations using momentum source wave-maker applied to rans equation model. Coastal Engineering 56, 1043–1060.

Chorin, A.J., 1968. Numerical solution of the navier-stokes equations. Mathematics of computation 22, 745–762.

Clauss, G.F., 2002. Dramas of the sea: episodic waves and their impact on offshore structures. Applied Ocean Research 24, 147–161.

Courant, R., Friedrichs, K., Lewy, H., 1928. Über die partiellen differenzengleichungen der mathematischen physik. Mathematische Annalen 100, 32–74.

Courant, R., Isaacson, E., Rees, M., 1952. On the solution of nonlinear hyperbolic differential equations by finite differences. Communications on Pure and Applied Mathematics 5, 243–255.

Croce, R., Griebel, M., Schweitzer, M.A., 2010. Numerical simulation of bubble and droplet deformation by a level set approach with surface tension in three dimensions. International Journal for numerical methods in fluids 62, 963–993.

Dalzell, J., 1999. A note on finite depth second-order wave–wave interactions. Applied Ocean Research 21, 105–111.

Durbin, P., 2009. Limiters and wall treatments in applied turbulence modeling. Fluid dynamics research 41, 012203.

Engquist, B., Majda, A., 1977. Absorbing boundary conditions for numerical simulation of waves. Proceedings of the National Academy of Sciences 74, 1765–1766.

Eymard, R., Gallouët, T., Herbin, R., 2000. Finite volume methods. Handbook of numerical analysis 7, 713–1018.

Fine, R.A., Millero, F.J., 1973. Compressibility of water as a function of temperature and pressure. The Journal of Chemical Physics 59, 5529–5536.

Forristall, G.Z., 2000. Wave crest distributions: Observations and second-order theory. Journal of physical oceanography 30, 1931–1943.

Gresho, P.M., Chan, S.T., Lee, R.L., Upson, C.D., 1984. A modified finite element method for solving the time-dependent, incompressible navier-stokes equations. part 1: Theory. International Journal for Numerical Methods in Fluids 4, 557–598.

Griebel, M., Dornseifer, T., Neunhoeffer, T., 1997. Numerical simulation in fluid dynamics: a practical introduction. volume 3. Siam.

Harten, A., 1983. High resolution schemes for hyperbolic conservation laws. Journal of computational physics 49, 357–393.

Harten, A., Engquist, B., Osher, S., Chakravarthy, S.R., 1987. Uniformly high order accurate essentially non-oscillatory schemes, iii, in: Upwind and High-Resolution Schemes. Springer, pp. 218–290.

Hasselmann, K., Barnett, T., Bouws, E., Carlson, H., Cartwright, D., Enke, K., Ewing, J., Gienapp, H., Hasselmann, D., Kruseman, P., et al., 1973. Measurements of wind-wave growth and swell decay during the Joint North Sea Wave Project (JONSWAP). Technical Report. Deutches Hydrographisches Institut.

Hossain, M., Rodi, W., 1980. Mathematical modelling of vertical mixing in stratified channel flow, in: Proceedings of the 2nd Symposium on Stratified Flows, pp. 280–290.

Hughes, T.J., 2012. The finite element method: linear static and dynamic finite element analysis. Courier Corporation.

Ippen, A.T., Kulin, G., 1954. The shoaling and breaking of the solitary wave. Coastal Engineering Proceedings 1, 4.

Iwagaki, Y., Sakai, T., 1972. Shoaling of finite amplitude long waves on a beach of constant slope. Coastal Engineering Proceedings 1.

Jacobsen, N.G., Fuhrman, D.R., Fredsøe, J., 2012. A wave generation toolbox for the open-source cfd library: Openfoam®. International Journal for Numerical Methods in Fluids 70, 1073–1088.

Jiang, G.S., Shu, C.W., 1995. Efficient implementation of weighted ENO schemes. Technical Report. DTIC Document.

Johannessen, T.B., Swan, C., 1997. Nonlinear transient water waves part i. a numerical method of computation with comparisons to 2-d laboratory data. Applied Ocean Research 19, 293–308.

Johannessen, T.B., Swan, C., 2001. A laboratory study of the focusing of transient and directionally spread surface water waves, in: Proceedings of the Royal Society of London A: Mathematical, Physical and Engineering Sciences, The Royal Society. pp. 971–1006.

Kalita, J.C., Dalal, D., Dass, A.K., 2002. A class of higher order compact schemes for the unsteady two-dimensional convection–diffusion equation with variable convection coefficients. International Journal for Numerical Methods in Fluids 38, 1111–1131.

Kharif, C., Pelinovsky, E., Slunyaev, A., 2009. Observation of Rogue Waves. Springer.

Kim, J., Moin, P., Moser, R., 1987. Turbulence statistics in fully developed channel flow at low reynolds number. Journal of fluid mechanics 177, 133–166.

Kjeldsen, S.P., Myrhaug, D., 1978. Kinematics and dynamics of breaking waves. Vassdrags-og havnelaboratoriet ved Norges tekniske høgskole.

Koliopulos, P., 1988. Quasi-static and dynamic response statistics of linear sdof systems under morison-type wave forces. Engineering Structures 10, 24–36.

Krogstad, H., Arntsen, O., 2000. Linear wave theory. Norwegian University of Science and Technology, Trondheim, Norway [cited 17 March 2013]¡ Available at: http://folk. ntnu. no/oivarn/hercules_ntnu/LWTcourse .

Ladenburg, J., 2008. Attitudes towards on-land and offshore wind power development in denmark; choice of development strategy. Renewable Energy 33, 111–118.

Lyn, D.A., Goodwin, P., 1987. Stability of a general preissmann scheme. Journal of Hydraulic Engineering 113, 16–28.

Ma, Q., Wu, G., Eatock Taylor, R., 2001. Finite element simulation of fully non-linear interaction between vertical cylinders and steep waves. part 1: methodology and numerical procedure. International Journal for Numerical Methods in Fluids 36, 265–285.

MacCamy, R., Fuchs, R.A., 1954. Wave forces on piles: a diffraction theory. Technical Report. DTIC Document.

Mayer, S., Garapon, A., Sørensen, L., et al., 1998. A fractional step method for unsteady free-surface flow with applications to non-linear wave dynamics. International Journal for Numerical Methods in Fluids 28, 293–315.

Menter, F.R., 1994. Two-equation eddy-viscosity turbulence models for engineering applications. AIAA journal 32, 1598–1605.

Miller, R.L., Zeigler, J.M., 1964. The internal velocity field in breaking waves. University of Chicago, Department of the Geophysical Sciences, Fluid Dynamics and Sediment Transport Laboratory.

Morinishi, Y., Lund, T., Vasilyev, O., Moin, P., 1998. Fully conservative higher order finite difference schemes for incompressible flow. Journal of computational physics 143, 90–124.

Moser, R.D., Kim, J., Mansour, N.N., 1999. Direct numerical simulation of turbulent channel flow up to re= 590. Phys. Fluids 11, 943–945.

Myrhaug, D., Kjeldsen, S.P., 1986. Steepness and asymmetry of extreme waves and the highest waves in deep water. Ocean Engineering 13, 549–568.

Naot, D., Rodi, W., 1982. Calculation of secondary currents in channel flow. Journal of the Hydraulics Division 108, 948–968.

Ning, D., Zang, J., Liu, S., Taylor, R.E., Teng, B., Taylor, P., 2009. Free-surface evolution and wave kinematics for nonlinear uni-directional focused wave groups. Ocean Engineering 36, 1226–1243.

Osher, S., Sethian, J.A., 1988. Fronts propagating with curvature-dependent speed: algorithms based on hamilton-jacobi formulations. Journal of computational physics 79, 12–49.

Pierson, W.J., Moskowitz, L., 1964. A proposed spectral form for fully developed wind seas based on the similarity theory of sa kitaigorodskii. Journal of geophysical research 69, 5181–5190.

Roe, P., 1981. Numerical algorithms for the linear wave equation. Royal Aircraft Establishment.

Schäffer, H.A., 1996. Second-order wavemaker theory for irregular waves. Ocean Engineering 23, 47–88.

Sharma, J., Dean, R., et al., 1981. Second-order directional seas and associated wave forces. Society of Petroleum Engineers Journal 21, 129–140.

Shu, C.W., Osher, S., 1988. Efficient implementation of essentially non-oscillatory shock-capturing schemes. Journal of Computational Physics 77, 439–471.

Slunyaev, A., Didenkulova, I., Pelinovsky, E., 2011. Rogue waters. Contemporary physics 52, 571–590.

Smith, G., 1985. Numerical Solution of Partial Differential Equations: Finite Difference Methods. Oxford applied mathematics and computing science series, Clarendon Press. URL: `https://books.google.no/books?id=hDpvljaHOrMC`.

Sumer, B.M., Christiansen, N., Fredsøe, J., 1997. The horseshoe vortex and vortex shedding around a vertical wall-mounted cylinder exposed to waves. Journal of Fluid Mechanics 332, 41–70.

Svendson, I.A., Hansen, J.B., 1976. Deformation up to breaking of periodic waves on a beach. Coastal Engineering Proceedings 1.

Sweby, P.K., 1984. High resolution schemes using flux limiters for hyperbolic conservation laws. SIAM journal on numerical analysis 21, 995–1011.

Van der Vorst, H.A., 1992. Bi-cgstab: A fast and smoothly converging variant of bi-cg for the solution of nonsymmetric linear systems. SIAM Journal on scientific and Statistical Computing 13, 631–644.

Wagner, T.M., 2004. A very short introduction to the finite element method. Technical University of Munich .

Walker, D., Taylor, P., Taylor, R.E., 2004. The shape of large surface waves on the open sea and the draupner new year wave. Applied Ocean Research 26, 73–83.

Wilcox, D.A., 1994. Simulation of transition with a two-equation turbulence model. AIAA journal 32, 247–255.

Yang, J., Stern, F., 2009. Sharp interface immersed-boundary/level-set method for wave–body interactions. Journal of Computational Physics 228, 6590–6616.

Young, I., 1999. Wind Generated Ocean Waves. Elsevier Ocean Engineering Series, Elsevier Science. URL: `https://books.google.no/books?id=ph7GKZZGjyYC`.

Zang, J., Taylor, P.H., Morgan, G., Orszaghova, J., Grice, J., Stringer, R., Tello, M., 2010. Steep wave and breaking wave impact on offshore wind turbine foundations–ringing re-visited, in: Proc. 25th International Workshop on Water Waves and Floating Bodies, Harbin, China.